Universitat Ramon Llull

DOCTORAL THESIS

Title **New Insights in Photodynamic Therapy: Production, Diffusion and Reactivity of Singlet Oxygen in Biological Systems.**

Presented by **Ana Mª Jiménez Banzo**

Centre **Escuela Técnica Superior IQS**

Department **Organic Chemistry**

Directed by **Prof. Santi Nonell Marrugat**

C. Claravall, 1-3
08022 Barcelona
Tel. 936 022 200
Fax 936 022 249
E-mail: urlsc@sec.url.es
www.url.es

A mis padres y hermano.

A David.

Había dos niños que patinaban sobre una laguna congelada. Era una tarde nublada y fría pero los niños jugaban sin preocupación. De pronto el hielo se reventó y uno de los niños cayó al agua. El otro niño, viendo que su amigo se ahogaba debajo del hielo, tomó una piedra y empezó a golpear el hielo con todas sus fuerzas hasta que logró romperlo, y así salvar a su amigo. Cuando llegaron los bomberos y vieron lo que sucedió se preguntaron:

- ¿Cómo lo hizo? El hielo está muy grueso, es imposible que lo haya podido romper con esa piedra y sus manos tan pequeñas.

En ese instante apareció un anciano y dijo:

- Yo sé como lo hizo.
- ¿Cómo? - Le preguntaron al anciano. Él contestó:
- No había nadie a su alrededor que le dijera que no se podía hacer.

"Si lo puedes imaginar, lo puedes lograr"

"If you can imagine it, you can achieve it"

Arthur William Ward.

AKNOWLEDGEMENTS

Science is inevitably a team work, and that is what this thesis reflects.

Gracias al Dr. Santi Nonell por descubrirme la Ciencia, por su absoluta implicación en este trabajo, y por todas las oportunidades que me ha ofrecido para mi desarrollo cientifico y personal. Por compartir las alegrías y apoyarme en los momentos más difíciles de este periodo.

A mis compañeros pero sobre todo amigos de Fotoquímica: Noe, Víctor, Mireia, Xavi, Lourdes, Laia, Noemí, Adaya, María, Ignasi y Rubén. Por las risas, las confidencias, las charlas científicas y no tan científicas, por todo vuestro apoyo y ayuda incondicional. Mención especial merece Xavi, por su colaboración en el desarrollo instrumental y por su paciencia y disposición para escucharme en todo momento. También me gustaría agraceder a Víctor su amistad a pesar de la distancia, su buen humor y los ánimos que siempre me ha dado.

A la Dra. Flors, por prorpocionarnos las GFPs y darme la oportunidad de trabajar en ese proyecto, por compartir conmigo sus conocimientos y por su implicación en esta tesis. A Cris, por todos los buenos momentos vividos juntas, por nuestras largas conversaciones y tantas otras cosas que seguro echaré de menos.

Una parte importante de esta tesis se ha realizado en el Laboratorio de Vehiculización de Fármacos de la Facultad de Biología de la Universidad de Barcelona. Muchas gracias a la Dra. Margarita Mora y a la Dra. María Luisa Sagristà por acogerme en su laboratorio y hacerme sentir como una más, por su implicación y valiosos consejos y en general, por compartir este proyecto.

A mis compañeras y amigas del Laboratorio de Vehiculización de Fármacos: Ana, Begoña y Dra. Bogdanov. Sin vosotras este trabajo no hubiera sido posible. Muchas gracias por encontrar siempre un momento para ayudarme y por vuestra cálida acogida. También quiero agradecer a los chicos de Receptores los buenos momentos compartidos.

Thanks to Prof. Peter Ogilby, from the University of Aarhus (Denmark), for welcoming me in his lab and for his involvement in this work. Also thanks to Lars, John, Cecilia, Markus, Elsa, Nickolass, Sonja, Vijaykumar, Zhangquan, Paul and Mette for their help, and for making my stay in Aarhus very enjoyable. I am in debt with Jacob for what he taught me, his patience, and his advice but mainly for his friendship. Gracias, amigo!!!!

I am grateful to Prof. Cristiano Viappiani, from the University of Parma, for supplying us with the GFP samples and for his great involvement in this work.

A mis compañeros de sala, por su paciencia y compañía. A Violeta, por nuestras charlas y confidencias.

A todos los miembros del Laboratorio de Síntesis. Gracias por vuestra disposición para ayudarme en todo momento.

A la Dra. Agut, por interesase por este trabajo y por sus buenos consejos.

Gracias a todos mis amigos en los que he encontrado apoyo y alegría. Por hacer más llevaderos algunos momentos de esta etapa y "por estar ahí".

A las "supernenas" les tengo que agradecer tantas cosas que necesitaría muchas páginas para enumerarlas. Hemos compartido juntas los buenos momentos de esta etapa, pero también habéis estado conmigo en los momentos "menos buenos". Por esto y mucho más…gracias!!!!!

A Berta, la persona que nunca me ha fallado desde que me embarqué en la "aventura química". Espero que nuestro enlace covalente no se rompa nunca. Simplemente, gracias.

Y por último, lo más importante para mí, mi familia. A mis padres les tengo que agradecer todo lo que soy en esta vida. Sois mi mejor ejemplo y mi mayor orgullo. Gracias por todos vuestros esfuerzos para que haya llegado hasta aquí, por hacer desaparecer la distancia que nos separa y por darme aliento cuando más lo necesitaba. Sé que esta tesis os ha costado tanto o más esfuerzo que a mí. Por todo eso, y por tantas otras cosas que os tengo que agradecer, mi GRACIAS más sincero. A mi hermano, porque sin él tampoco habría sido posible. Gracias por hacerlo todo más sencillo. A David, el amor de mi vida. Gracias sobre todo por intentar comprender mi "amor por la química", por estar siempre a mi lado, por transmitirme tu optimismo y por toda tu ayuda durante la tesis. Sin tí habría sido todo mucho más difícil. A Cristina, Santos y Carolina, por vuestro interés y ánimos pero sobre todo, por hacerme sentir como una más de la familia.

The development of this thesis has been possible thanks to a predoctoral FI fellowship from the *Departament d'Universitats, Recerca i Societat de la Informació* of the Catalonian government and from the *Fons Social Europeu*, to the Spanish Ministry of Science and Technology (SAF2002-04034-C02-02 and BCQ2007-67763-C03/BQU) and to the Institut Químic de Sarrià.

SUMMARY

The kinetics of singlet oxygen ($^1O_2$) photosensitisation in human skin fibroblasts have been investigated by means of an ultrasensitive near-infrared spectrometer with submicrosecond time resolution. The results indicate that the $^1O_2$ kinetics are site-dependent. On one hand, the production of $^1O_2$ is slower in the lysosomes than in the nucleus. On the other hand, $^1O_2$ is able to escape out of the cells when photosensitised in the nucleus, while $^1O_2$ photosensitized in the lysosomes is confined. Despite showing a lifetime in the microsecond time domain, the decay of $^1O_2$ is governed by interactions with the biomolecules within the organelle where it is produced.

The uncertainty as to the intracellular site of $^1O_2$ production may be removed by the use of genetically-encoded photosensitisers, which can be expressed in any desired organelle. Towards this end, the ability of some fluorescent proteins (GFPs) to photosensitise $^1O_2$ has been studied. Some of the studied proteins are able to produce $^1O_2$ albeit with a very low quantum yield. The results obtained are compared to those of the synthetic GFP chromophore and indicates that the protein scaffold not only plays a role in modulating the photophysical properties of the chromophore but also has a protective function from collisional quenching.

Finally, the two-photon absorption properties of tetraphenylporphycene and its palladium (II) complex have been determined. These compounds are *ca.* 100-fold more efficient two-photon $^1O_2$ photosensitisers than their isomeric porphyrin counterparts, with two-photon absorption cross sections δ ~ 25 GM. Qualitative symmetry-based arguments are provided to explain the excellent two-photon properties and the prospects for photodynamic therapy are discussed.

RESUMEN

Se ha estudiado la cinética de fotosensibilización de $^1O_2$ en células eucariotas en suspensión, usando un espectrómetro de última generación con resolución temporal por debajo del microsegundo. Los estudios revelan que la cinética del $^1O_2$ depende de su lugar de formación. Por una parte, la producción de $^1O_2$ es más lenta en los lisosomas que en el núcleo. Por otra parte, el $^1O_2$ es capaz de escapar de las células cuando es fotosensibilizado en el núcleo, mientras que queda confinado en el interior si se fotosensibiliza en los lisosomas. A pesar de que el tiempo de vida del $^1O_2$ se encuentra en los microsegundos, la desactivación principal viene dada por interacciones con las biomoléculas características de cada orgánulo.

La incerteza respecto a la producción de $^1O_2$ en un orgánulo determinado puede ser eliminada mediante el uso de fotosensibilizadores modificados genéticamente ya que pueden ser expresados selectivamente. Con este fin, se evalúan las propiedades fotosensibilizantes de mutantes de proteína fluorescente verde (GFP). Algunas de las GFPs estudiadas sensibilizan la formación de $^1O_2$ aunque con baja eficiencia. Los resultados obtenidos se comparan con los del cromóforo de la GFP y muestran que la estructura proteica, además de modular las propiedades fotofísicas del cromofóro, también lo protege de la desactivación colisional.

Finalmente, se estudian las propiedades de absorción bifotónica del 2,7,12,17-tetrafenilporficeno y de su complejo de paladio (II). La eficacia de formación de $^1O_2$ de ambos compuestos, tras la absorción simultánea de dos fotones, es aproximadamente 100 veces superior a la de sus análogos porfirínicos, con secciones de absorción bifiónica $\delta \sim 25$ GM. Las excelentes propiedades de estos compuestos se explican mediante argumentos cualitativos y se analizan sus perspectivas de cara a su uso en terapia fotodinámica.

RESUM

S'ha estudiat la cinètica de fotosensibilització de l'oxigen singlet ($^1O_2$) en cèl·lules eucariotes en suspensió mitjançant un espectròmetre d'última generació amb resolució temporal per sota del microsegon. Els estudis revelen que la cinètica del $^1O_2$ depèn del seu lloc de formació. Per una banda, la producció del $^1O_2$ es més lenta en els lisosomes que en el nucli. Per altra banda, el $^1O_2$ es capaç d'escapar de les cèl·lules quan es fotosensibilitza en el nucli, però es queda confinat al interior si es fotosensibilitza en els lisosomes. Malgrat que el temps de vida del $^1O_2$ es troba en els microsegons, la desactivació principal ve donada per interaccions amb les biomolècules característiques de cadascú dels orgànuls.

La incertesa respecte a la producció de $^1O_2$ en un orgànul determinat es pot eliminar mitjançant l'ús de fotosensibilitzadors modificats genèticament, ja que aquets poden ésser expressats selectivament. Amb aquesta finalitat, s'avaluen les propietats fotosensibilitzants de mutants de proteïna fluorescent verd (GFP). Algunes de les GFPs estudiades sensibilitzen la formació del $^1O_2$ malgrat amb baixa eficiència. Els resultats obtinguts es comparen amb els del cromòfor de la GFP i mostren que l'estructura proteínica, a sobre de modular les propietats fotofísiques del cromòfor, també el protegeix de la desactivació col·lisional.

Finalment, s'estudien les propietats d'absorció bifotónica del 2,7,12,17-tetrafenilporficé i del seu complex de pal·ladi (II). L'eficiència de formació del $^1O_2$ per part dels dos compostos, després de l'absorció simultània de dos fotons, es aproximadament 100 vegades superior a la dels seus anàlegs porfirínics, amb seccions d'absorció bifotòniques $\delta \sim 25$ GM. Les excel·lents propietats d'aquestos compostos s'expliquen mitjançant arguments qualitatius i s'analitzen les seves perspectives de cara al seu ús en teràpia fotodinámica.

LIST OF ABBREVIATIONS

A	adenine
ADC	analog-to-digital conversion
BP3	4-methoxy-2-hydroxy-benzophenone
Bu_4TAP	tetra-*tert*-butylporphyrazine
BSA	bovine serum albumin
C	cytosine
CALI	Chromophore-Assisted Light Inactivation
CHES	2-(*N*-cyclohexylamino)ethane sulfonic acid
CNPhVB	2,5-dicyano-1,4-bis(2-(4-diphenyl-aminophenyl)-vinyl)-benzene
DABCO	1,4-diazabicyclo[2.2.2]octane
D-CHES	deuterated 2-(*N*-cyclohexylamino)ethane sulfonic acid buffer
DFT	density functional theory
DMEM	Dulbecco's Modified Eagle's Medium
DMSO	dimethylsulfoxide
DNA	deoxyribonucleic acid
D-PBS	deuterated phosphate buffered saline
EDTA	ethylenediaminetetraacetic acid
EGFP	enhanced green fluorescent protein
ELISA	Enzyme-Linked Immunosorbent Assay
ER	endoplasmic reticulum
FCS	fluorescence correlated spectroscopy
FDA	Food and Drug Administration
FHWM	full width at half maximum
G	guanine
GdnHCl	guanidinium chloride
GFP	green fluorescence protein
GM	Göppert-Mayer
GPC	gated photon counting
HBDI	4-hydroxybenzylidene-1,2-dimethylimidazoline
HPD	hematoporphyrin derivate
IR	infrared
IRF	Instrument's response function
LDL	low density lipoprotein
LED	light-emitting diode
MCS	multichannel scaling

MTT	3-[4,5-dimethylthiazol-2-yl]-2,5-diphenyltetrazolium bromide
NIR	near infrared radiation
$^1O_2$, O_2 ($a^1\Delta_g$)	singlet oxygen
$O_2^{\bullet -}$	superoxide radical
OPA	optical parametric amplifier
OPO	optical parametric oscillator
PBS	phosphate buffered saline
Pc	phthalocyanine
PDD	photodynamic photodiagnosis
PDT	photodynamic therapy
PdTPPo	palladium (II)-2,7,12,17-tetraphenylporphycene
PMT	photomultiplier tube
PN	phenalenone
PS	photosensitiser
PtOEP	platinum(II)-2,3,7,8,12,13,17,18-octaethyl-21*H*,23*H*-porphine
ROS	reactive oxygen species
SDS	sodium dodecyl sulphate
SNR	signal-to-noise ratio
T	thymine
TBP	tetrabenzoporphyrin
TCSPC	time-correlated single photon counting
TMPyP	5,10,15,20-tetrakis(*N*-methyl-4-pyridyl)-21*H*,23*H*-porphine
TPA	two-photon absorption
TPP	5,10,15,20-tetraphenyl-21*H*,23*H*-porphine
TPPo	2,7,12,17-tetraphenylporphycene
TPPS	5,10,15,20-tetrakis-(4-sulfonatophenyl)-21*H*,23*H*-porphine
TRPD	time-resolved phosphorescence detection
TTS	transit-time-spread
UV	ultraviolet
VIS	visible

INDEX

Chapter 1

Introduction

A general introduction to the subject of this thesis and the aim of this work is given in this chapter. The history and the basis of photodynamic therapy for the treatment of cancer are reviewed and new perspectives for this therapy are also presented.

1.1. FROM LIGHT TO PHOTODYNAMIC THERAPY

Light has been used as therapy for more than three thousand years. Ancient Egyptian, Chinese and Indians civilizations used the combined action of natural plant extracts with sunlight in attempts to cure disorders such as vitiligo, rickets, psoriasis, skin cancer and psychosis [1]. The start of a modern quantitative and experimental approach to the study of light-sensitized reactions took place near the turn of the last century:

> "*During the winter of 1897, Oscar Raab, a student in the laboratory of Prof. Tappeiner, was set to study the toxicity of a dye, acridine, for paramecia. To this end he measured the time required to kill these organisms when they were placed in solutions of different dye concentrations, and found, to his surprise, that the time varied widely for different experiments in which the same concentration was used. He quickly recognized that the time required to kill was related to the intensity of light in the laboratory, and, following this lead, was able to show that paramecia swimming in solutions containing dye were rapidly killed when exposed to the sun's rays, whereas when no dye was present they survived for long periods in sunlight."* [2]

Under the driving force of Prof. Tappeiner, this discovery initiated a large burst of research activity which led to the identification of many photosensitizing compounds, such as anthracences, tetrapyrroles, thiazines and xantenes. Moreover, the presence of oxygen was shown to be a necessary requirement to obtain photosensitization. In order to distinguish these phenomena from the sensitization of photographic plates by dyes, the term *photodynamische Wirkung* (photodynamic effect) was coined for the oxygen-requiring photosensitized reactions in biological systems.

The application of photodynamic reactions to medicine was rapidly exploited but it was not until 1950s when the ability of certain tetrapyrrolic compounds (porphyrins) to selectively accumulate in certain tissues was reported. This fact, coupled with the photosensitising ability of many such porphyrin compounds, has led to the beneficial use of photosensitization in the treatment of several tumours, as well as for other non oncological diseases [3], in what is currently known as photodynamic therapy (PDT).

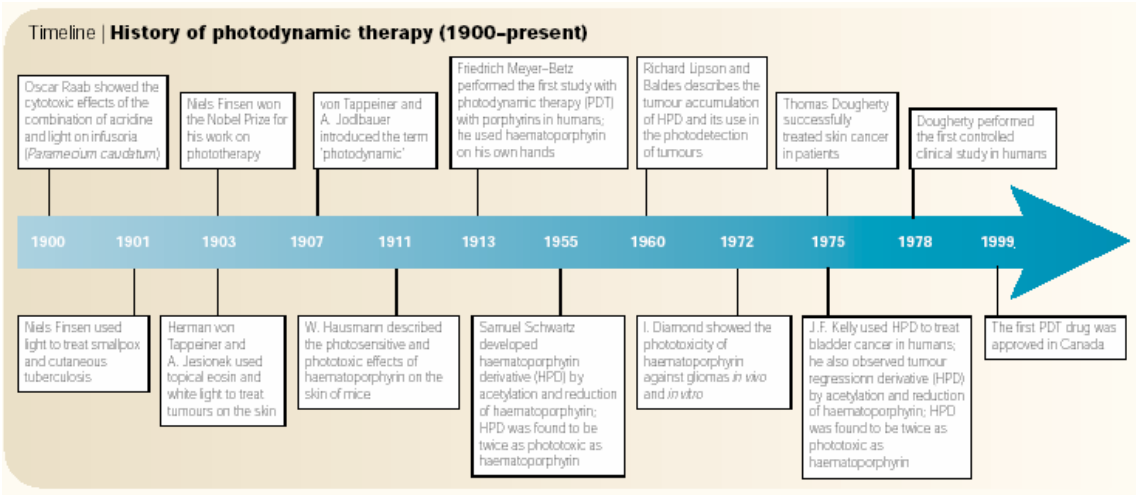

Fig. 1: Brief summary of the more relevant dates and achievements related to photodynamic therapy. From Dolmans *et al.* in [4].

1.2. PHOTODYNAMIC THERAPY FOR CANCER: general aspects

Photodynamic therapy (PDT) involves three individually non-toxic components that are combined to induce cellular and tissue effects. The first component of PDT is a *photosensitiser*, a photosensitive molecule that localizes preferentially in certain kinds of cells and/or tissues. The second component involves the administration of *light* of a specific wavelength. None of these factors is harmful by itself but in the presence of *oxygen*, the third and last required component, produce *reactive oxygen species* (ROS), cytotoxic agents that can inactivate tumour cells. Therefore, this treatment shows a dual selectivity that is produced by both a preferential uptake of the photosensitiser by the diseased tissue and its ability to confine activation of the photosensitiser by restricting the illumination to that specific area [4-6].

1.2.1 Mechanisms of selective tumour uptake

The mechanisms involved in the preferential distribution of photosensitisers in tumours are not fully understood yet. Properties of tumour tissue may contribute to such selective distribution:

- Cancer cells require more cholesterol for membrane biosynthesis. Many types of tumour cells express a high number of membrane receptors for low-density lipoproteins (LDL). These kinds of proteins are the main carriers of hydrophobic

sensitisers in the bloodstream, so they act as delivery systems of these compounds into cells *via* endocytotic pathways.

- Tumour-associated macrophages can make up to 20-50% of the cellular content in tumour cells. They can contribute to the photosensitisers' preferential distribution in tumours since it has been demonstrated that these macrophages take up large amounts of photosensitisers.
- A decreased intratumoral pH, caused by an increased concentration in lactic acid, can affect the ionisation of the sensitisers with weakly acidic pKa values, thus retaining them inside the tumours.

Also, other features of the abnormal structure of tumour stroma, characterized by large interstitial space, a leaky vasculature, compromised lymphatic drainage, a high amount of lipid and newly synthesized collagen, may also favour a preferential distribution of the photosensitizers within the tumour tissues [6,7].

Increased and/or more selective accumulation of sensitisers at the targeted site can be achieved with active or passive delivering vehicles [8,9]. Examples of active carriers include the use of antitumoral monoclonal antibodies- or hormone-photosensitiser conjugates that selectively bind to the appropriate receptor of neoplasic cells. Passive carriers such as dendrimers, micelles or liposomes improve the photophysical properties of many photosensitisers preventing their aggregation and can also influence their binding to LDL, increasing the uptake by tumours. Then, delivering vehicles broaden the clinical repertoire of sensitizers and minimize the amount of precision that is needed in light delivery.

Delivering vehicles can also influence the photosensitiser's subcellular localisation. Other features of the photosensitisers, such as the lipid/water partition coefficient, the molecular weight and the charge distribution (symmetry/asymmetry), seem to play an important role [10]. In general, cationic sensitisers bind to DNA through intercalation and then localise in the nucleus whereas cationic ones with long side-chains and thus, high lipophilicity solely accumulate in the mithocondria. Hydrophobic photosensitisers tend to stick to membrane structures and hydrophilic compounds are likely to be taken up by pinocytosis and/or endocytosis and therefore, become localized in lysosomes or endosomes [9]. The subcellular localisation of a given photosensitiser is considered a significant parameter for PDT treatments since several studies have shown a correlation between photosensitiser's subcellular localisation and its photodynamic efficacy for tumour destruction [11,12].

1.2.2 Mechanisms of tumour destruction

While it has long been known that the basis mode of cell death in PDT is mediated through singlet oxygen generation and other reactive oxygen species, and that direct cellular damage and vascular shutdown contribute to destruction of the tumour, only in recent years the importance of immune responses have been recognized [3].

Direct cellular damage. It has been shown that exposure of tumours to PDT *in vivo* can reduce the clonogenic tumour cells thought direct photodamage, *i.e.*, those cells able to reproduce a tumour. However, complete tumour eradication is not always fully realized by this mechanism mainly due to two reasons: non-homogeneous distribution of the photosensitiser within the tumour and oxygen availability within the tissue that is targeted by PDT [4,6].

Vascular damage. The viability of tumour cells also depends on the amount of nutrients supplied by the blood vessels, which in turn depend on growth factors produced by tumour or host cells. The mechanisms underlying the vascular effects of PDT differ greatly with different photosensitizers but vascular constriction, thrombus formation and inhibition of tumour growth have been identify among the most important ones [13].

Immune responses. Several studies have reported that infiltration of lymphocytes, leukocytes and macrophages into PDT-treated tissue produced an activation of the immune response that consequently eliminates surviving tumour cells that have escaped to the direct effects of PDT [14-16].

PDT effects on all these targets may influence each other, producing a plethora of responses. However, the relative importance of each for the overall tumour response is yet to be defined. Further, it is known that both necrosis and apoptosis occur following PDT [17,18], albeit to different degrees depending on the photosensitiser and treatment conditions.

Necrosis or passive cell death can either result from extreme external physical conditions or severe cellular damage induced by chemical processes. It is usually accompanied by a loss of membrane integrity and associated with characteristic morphological changes such as organelle and cell swelling, bleb formation, loss of integrity of mitochondrial, lysosomal and plasma membranes and eventual breakdown of the cell, leading to release of its contents into the surrounding area [19].

Apoptosis represents regulated cell suicide. It is a mechanism whereby organisms initiate cellular death *via* a process that is normally part of the genetic apparatus [20]. The end result is fragmentation of nuclear DNA and dissociation of the cell into membrane-bound particles that are phagocyted by neighbouring cells, preventing uncontrolled leakage of intracellular material to the environment and thereby avoiding damage to neighbouring cells and tissue inflammation [21]. Apoptosis has been shown to be a rapid and dominant form of cell death following PDT in multiple experimental settings utilising various photosensitisers and cell types [22-24].

1.2.3 Molecular basis of photodynamic therapy

Photodynamic therapy involves the administration of a tumour-localising photosensitiser that requires activation by light of the appropriate wavelength to produce *reactive oxygen species*. At a molecular level, after a molecule absorbs light and accesses an electronically-excited state it does deactivate and return to its ground state through different pathways that can be classified in three main groups:

a) Non-radiative processes. The excited state species are transformed in other electronic or vibrational states, releasing the excess of energy as heat. There are three non-radiative kinds of processes:

- *Vibrational relaxation*: the excited molecule decreases its vibrational energy within a single electronic state.
- *Internal conversion*: it is the isoenergetic transition between two electronic states with the same spin multiplicity, generally followed by vibrational relaxation.
- *Intersystem crossing*: it is the isoenergetic transition between two electronic states with different spin multiplicity, generally followed by vibrational relaxation.

b) Radiative processes. The excited state species are transformed into lower-energy electronic states, returning the excess of energy as electromagnetic radiation. There are two kinds of radiative processes:

- *Fluorescence*: spontaneous emission of radiation upon transition between two electronic states with the same spin multiplicity.
- *Phosphorescence*: spontaneous emission of radiation upon transition between two electronic states with different spin multiplicity.

The above processes are depicted in the Jablonski diagram show in Fig. 2:

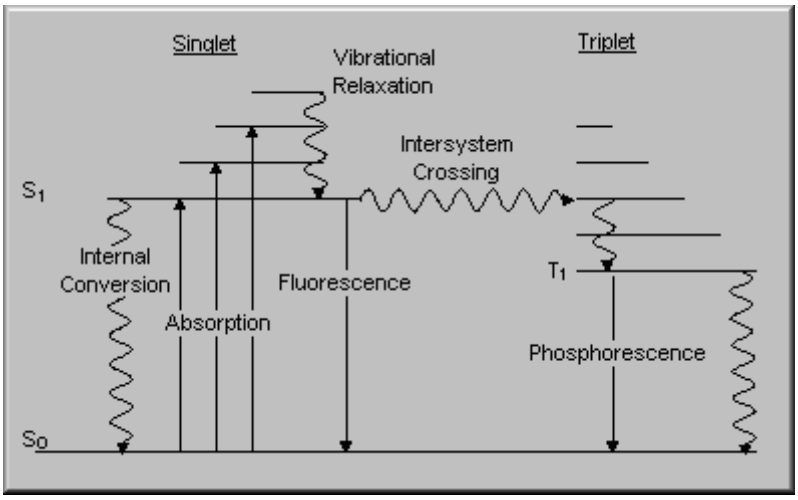

Fig. 2: Jablonski diagram depicting the possible photophysical processes.

c) Other deactivation processes. The excited state molecules can undergo photochemical or photophysical reactions or photosensitisation.

Photosensitisation is the process by which a photochemical or photophysical alteration occurs in one molecular entity (A) as a result of initial absorption of radiation by another molecular entity called photosensitiser (PS) [25]. It can schematically be represented as follows:

$$PS + h\nu \rightarrow PS^*$$

Photochemical: $PS^* + A \rightarrow PS' + B$

Photophysical: $PS^* + A \rightarrow PS + A^*$

When molecular oxygen is involved in photosensitization, such process is termed “photodynamic action” and two different mechanisms are possible:

- *Type I mechanism:* in this mechanism the photosensitiser in its singlet or triplet excited state reacts with a substrate *via* electron transfer (a) or hydrogen abstraction (b) to yield free radicals, which will readily react with oxygen to form peroxides radicals, and in turn starting a radical chain reaction.

$$PS + h\nu \rightarrow PS^*$$

a) $PS^* + R \rightarrow PS^{\bullet-} + R^{\bullet+}$

$PS^{\bullet-} + {}^3O_2 \rightarrow PS + O_2^{\bullet-}$

$R + O_2^{\bullet-} \rightarrow R^{\bullet-} + {}^3O_2$

b) $PS^* + RH \rightarrow PSH^{\bullet} + R^{\bullet}$

$R^{\bullet} + {}^3O_2 \rightarrow ROO^{\bullet}$

$ROO^{\bullet} + RH \rightarrow ROOH + R^{\bullet}$

- *Type II mechanism:* in this process, the sensitizer in its excited state (commonly in its triplet state) transfers its energy to ground-state molecular oxygen, giving rise to the photosensitiser in its ground state and singlet oxygen ($^1O_2$), a very reactive oxygen species towards electron rich substrates such as alquenes, aromatic rings, phenols, amines and thioethers [26].

$$PS + h\nu \rightarrow PS^*$$
$$PS^* + {}^3O_2 \rightarrow PS + {}^1O_2$$

In biological media, photodynamic effect, by either the two mechanisms (Fig. 3), can produce the photooxidation of relevant biomolecules, such as aminoacids, nucleic bases and lipids, which leads to damage on proteins, DNA and membranes, and end in cell death.

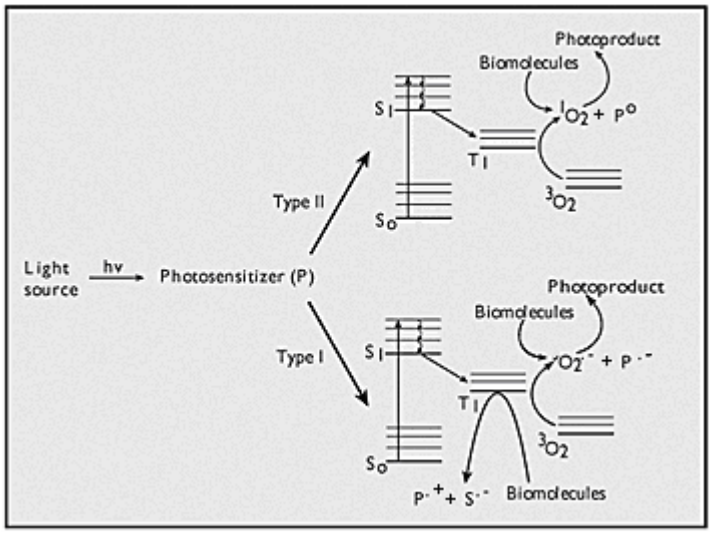

Fig. 3: Mechanisms of ROS generation by combination of light, photosensitiser and ground-state oxygen. Ground-state photosensitiser (S_0) is irradiated with visible light generating excited-state photosensitiser (S_1). S_1 can relax back to excited-triplet photosensitiser state (S_T), generating radicals (Type I mechanism) and / or singlet oxygen (Type II mechanism).

In general, both mechanisms occur simultaneously. The relative importance of one mechanism over the other will depends, among other factors, on the substrate and oxygen concentrations and on the distance between the photosensitiser and the substrate. In biological media, it is generally accepted that type I processes contribute to photoinduced cell death but that the predominant mechanism is a type II process *via* singlet oxygen.

1.2.4 Singlet oxygen and its relation to cell death mechanisms

Singlet oxygen ($^1O_2$ or $O_2(a^1\Delta_g)$ is a member of the general class of reactive species called *reactive oxygen species* (ROS) that includes the free radicals hydroxyl ($OH^{\bullet}$) and superoxide ($O_2^{\bullet -}$), together with other molecules such as hydrogen peroxide (H_2O_2) and hypochlorous acid (HClO). All these species are able to oxidize biomolecules and promote cell death by necrosis and/or apoptosis pathways. Because $^1O_2$ is an excited state, its properties differ in several ways from those of other ROS. For example, whereas many ROS can be produced by physiologic processes and interconversion between them is feasible, $^1O_2$ is generated by photosensitisation of endo and/or exogenous photosensitisers (*vide supra*) and does not interconvert to other ROS.

The most important feature of $^1O_2$ in relation to PDT is the inherent upper value of its lifetime. The term *lifetime* indicates the time for diminution of the concentration by 1/*e*, or to ~37 % of the original concentration. $^1O_2$ can exist in its excited state only for a certain period of time before returning to its ground state by transferring its energy to vibrational modes of the solvent. Then, the upper value of the lifetime is determined by the unimolecular rate constant of a given solvent, k_d, and defines how long $^1O_2$ exist in the absence of reactive molecules. $^1O_2$ lifetime is well documented in a variety of solvents and in the gas phase [27] but it is not clear yet which the value of this parameter is in a cellular environment where $^1O_2$ can react with several biomolecules.

In any case, the inherent excited state lifetime of $^1O_2$ determines an upper limit on its mobility from its site of generation. Using the Einstein-Smoluchowski two-dimensional diffusion model (equation 1), $D = 2 \cdot 10^{-5}$ cm^2s^{-1} for the $^1O_2$ diffusion constant in water [28], and considering that cells are predominantly aqueous systems, the maximum distance (δ) that $^1O_2$ could diffuse before returning to its ground state (t=5τ, τ ~3.5 μs in water [27]) is ~270 nm.

$$\delta = \sqrt{2Dt} \qquad \textbf{(1)}$$

This is a very small distance on the scale of cell dimensions. Typical eukaryotic cells have diameter of 10-30 μm, mitochondria are around 500 nm and membranes are less 10 nm thick [29]. Consequently, the primary reactions of $^1O_2$ in a cell occur within its short diffusion distance, *i.e.*, at a molecular level. These primary $^1O_2$ reactions with biomolecules can trigger a cellular response, and that will be different if $^1O_2$ is generated in another cellular site.

As already outlined, many photosensitisers show a preferential subcellular localisation due to the unique composition and properties of each organelle. In addition, the size of these organelles is in the same range of the maximum diffusion distance of singlet oxygen, *i.e.,* in the nanometre domain. Then, the unique composition of each organelle indicates that the biochemical mechanisms initiated by the primary reactions of singlet will be organelle specific. For example:

- The main consequence of mitochondria localisation is photodamage to the anti-apoptotic proteins Bcl-2 and Bcl-xL. This damage is considered the trigger of the apoptotic outcome. Subsequent responses are the release of cytochrome c and an alteration in the mitochondrial membrane potential [11].
- Photoproduction of $^1O_2$ in lysosomes induced photooxidation reactions that lead to membrane disruption and the release of lysosomal enzymes into the cytoplasm. One or more of these enzymes initiates a process that ultimately results in the cleavage of the proapoptotic protein Bid to a truncated form that lead to an indirect apoptotic response [11].
- $^1O_2$ photosensitised in the endoplasmic reticulum (ER) induced calcium release from its site of storage, the ER. This is likely only one step in a complex cascade of events that trigger the apoptosis [30,31].

Finally, the primary reactions of $^1O_2$ with neighbouring molecules can produce species that are capable of diffusing and then, cause further oxidation reactions at a cellular level. These species are considered to be *secondary ROS*. For example, $^1O_2$ formed in membranes reacts with proteins and unsaturated lipids to produce hydroperoxides that can break down to free radicals and initiate chain oxidation reactions of other compounds [32]. These longer-lived peroxides and free radicals are able to diffuse longer distances in cells to cause remote oxidative damage. Effects of membrane-localised photosensitisers seem not likely to initiate the apoptotic program but could produce irreparable damage that lead to cell death by necrosis.

In summary, although the lifetime of $^1O_2$ restricts its diffusion within the cells, generation of this highly reactive species at different subcellular sites does not produce the same cellular response or if it is produced, as in the case of both mitochondria- and lysosome-associated photosensitisers, it is through a different mechanism.

1.4. FUTURE DIRECTIONS OF PHOTODYNAMIC THERAPY

Photodynamic therapy has evolved rapidly since receiving approval for the treatment of refractory superficial bladder cancer in Canada in 1993. Photofrin®, the first drug approved by the Food and Drug Administration (FDA) for PDT purposes, is still the most commonly used photosensitiser, although it is far from being the ideal compound for PDT applications. First, it consists of complex and variable mixture of more than 60 compounds with different properties and activity. Second, PDT clinical applications require red light irradiation in order to reach deeper penetration into the tissues but Photofrin®, and porphyrins in general, do not absorb strongly in this region. Finally, Photofrin® causes long-lasting cutaneous photosensitivity due to its low selectivity for tumour tissues and its slow elimination rate from the body. As a result, the main current efforts in relation to PDT are related to: 1) the development of new photosensitisers with better properties, 2) improve the selectivity of the treatment thus minimising its side-effects.

1.4.1 Photosensitisers

Owing to the disadvantages presented by Photofrin® [33], many new compounds have been synthesised in an attempt to create better photosensitisers, the so-called second generation photosensitisers. Among other features, second-generation photosensitisers present stronger absorption coefficients at longer wavelengths and thus, a PDT treatment with any of these compounds would require lower doses of drug and light for efficacy. The main classes are synthetic porphyrin, porphycenes, chlorins and bacteriochlorins, phthalocyanines and naphthalocyanines, azaporphyrins, and expanded porphyrins such as texaphyrins. Their core structures are depicted in Fig. 4.

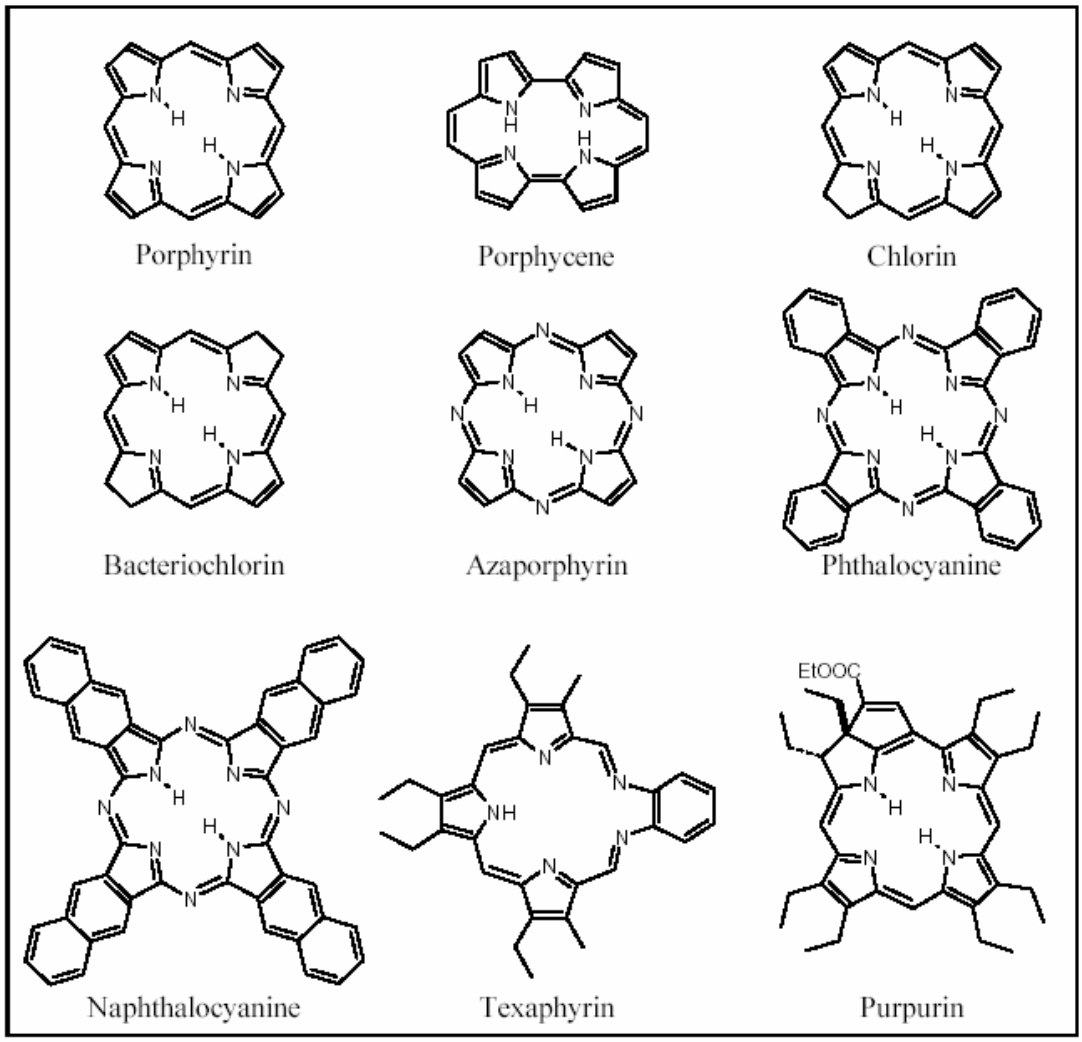

Fig. 4: core structures of the main kinds of second generation photosensitisers.

Our group has focused their interest in the porphycene's family. Porphycenes are structural isomers of porphyrins that have many unique properties and features. Since the synthesis of the first porphycene in 1986 [34], a variety of substituted derivatives have been prepared, including the 2,7,12,17-tetraphenylporphycene [35], as well as several of its metal-ion complexes [36]. The excellent porphycene's photophysical properties, as well as its ability to photoinactivate several cell lines [36-39], promote the porphycenes as promising photosensitisers for PDT treatments.

Some other photosensitisers that belong to the former families are currently under clinical trials for the treatment of several kinds of cancer. Their structures are depicted in Fig. 5. However, most of these sensitisers show only a slight preference for malignant cells. Then, selectivity should be improved by other approaches.

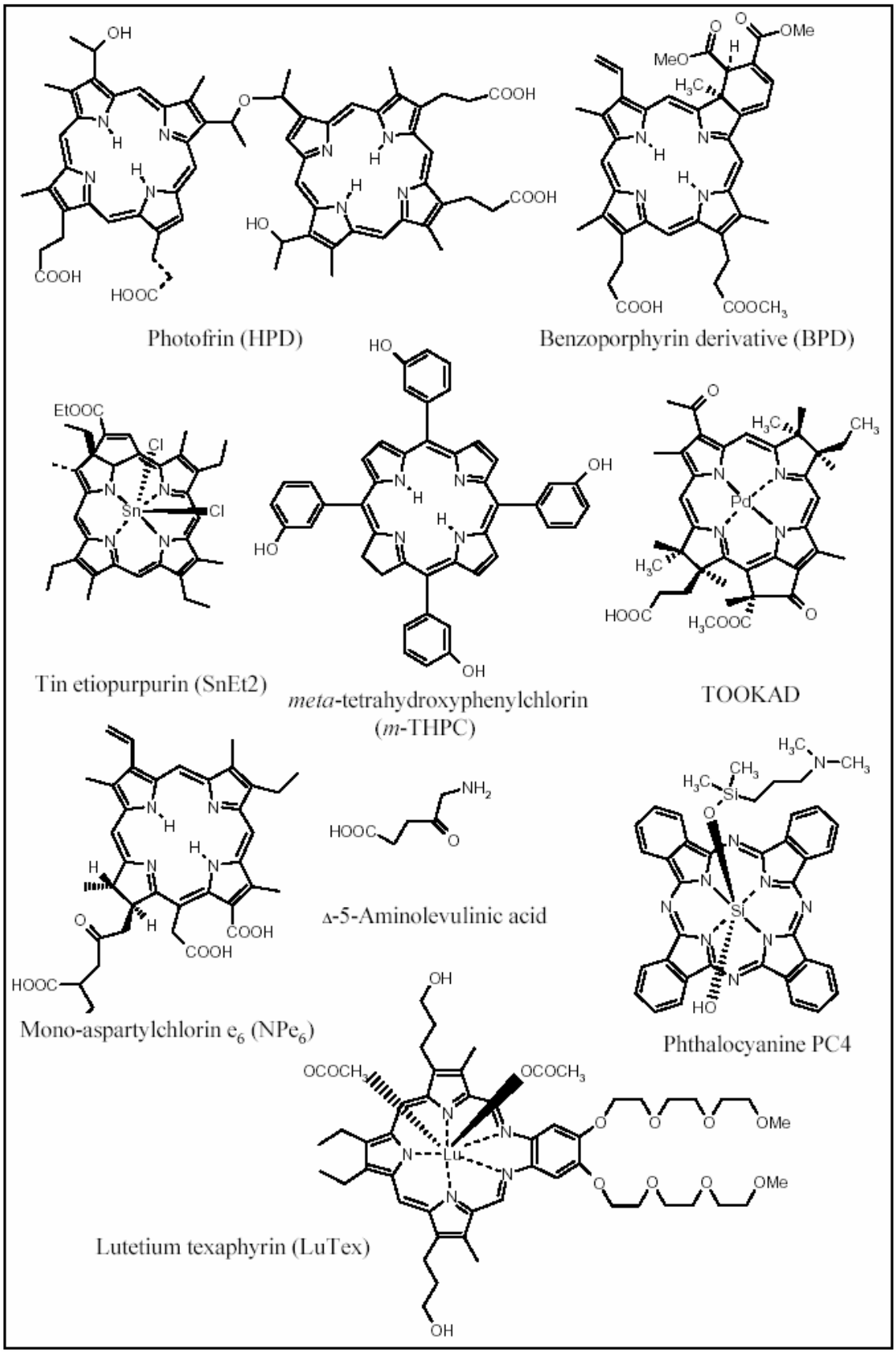

Fig. 5: photosensitisers used for PDT trials. Δ-5-Aminolevulinic acid is a prodrug that is enzimatically converted into Protoporphyrin IX, the actual photosensitiser.

1.4.2 Selectivity

The main advantage of PDT in comparison with other treatments is the reduced side-effects due to its high and dual selectivity. Ideally, this selectivity is achieved by preferential accumulation of the photosensitiser in tumour tissues as well as by strict irradiation of that area. However, most sensitisers currently under PDT trails are not as selective for tumour tissues as they should be, and irradiation of the photosensitiser requires illumination along the entire path of the laser. These two factors altogether lead to a large amount of damage to healthy tissue.

Two strategies can be used to overcome this problem:

1) design of new photosensitisers which are active-targeted towards diseased tissue, e.g., by attaching different systems, such as antibodies, serum proteins, and other molecules, which fit a receptor site on the tumour cell, to the first- and second-generation sensitisers (*vide supra*). The current research is focused in the kind of receptors overexpressed in tumoral cell lines that will allow the design and synthesis of ligand- sensitiser conjugates.

Active-targeted photosensitisers will increase the selectivity for tumour tissues, but the ideal selectivity would be realised if a photosensitiser is efficiently and exclusively confined in those malignant tissues. In relation to that, it is worthy to be note that very recently, the first genetically-encoded photosensitiser has been reported [40], namely a phototoxic homolog of the green fluorescence protein (GFP) designed to produce $^1O_2$ upon irradiation with green light. Also, recent studies on nude mice demonstrated accumulation of GFP-expressing bacteria or viruses within various tumours [41]. Bacteria or viruses expressing a genetically encoded photosensitiser might also allow light-induced killing of tumour cells, both spatially and temporally controlled. Although in its initial steps of research, genetically encoded photosensitisers would open new perspectives for photodynamic therapy.

2) An alternative approach is the use of the nonlinear-optical effect of two-photon absorption (TPA) [42]: a sensitiser excited state is populated as a consequence of the simultaneous absorption of two photons of comparatively low energy. The transition proceeds *via* a virtual state but, irrespective of the excitation method and which state is populated first, and due to rapid relaxation, all the subsequent processes originate from one common state: the lowest excited singlet state, S_1. The principle of $^1O_2$ photosensitisation by both one- and two-photon excitation of the sensitiser has been demonstrated [43] and is illustrated in Fig. 6:

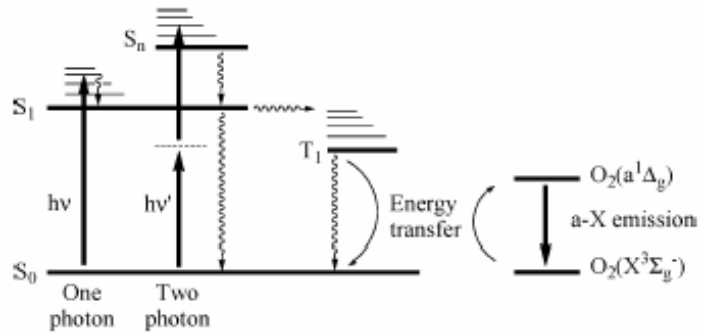

Fig. 6: $^1O_2$ photosensitisation processes upon conventional (one-photon) and two-photon excitation of the photosensitiser. From Arnbjerg *et al.* in [44].

Two-photon irradiation has some important advantages. First, the excitation can be confined to a femtoliter volume at the focus whereas in conventional irradiation (one-photon excitation processes) the photosensitiser is necessarily excited along the entire path of the laser, leading to a large amount of damage to healthy tissue. Second, the energy of the photons required for TPA is comparatively lower than for one-photon excitation and fit into the therapeutic window, *i.e.*, 800-1000 nm, allowing deeper penetration of the light. Finally, due to the nature of TPA, the photophysical properties of the photosensitisers remain the same and the information already gathered for conventional PDT is still valid for two-photon excitation PDT [45,46].

Although two-photon initiated PDT is also in the initial stages of research, it is a very promising therapy for the treatment of some diseases due to its advantages in comparison to conventional PDT. For instance, one disease that could benefit from highly-localised two-photon excitation is the wet-form of age-related macular degeneration, a major cause of blindness in the older population, and the most popular application of PDT nowadays.

1.5. PDT FOR THE TREATMENT OF OTHER DISEASES

Today, PDT is extensively used for the treatment of age-related macular degeneration and other eye diseases related to neo-vascularization [47], as well as in dermatology for treating psoriasis and scleroderma [48,49]. PDT has also been applied in cardiovascular diseases and in the rheumatology field, where it is being tested to treat arthritis [50]. PDT is also useful for detection of cancer and pre-cancerous lesions due to photosensitisers' fluorescence in the related field of photodynamic diagnosis (PDD) [51]. Finally, PDT is going back to its origins in microbiology and being used for photoinactivation of virus and bacteria [52,53].

1.6. OBJECTIVES

The main goal of this thesis is to unravel the details of $^1O_2$ photosensitisation in cells as well as to assess the potential of genetically-encoded sensitisers and two-photon excitation in photodynamic therapy. This is divided in the following specific objectives:

- Assess the potential of the novel development in the optoelectronic industry for the real-time monitory of $^1O_2$ in cells.
- Study the $^1O_2$ photosensitisation kinetics as a function of the subcellular site in human skin fibroblasts.
- Investigate the ability of GFP-like proteins to photosensitise $^1O_2$.
- Characterize the two-photon absorption properties of tetraphenylporphycenes.

1.7. REFERENCES

[1] Spikes, J. D. Historical review: photodynamic action: from paramecium to photochemotherapy. *Photochem. Photobiol.* **65S**:142S-147S; 1997.

[2] Blum, H. F. *Photodynamic action and diseases caused by light*: New York: Hafner Publishing Company; 1964.

[3] Dougherty, T. J. An update on photodynamic therapy applications. *J. Clin. Laser. Med. & Surg.* **20**:3-7; 2002.

[4] Dolmans, D. E. J. G.; Fukumura, D.; Jain, R. K. Photodynamic therapy for cancer. *Nat. Rev. Cancer* **3**:380-387; 2003.

[5] Henderson, B. W.; Dougherty, T. J. How does photodynamic therapy work? *Photochem. Photobiol.* **55**:145-157; 1992.

[6] Dougherty, T. J.; Gomer, C. J.; Henderson, B. W.; Jori, G.; Kessel, D.; Korbelik, M.; Moan, J.; Peng, Q. Photodynamic therapy. *J. Natl. Cancer Inst.* **90**:889-905; 1998.

[7] Hamblin, M. R.; Newman, E. L. On the mechanism of the tumor-localizing effect in photodynamic therapy. *J. Photochem. Photobiol. B:Biol.* **23**:3-8; 1994.

[8] Konan, Y.; Gurny, R.; Allémann, E. State of the art in the delivery of photosensitizers for photodynamic therapy. *J. Photochem. Photobiol. B:Biol.* **66**:89-106; 2002.

[9] Stockert, J. C.; Juarranz, A.; Villanueva, A.; Nonell, S.; Horobin, R. W.; Soltermann, A. T.; Durantini, E. N.; Rivarola, V.; Colombo, L. L.; Espada, J.; Canete, M. Photodynamic therapy: selective uptake by photosensitising drugs into tumor cells. *Curr. Top. Pharmacol.* **8**:185-217; 2004.

[10] Boyle, R. W.; Dolphin, D. Structure and Biodistribution relationships of photodynamic sensitizers. *Photochem. Photobiol.* **64**:469-485; 1996.

[11] Kessel, D. Correlation between subcellular localization and photodynamic efficacy. *J. Porphyrins Phthalocyanines* **8**:1009-1014; 2004.

[12] Peng, Q.; Moan, J.; Nesland, J. M. Correlation of subcellular and intratumoral photosensitizer localization with ultrastructural features after photodynamic therapy. *Ultrastruct. Pathol.* **20**:109-129; 1996.

[13] Krammer, B. Vascular effects of photodynamic therapy. *Anticancer Res.* **21**:4271-4277; 2001.

[14] Gollnick, S. O.; Vaughan, L.; Henderson, B. W. Generation of effective antitumor vaccines using photodynamic therapy. *Cancer Res.* **62**:1604-1608; 2002.

[15] Korbelik, M.; Dougherty, G. J. Photodynamic therapy-mediated immune response against subcutaneous mouse tumors. *Cancer Res.* **59**:1941-1946; 1999.

[16] Korbelik, M.; Krosl, G.; Krosl, J.; Dougherty, G. J. The role of host lymphoid populations in the response of mouse EMT6 tumor to photodynamic therapy. *Cancer Res.* **56**:5647-5652; 1996.

[17] Buja, L. M.; Eigenbrodt, M. L.; Eigenbrodt, E. H. Apoptosis and Necrosis - Basic Types and Mechanisms of Cell-Death. *Arch. Pathol. Lab. Med.* **117**:1208-1214; 1993.

[18] Plaetzer, K.; Kiesslich, T.; Verwagen, T.; Krammer, B. The modes of cell death induced by PDT: an overview. *Med. Laser. Appl.* **18**:7-19; 2003.

[19] Zhou, C. N. New trends in photobiology: mechanisms of tumor necrosis induced by photodynamic therapy. *J. Photochem. Photobiol. B:Biol.* **3**:299-318; 1989.

[20] Vaux, D. L.; Strasser, A. The molecular biology of apoptosis. *Proc. Natl. Acad. Sci. USA* **93**:2239-2244; 1996.

[21] Savill, J.; Fadok, V.; Henson, P.; Haslett, C. Phagocyte recognition of cells undergoing apoptosis. *Immunol. Today* **14**:131-136; 1993.

[22] Luo, Y.; Chang, C. K.; Kessel, D. Rapid initiation of apoptosis by photodynamic therapy. *Photochem. Photobiol.* **63**:528-534; 1996.

[23] Plaetzer, K.; Kiesslich, T.; Oberdanner, C. B.; Krammer, B. Apoptosis following photodynamic tumor therapy: Induction, mechanisms and detection. *Curr. Pharm. Des.* **11**:1151-1165; 2005.

[24] Oleinick, N. L.; Morris, R. L.; Belichenko, T. The role of apoptosis in response to photodynamic therapy: what, where, why, and how. *Photochem. Photobiol. Sci.* **1**:1-21; 2002.

[25] Braslavsky, S. E.; Houk, K. N.; Verhoeven, J. W. *Glossary of terms used in photochemistry*: 1996.

[26] Foote, C. S.; Valentine, J. S.; Greenberg, A.; Liebman, J. F. e. *Active Oxygen in Biochemistry*: Blackie Academic and Professional; 1995.

[27] Wilkinson, F.; Helman, W. P.; Ross, A. B. Rate constants for the decay and reactions of the lowest electronically excited singlet state of molecular oxygen in solution. An expanded and revised compilation. *J. Phys. Chem. Ref. Data* **24**:663-1021; 1995.

[28] Moan, J. On the diffusion length of singlet oxygen in cells and tissues. *J. Photochem. Photobiol. B:Biol.* **6**:343-347; 1990.

[29] Redmond, R. W.; Kochevar, I. E. Spatially resolved cellular responses to singlet oxygen. *Photochem. Photobiol.* **82**:1178-1186; 2006.

[30] Breckenridge, D. G.; Germain, M.; Mathai, J. P.; Nguyen, M.; Shore, G. C. Regulation of apoptosis by endoplasmic reticulum pathways. *Oncogene* **22**:8608-8618; 2003.

[31] Orrenius, S.; Zhivotovsky, B.; Nicotera, P. Regulation of cell death: the calcium-apoptosis link. *Nat. Rev. Mol. Cell Biol.* **4**:552-565; 2003.

[32] Davies, M. J.; Fu, S. L.; Dean, R. T. Protein hydroperoxides can give rise to reactive free-radicals. *Biochem. J.* **305**:643-649; 1995.

[33] Pottier, R.; Truscott, T. G. The photochemistry of haematoporphyrin and related systems. *Int. J. Radiat. Biol.* **50**:421-452; 1986.

[34] Vogel, E.; Kocher, M.; Schmickler, H.; Lex, J. Porphycene: a novel porphin isomer. *Angew. Chem. Int. Ed. Engl.* **25**:257-259; 1986.

[35] Nonell, S.; Bou, N.; Borrell, J. I.; Teixido, J.; Villanueva, A.; Juarranz, A.; Canete, M. Synthesis of 2,7,12,17-tetraphenylporphycene (TPPo): first aryl-substituted porphycene for the photodynamic therapy of tumors. *Tetrahedron Lett.* **36**:3405-3408; 1995.

[36] Cañete, M.; Ortiz, A.; Juarranz, A.; Villanueva, A.; Nonell, S.; Borrell, J. I.; Teixidó, J.; Stockert, J. C. Photosensitizing properties of palladium-tetraphenylporphycene on cultured tumour cells. *Anti-Cancer Drug Des.* **15**:143-150; 2000.

[37] Cañete, M.; Lapena, M.; Juarranz, A.; Vendrell, V.; Borrell, J. I.; Teixido, J.; Nonell, S.; Villanueva, A. Uptake of tetraphenylporphycene and its photoeffects on actin and cytokeratin elements of HeLa cells. *Anti-Cancer Drug Des.* **12**:543-554; 1997.

[38] Villanueva, A.; Cañete, M.; Nonell, S.; Borrell, J. I.; Teixido, J.; Juarranz, A. Photodamaging effects of tetraphenylporphycene in a human carcinoma cell line. *Anti-Cancer Drug Des.* **11**:89-99; 1996.

[39] Canete, M.; Ortega, C.; Gavalda, A.; Cristobal, J.; Juarranz, A.; Nonell, S.; Teixido, J.; Borrell, J. I.; Villanueva, A.; Rello, S.; Stockert, J. C. Necrotic cell death induced by photodynamic treatment of human lung adenocarcinoma A-549 cells with palladium(II)-tetraphenylporphycene. *Int. J. Onc.* **24**:1221-1228; 2004.

[40] Bulina, M. E.; Chudakov, D. M.; Britanova, O. V.; Yanushevich, Y. G.; Staroverov, D. B.; Chepurnykh, T. V.; Merzlyak, E. M.; Shkrob, M. A.; Lukyanov, S.; Lukyanov, K. A. A genetically encoded photosensitizer. *Nat. Biotechnol.* **24**:95-99; 2006.

[41] Yong, P.; Timiryasova, T.; Zhang, Q.; Beltz, R.; Szalay, A. A. Optical imaging: bacteria, viruses, and mammalian cells encoding light-emitting proteins reveal the locations of primary tumors and metastases in animals. *Anal. Bioanal. Chem.* **377**:964-972; 2007.

[42] McClain, W. M. Two-photon molecular spectroscopy. *Acc. Chem. Res* **7**:129-135; 1974.

[43] Frederiksen, P. K.; Jorgensen, M.; Ogilby, P. R. Two-photon photosensitized production of singlet oxygen. *J. Am. Chem. Soc.* **123**:1215-1221; 2001.

[44] Arnbjerg, J.; Johnsen, M.; Frederiksen, P. K.; Braslavsky, S. E.; Ogilby, P. R. Two-photon photosensitized production of singlet oxygen: Optical and optoacoustic characterization of absolute two-photon absorption cross sections for standard sensitizers in different solvents. *J. Phys. Chem. A* **110**:7375-7385; 2006.

[45] Karotki, A.; Kruk, M.; Drobizhev, M.; Rebane, A.; Nickel, E.; Spangler, C. W. Efficient singlet oxygen generation upon two-photon excitation of new porphyrin with enhanced nonlinear absorption. *IEEE J. Select. Top. Quant. Electron.* **7**:971-975; 2001.

[46] Bhawalkar, J. D.; Kumar, N. D.; Zhao, C.-F.; Prasad, P. N. Two-photon photodynamic therapy. *J. Clin. Laser. Med. & Surg.* **15**:201-204; 1997.

[47] Bressler, N. M.; Bressler, S. B. Photodynamic therapy with verteporfin (visudyne): impact on ophthalmology and visual sciences. *Invest. Ophthalmol. Vis. Sci.* **41**:624-628; 2000.

[48] Fritsch, C.; Goerz, G.; Ruzicka, T. Photodynamic therapy in dermatology. *Arch. Dermatol.* **134**:207-214; 1998.

[49] Allison, R. R.; Sibata, C. H.; Downie, G. H.; Cuenca, R. E. A clinical review of PDT for cutaneous malignancies. *Photodiag. Photodyn. Ther.* **3**:214-226; 2006.

[50] Trauner, K. B.; Gandour-Edwards, R.; Bamberg, M.; Shortkroff, S.; Sledge, C.; Hasan, T. Photodynamic synovectomy using benzoporphyrin derivative in an antigen-induced arthritis model for rheumatoid arthritis. *Photochem. Photobiol.* **67**:133-139; 1998.

[51] Kelty, C. J.; Brown, N. J.; Reed, M. W. R.; Ackroyd, R. The use of 5-aminolaevulinic acid as a photosensitiser in photodynamic therapy and photodiagnosis. *Photochem. Photobiol. Sci.* **1**:158-168; 2002.

[52] Merchat, M.; Spikes, J. D.; Bertoloni, G.; Jori, G. Studies on the mechanism of bacteria photosensitization by meso-substituted cationic porphyrins. *J. Photochem. Photobiol. B:Biol.* **35**:149-157; 1996.

[53] Wainwright, M. Photoinactivation of viruses. *Photochem. Photobiol. Sci.* **3**:406-411; 2004.

Chapter 2

General Techniques and Methods

This chapter describes the common photophysical techniques and specific methods used for the determination of photophysical properties in the light-induced reaction processes involved in this work. Specific details will be described in the experimental section of each chapter.

2.1. STEADY-STATE OPTICAL TECHNIQUES

2.1.1. Absorption.

Spectra were recorded in a Varian Cary 4E spectrophotometer periodically calibrated with a holmiun oxide filter.

For the experiments performed in Prof. Ogilgy's lab at Aarhus University, spectra in the UV-VIS region were recorded using a Hewlett-Packard/Agilent model 8453 diode array spectrometer, while near-IR spectra were recorded on a Shimadzu UV-3600 spectrophotometer.

2.2.2. Transmittance.

Transmittance measurements were recorded in a Varian Cary 4E spectrophotometer equipped with a 110 mm diameter integrating sphere and a high performance photomultiplier tube. Integrating spheres have the ability to collect most reflected or transmitted radiation from turbid, translucent or opaque samples, remove any directional preferences and present an integrated signal to the detector.

2.2.3. Emission.

Emission and excitation spectra were recorded in a Jobin-Ybon Spex Fluoromax-2 spectrofluorometer, ensuring that the absorbance of the sample was less than 0.05 in the overlap region between absorption and emission to avoid inner filter effects in the measurement of fluorescence.

2.2. TIME-RESOLVED OPTICAL TECHNIQUES

The time-resolved techniques used in this work involve the observation, through absorption or emission, of excited states or other reaction intermediates generated upon pulsed-laser irradiation of a sample. The formation of a large concentration of transient species upon absorption of light produces a change in the intensity of an analyzing beam (in the case of absorption spectroscopy) or in the intensity that emerges from the sample (in the case of emission spectroscopy), which the system is able to monitor with time resolution.

2.2.1. Time-Correlated Single Photon Counting (TCSPC)

Time-Correlated Single Photon Counting is the most commonly used technique for singlet state lifetime determination. It is based on the detection of single photons of a periodical light signal, the measurement of the detection times of the individual photons and the reconstruction of the waveform from the individual time measurements. TCSPC technique makes use of the fact that for low-level, high-repetition-rate pulses, the produced light intensity is so low that the probability of detecting one photon in one signal period is less than one. Therefore, is not necessary to provide for the possibility of detecting several photons in one signal period. It is sufficient to record the photons, measure their time in the signal period, and build up a histogram of the photon times.

The principle is shown in Fig. 1:

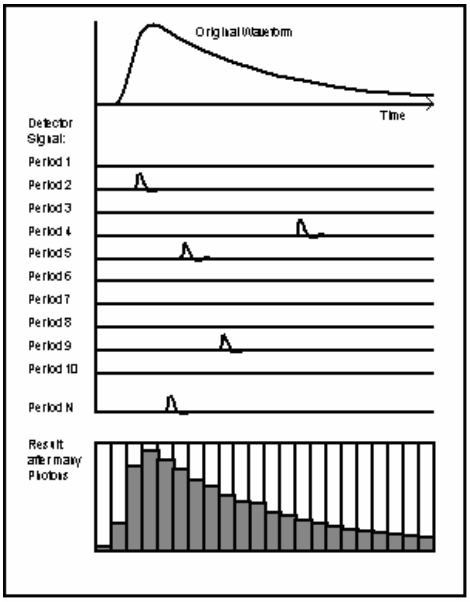

Fig. 1: schematic representation of the TCSPC technique. From [1].

In most cases, the lifetime of the sample to be measured is on the same time scale as the response function of the system. In these cases, the actual decay may be obtained by deconvolution of the measured signal using an *instrumental response function* (IRF) generated from a light scattering sample.

TCSPC experiments were carried out using a PicoQuant Fluotime 200 fluorescence lifetime system. Excitation was achieved by means of picosecond diode lasers or LEDs (PicoQuant, 10 MHz repetition rate) and the counting frequency was always below 1 %. Singlet state lifetimes were determined using the PicoQuant FluoFit data analysis software.

Methods

- **Singlet lifetime (τ_S)**

A solution of the sample in the proper solvent was prepared ensuring that the absorbance of the sample was less than 0.05 in the overlap region between absorption and emission to avoid inner filter effects. The deconvolution of the TCSPC fluorescence signal with the IRF signal from a light scattering sample yields the singlet lifetime.

2.2.2. Time-resolved NIR phosphorescence detection (TRPD)

This technique is commonly used for monitoring the formation and decay of singlet oxygen ($^1O_2$ or $O_2(a^1\Delta_g)$), the measurement of its lifetime (τ_Δ) and its quantum yield of formation (Φ_Δ) [2]. It is based on the detection of the weak $O_2(a^1\Delta_g)$ phosphorescence, centred at 1270 nm. In this work, singlet oxygen detection in time-resolved mode has been achieved upon either one-or two-photon excitation of the photosensitiser. For one-photon excitation, detection of singlet oxygen phosphorescence has been carried out in both analogic and photon counting mode. A detailed comparison between these two approaches is given in Chapter 3.

2.2.2.1. One-photon excitation

Analog Mode. In a time-resolved NIR phosphorescence experiment the 2nd or 3rd harmonic of a Continuum Surelite Nd:YAG laser was used for either sample excitation or pumping an OPO for tunability. In order to block NIR background radiation from the excitation source, a KG-5 filter (CVI Laser Corporation, ALburquerque, USA) was placed at the exit port of the laser. A Si photodiode (Laser-Optotronic BPX 65) was used to trigger the system and the energy of the beam was measured by means of a

pyroelectric energy meter (RJP 735 and RJP) from laser Precisition Corp. The $O_2(a^1\Delta_g)$ phosphorescence was detected at 90º with an liquid-nitrogen cooled germanium diode (North-Coast, EO-817P, time response ~250 ns) behind a cut-off silicon filter at 1050 nm and an interference filter at 1270 nm to prevent fluorescence from reaching the detector. The output of the detector was transferred to a Lecroy 9410 oscilloscope and then stored in a PC. The signals were analysed with the home-developed FitLabWindows software.

The laser set-up used for these experiments is shown in Fig. 2:

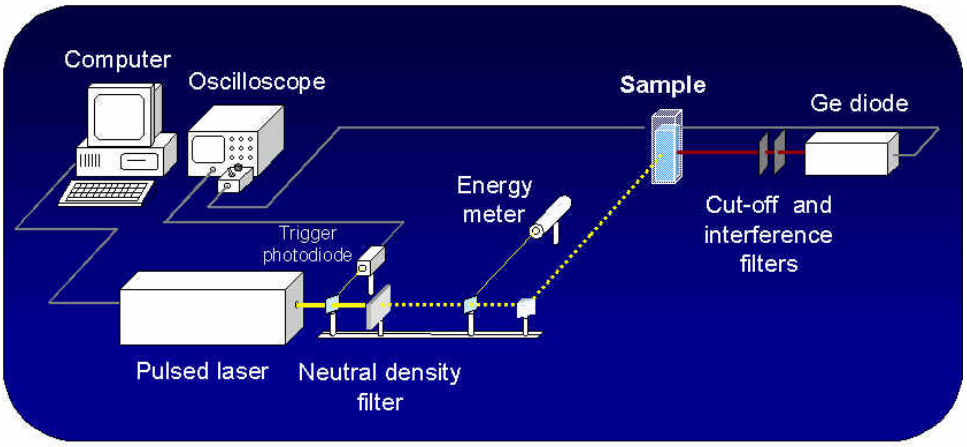

Fig. 2: Experimental set-up for time-resolved phosphorescence detection in analogic mode.

Photon Counting Mode. The singlet oxygen spectrophotometer used is based on the Picoquant Fluotime 200 fluorescence lifetime system which has been subject to the following modifications: (1) A diode-pumped solid-state Q-switched Nd:YAG laser (CryLas, FTQ355-QS) is used for excitation. This laser works at 10 kHz repetition rate, producing *ca.* 1 ns pulsewidth laser pulses at either 355 nm (5 mW, 0.5 μJ per pulse) or at 532 nm (12 mW, 1.2 μJ per pulse). (2) The original single-grating monochromator was replaced by a dual grating one, which allows extending its dispersion range from 200 to 2000 nm. A flip mirror is used to direct the dispersed light beam either to the visible or to near-IR detector ports. (3) A TE-cooled Hamamatsu near-IR photomultiplier (model H9170-45), sensitive from 950 to 1400 nm, is used to detect the weak $O_2(a^1\Delta_g)$ phosphorescence. (4) The output of the PMT is sent to a mutichannel scaler (Becker and Hickl, model MSA300). In order to block NIR background radiation from the excitation source, a KG-5 filter (CVI Laser Corporation, ALburquerque, USA) is placed at the exit port of the laser. Likewise, a cold mirror (Edmund Scientific, Barrington, USA) is placed at the entry port of the dual grating monocromator to prevent any visible radiation form reaching the detector. Data was processed using PicoQuant's FluoFit software.

2.2.2.2. Two-photon excitation

Photon Counting Mode. This technique has been used at Prof. Peter R. Ogilby's group in the Chemistry Department of the University of Århus in Denmark. All experiments were performed using a femtosecond (fs) excitation source and optical detection apparatus that have been described in detail elsewhere [3,4]. Briefly, the output of a Ti:sapphire laser (Spectra Physics, Tsunami 3941) was regeneratively amplified (Spectra Physics, Spitfire), resulting in tunable fs pulses over the wavelength range ~765-850 nm. In addition, an optical parametric amplifier (Spectra Physics, OPA-800CF) pumped by the Spitfire delivered fs pulses that could be tuned over the range 300-3000 nm. For the present experiments, the laser polarization at the sample was linear, and the spectral output characteristics were measured using a fiberoptic spectrometer (Avantes AVS-USB2000). The laser power was controlled by adjusting a Glan-Taylor polarizer, and for experiments performed at 1100 nm a long-pass filter (Schott, 830 nm cut-off) was inserted to eliminate higher harmonics from the OPA and residuals from the Spitfire pump beam. For all experiments, the pulse repetition rate was 1 kHz. Typical peak intensities of the irradiating laser were 1-10 GW/cm^2, with a pulse duration of ~ 120 fs and laser beam waist of ~ 500 μm.

The sample was contained in a 1 cm path length quartz cuvette mounted in a light-tight housing with a small entrance hole for the laser beam. Singlet oxygen phosphorescence from the sample was collected and focused onto the active area of an IR photomultiplier tube, PMT (Hamamatsu model R5509-42). The 1270 nm phosphorescence of singlet oxygen was spectrally isolated using an interference filter (Barr Associates, 50 nm fwhm). The output of the PMT was amplified (Stanford Research Systems model 445 preamplifier) and sent to a photon counter (Stanford Research Systems model 400), operated using a program written in LabView (National Instruments, Inc.).

The experimental set-up used for these experiments is shown in Fig. 3:

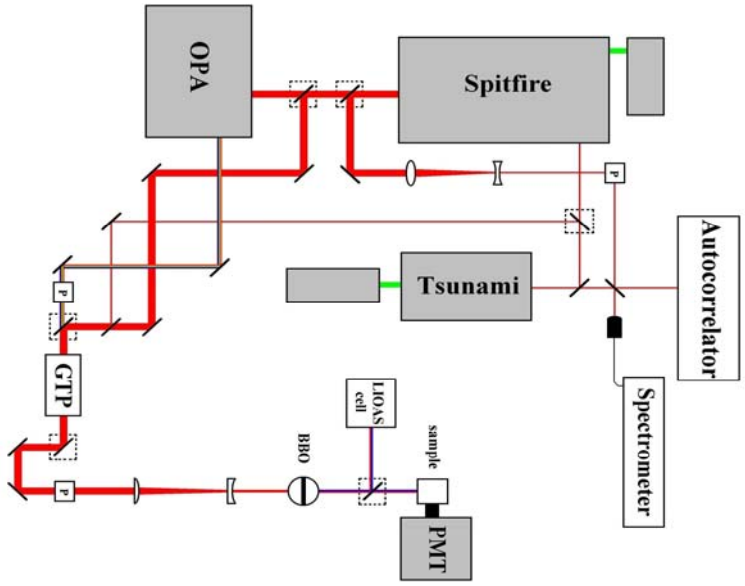

Fig. 3: Experimental set-up for two-photon time-resolved phosphorescence detection.

Methods

- **$O_2(a^1\Delta_g)$ lifetime (τ_Δ)**

Singlet oxygen lifetime was obtained by fitting Eq. 1 to the signal detected at 1270 nm,

$$S(t) = S(0) \cdot \frac{\tau_\Delta}{\tau_T - \tau_\Delta} \cdot \left(e^{-t/\tau_T} - e^{-t/\tau_\Delta} \right) \qquad (1)$$

where *S(0)* is the zero-time amplitude of the signal and τ_T and τ_Δ are the actual lifetimes of the photosensitiser triplet state and singlet oxygen, respectively.

- **Quantum yield of $O_2(a^1\Delta_g)$ formation (Φ_Δ)**

The quantum yield of singlet oxygen photosensitisation is defined as the number of photosensitized $^1O_2$ molecules *per* absorbed photon. The pre-exponential factor *S(0)*, which is proportional to Φ_Δ, was determined by fitting Eq. 1 to the time-resolved phosphorescence intensity at 1270 nm. The quantum yields of $^1O_2$ production were determined from the comparison of S(0) to that produced by an optically matched reference in the same solvent and at the same excitation wavelength and intensity (Eq. 2) [2].

$$\Phi_\Delta(sample) = \frac{S(0)_{sample}}{S(0)_{ref}} \cdot \Phi_\Delta(ref) \qquad (2)$$

- **Two-photon absorption cross sections**

To obtain two-photon parameters from a given molecule, the intensity of $O_2(a^1\Delta_g)$ phosphorescence produced by that molecule was compared to that produced by a standard in the same conditions. For the experiments performed over the wavelength range 750 - 850 nm, 2,5-dicyano-1,4-bis(2-(4-diphenyl-aminophenyl)-vinyl)-benzene, CNPhVB, was used as standard because its two-photon absorption spectrum and absolute values of its absorption cross section, δ, are reported in the literature [3]. For the experiments performed at 1100 nm, TPP was used as the reference molecule. As the experiments were performed under identical conditions, it was not necessary to characterize the temporal and spatial properties of the laser beam at each excitation wavelength.

Values for the two-photon absorption cross section at a given wavelength, λ, were obtained through the use of Eq. 3:

$$\delta(\lambda) = \frac{S(\lambda)\Phi_{\Delta,r}C_r P_r^2}{S_r(\lambda)\Phi_\Delta C P^2}\delta_r(\lambda) \qquad (3)$$

where the subscript *r* refers to the reference compound, with *S*, *P*, *C* and Φ_Δ being the observed $O_2(a^1\Delta_g)$ signal, irradiation power at the sample, sensitizer concentration and singlet oxygen quantum yield, respectively.

- **Two-photon absorption spectrum**

The plot of the δ values, obtained upon two-photon irradiation of the sensitizers in incremental wavelength steps of 10 nm, *vs* wavelength yield the two photon absorption spectrum.

2.3. CELL CULTURE

2.3.1. Cell Lines

Human skin fibroblast cells (Foreskin cells, ATCC CRL-1635) were cultured at 37 ºC in a humidified sterile atmosphere of 95% air and 5% CO2, using DMEM supplemented with fetal calf serum (10% v/v), glucose (4.5 g/l), *L*-glutamine (292 mg/l) and streptomycim sulphate (10 mg/l) and potassium penicillin (10000 U/l). Human skin fibroblast cells were maintained frozen in DMEM with 10% DMSO. 1.8 ml CryoTubesTM (Nunc, Nalge Nunc Interational, IL, USA) were filled with the cellular suspension and were placed in a cell Cryo 1ºC Freezing Container (Nalgene, Nalge Nunc International, IL, USA) to be frozen slowly down to -80 ºC at a cooling rate of -1ºC/min for successful cell cryopreservation. Frozen cells were rapidly transferred to a liquid nitrogen container (-196ºC) and stored. Skin fibroblasts are adherent cells which grow up to form cellular monolayers toward confluence after inoculation.

Human skin fibroblasts were seeded in 75 cm^2 tissue culture flasks (Techno Plastic Products, Trasadingen, Switzerland) and were cultured toward 80-85% confluence in order to control the uptake of porphyrins by the cells

2.3.2. Dark toxicity

The photosensitizers' effect on cell viability in the absence of light was determined by the MTT colorimetric assay [5].This assay detects living but not dead cells and it is based on the reduction of a tetrazolium salt to form a formazan dye. The electrons required for this process are given by the mitochondrion of the viable cells.

Method

Human skin fibroblasts were seeded in 96-well plates and cultured until 80-85% confluence. They were then incubated in the dark with 1 to 100 μM photosensitizer concentration from 20 minutes to 24 hours. After washing with PBS, 200 μl of DMEM containing 2 mg MTT/ml were added to each well. After 1 hour incubation in the dark at 37ºC, the MTT solution was replaced by 100 μl DMSO. The plate was finally vortexed for 15 min on a shaker and the absorbance at 550 nm was read on a microplate reader (ELISA System MIOS, Merck). Experiments were performed in triplicate using Eq. 4:

$$\%\,\text{cell viability} = \frac{Abs_{\text{sample}} - Abs_{\text{backgr}}}{Abs_{\text{control}} - Abs_{\text{backgr}}} \times 100 \qquad (4)$$

where Abs_{sample}, Abs_{backgr} and $Abs_{control}$ refer to the absorbance of the sample, background (wells without cells) and control (wells with cell but without photosensitizer), respectively.

2.3.3. Photosensitizer uptake and quantification

The uptake of the studied photosensitizers by skin human fibroblasts was determined by fluorescence spectroscopy.

Method

An appropriate number of human skin fibroblasts cells were seeded in 75 cm^2 tissue culture flasks and were cultured toward 80-85% confluence. Cells were then incubated in the dark with 10 ml of medium containing 1, 10 or 100 μM concentration of the photosensitizer and for different times ranging from 30 minutes to 24 hours. Afterwards, the medium was discarded and the cells were washed three times with PBS, trypsinized with PBS containing 0.2% trypsin and 0.5 mM EDTA, and resuspended in 700 μl of 2% sodium dodecyl sulphate (SDS) in PBS. The resulting suspension was kept for 20 minutes in the dark at room temperature and centrifuged at 10000 rpm for 10 minutes. The extent of photosensitizer uptake was then assessed by comparison of its fluorescence in this supernatant to that of standard solutions under the same conditions. The fluorescence intensity values obtained for each sample were normalized by the total number of cells in the suspension to correct for variations between samples. Each experiment was repeated twice.

2.3.4. Subcellular localisation

The distribution of photosensitizer within the cells was assessed by fluorescence microscopy.

Method

The cells were grown on glass slides, incubated in the dark as described above, washed three times with PBS cooled at 4 ºC and studied for less than 5 minutes to avoid photobleaching. The cells were studied using a fluorescence microscope (Leika DMIRB, Germany) equipped with a high pressure xenon lamp, a 515-560 nm bandpass filter for green excitation, and a dichroic mirror (580 nm), a cut-on red filter (590 nm) and magnification objectives (x10, x20) for red detection. Photographs were acquired

and analysed by means of a personal computer-controlled Leika camera supplied with Axiovision 3.0 image capture and specific software analysis (Leika DMIRB, Germany).

2.3.5. Spectroscopic measurements in cell suspensions

Spectroscopic measurements were recorded on the systems previously described. Cell suspension samples were prepared using the following method.

Method

An appropriate number of cells were seeded in 75 cm^2 tissue culture flasks and were cultured toward 80-85% confluence. They were then incubated in the dark with the desired amount of photosensitizer for a given period of time. The medium was discarded and the cells were washed three times with PBS, trypsinized and resuspended in PBS to a final concentration of ~50 x 10^6 cells/ml. Measurements were then performed within the following 45 minutes and cell suspensions were continuously stirred.

2.4. REFERENCES

[1] Becker, W. *Advanced Time-Correlated Single Photon Counting Techniques*: Germany: Springer; 2005.

[2] Nonell, S.; Braslavsky, S. E. Time-resolved singlet oxygen detection. In: *Methods in Enzymology:* San Diego: Academic Press; 2000.

[3] Arnbjerg, J.; Johnsen, M.; Frederiksen, P. K.; Braslavsky, S. E.; Ogilby, P. R. Two-photon photosensitized production of singlet oxygen: Optical and optoacoustic characterization of absolute two-photon absorption cross sections for standard sensitizers in different solvents. *J. Phys. Chem. A* **110**:7375-7385; 2006.

[4] Frederiksen, P. K.; McIlroy, S. P.; Nielsen, C. B.; Nikolajsen, L.; Skovsen, E.; Jorgensen, M.; Mikkelsen, K. V.; Ogilby, P. R. Two-photon photosensitized production of singlet oxygen in water . *J. Am. Chem. Soc.* **127**:255-269; 2005.

[5] Mosmann, T. Rapid colorimetric assay for cellular growth and survival: application to proliferation and cyto-toxicity assays. *J. Immunol. Meth.* **65**:55-63; 1983.

Chapter 3

Photon-Counting *vs*. Analog Time-Resolved Singlet Oxygen Phosphorescence Detection

Two recent advances in optoelectronics, namely novel near-IR sensitive photomultipliers and inexpensive yet powerful diode-pumped solid-state lasers working at kHz repetition rate, enable the time-resolved detection of singlet oxygen ($O_2(a^1\Delta_g)$) phosphorescence in photon-counting mode, thereby boosting the time-resolution, sensitivity, and dynamic range of this well-established detection technique. Principles underlying this novel approach and selected examples of applications are provided in this chapter, which illustrate the advantages over the conventional analog detection mode.

The work described in this chapter is derived from the lecture given at the X School of Pure and Applied Biophysics "Time-resolved spectroscopic methods in biophysics" held in Venice in January 2006. It is submitted for publication in *Photochem. Photobiol. Sci.*

3.1. INTRODUCTION

The lowest electronic excited state of molecular oxygen, singlet oxygen or $O_2(a^1\Delta_g)$, is a non-radical, highly-reactive oxidising species (ROS) that is produced very often in chemical [1], enzyme [2] or photochemical reactions [3]. Photosensitised $O_2(a^1\Delta_g)$ production is indeed a very general process that results from the interaction of a light-activated molecule, referred to as the photosensitiser, with ambient molecular oxygen. It is also a most convenient method to create a controlled population of $O_2(a^1\Delta_g)$ molecules in a system under study. Thus, the electronically-excited states of the photosensitiser, particularly the longer-lived triplet state, are efficiently quenched by molecular oxygen, energy transfer between the two species resulting in the production of $O_2(a^1\Delta_g)$:

$$\begin{aligned} \text{sens} + h\nu &\rightarrow {}^1\text{sens}^* \\ {}^1\text{sens}^* &\rightarrow {}^3\text{sens}^* \\ {}^3\text{sens}^* + {}^3\text{O}_2 &\rightarrow \text{sens} + \text{O}_2(a^1\Delta_g) \end{aligned}$$

$O_2(a^1\Delta_g)$ is a strong electrophile and thus reacts readily with electron-rich substrates such as unsaturated hydrocarbons, phenols, amines or sulfides [4]. This is relevant for biological systems because such reactive substrates are ubiquitous in membrane lipids, proteins, and DNA [5-8]. Not surprisingly, $O_2(a^1\Delta_g)$ plays a major role in several biomedical and biological processes ranging from photodynamic therapy (PDT)[9] to plant defense [10], where it is being increasingly regarded as a signaling species [11-13]. $O_2(a^1\Delta_g)$ can also be deactivated by physical interactions with surrounding molecules. In non-reactive systems, such interactions are the major deactivation mode for $O_2(a^1\Delta_g)$ and ultimately determine its lifetime, which ranges from 3.3 μs in neat water to hundreds of milliseconds in the gas phase [14]. A minor fraction of $O_2(a^1\Delta_g)$ molecules decays by emitting a photon at *ca.* 1270 nm (Fig. 1). The quantum yield of such emission is extremely low, ranging from 10^{-5} to 10^{-7} depending on its environment [15]. Nevertheless, the time-resolved detection of $O_2(a^1\Delta_g)$ phosphorescence (TRPD) is regarded as the most direct and specific means for monitoring this species, with the added benefit of providing information about the kinetics of its production and decay.

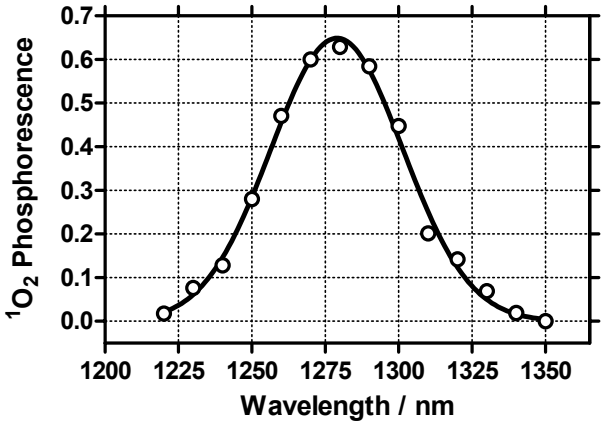

Fig.1: Near-infrared phosphorescence spectrum of $O_2(a^1\Delta_g)$.

TRPD is typically accomplished by coupling a near-IR sensitive detector to a conventional laser flash photolysis system. With minor variations, the set-up uses a pulsed laser for excitation, working at 1-25 Hz repetition rate and delivering millijoules pulses of 1-20 ns pulse duration. The emission arising from the sample is monitored at 90 degrees through either a monochromator or a combination of long-pass and interference filters, which block the excitation wavelengths and isolate the $O_2(a^1\Delta_g)$ phosphorescence. The conditioned emission is detected in analogue mode using either a germanium or indium-gallium arsenide photodiode and recorded using a digital oscilloscope [16]. This approach has been around for almost three decades and has provided most of the $O_2(a^1\Delta_g)$ data underpinning the current understanding of this intermediate species. Despite a long list of successes, analog optical techniques suffer from a number of problems (*vide infra)*, which have limited the detection of $O_2(a^1\Delta_g)$ in biological samples in a time-resolved manner. The remarkable evolution of optolectronics over the last few years makes now possible to overcome such difficulties. Specifically, the availability of near-infrared photomultiplier tubes (PMTs), in conjunction with inexpensive diode-pumped high-repetition pulsed lasers, allows the detection of $O_2(a^1\Delta_g)$ phosphorescence in photon counting mode, improving the time resolution and sensitivity of $O_2(a^1\Delta_g)$ detection. This concept was pioneered in the early nineties by Egorov *et al.* using a custom-made PMT [17]. With the recent advent of commercially-available near-IR PMTs, a number of laboratories are rapidly adopting it [18-24]. In this chapter, the two approaches are compared and examples that illustrate the advantages of the photon counting technique over the analog mode for $O_2(a^1\Delta_g)$ detection are discussed.

3.2. EXPERIMENTAL SECTION

***Materials*:** 1,4-diazabicyclo[2.2.2]octane (DABCO) purchased from Aldrich, as well as platinum(II)-2,3,7,8,12,13,17,18-octaethyl-21*H*,23*H*-porphine (PtOEP) from Frontier Scientific, were used as received. Palladium(II)-2,7,12,17-tetraphenylporphycene (PdTPPo) were synthesised as described elsewhere [25]. Toluene of spectroscopic grade were purchased from Solvents Documentation Syntheses (SDS).

3.3. SPECTROPHOTOMETER DESIGN

A. Overview of photon counting techniques. Photon counting detection arises naturally from the response of photomultiplier tubes to detected photons, as the intrinsic response of a PMT to a photon striking its surface is a pulse of electrical current. There are basically three main photon counting techniques for time-resolved measurements: *gated photon counting* (GPC), *multichannel scaling* (MCS)*, and time-correlated single photon counting* (TCSPC). The reader is referred to recent books for a thorough in-depth discussion [26,27]. Only a brief summary is presented here.
In TCSPC, only one photon, the first one striking the detector, is counted *per* laser shot. This approach provides the most accurate timing of the photon among all photon counting techniques, down to a few ps per channel. Thus, TCSPC is the technique of choice when time resolution is the prime need, at the expense of a much longer acquisition times in order to build the complete signal profile.

In GPC, all pulses in a pre-set time window above a minimum threshold are counted. Repeating the measurements at different time delays allows building up the waveform. Gated photon counting is used to select only a portion of the total emitted photons. A typical application is to discriminate between prompt and delayed emissions, *e.g.*, fluorescence from phosphorescence, or to remove light scattering after excitation. The main disadvantage of GPC is, again, that it does not count all detected photons but only those within the gate. The minimum gate width is currently ~ 500 ps. Reconstruction of the signal's time profile requires repeating the acquisition at several delays between excitation and the counting window, which results in long acquisition times.

MCS finally can be viewed as a multi-gated photon counting in which **all** detected photons are counted and sorted out in the different positions of the board memory. The time distribution of all detected photons is thus obtained at once. The time resolution of the technique is given by the memory speed and is currently *ca.* 1 ns/channel, enough for

$O_2(a^1\Delta_g)$ applications (*vide infra*). Fig. 2 gives a pictorial representation of the three techniques.

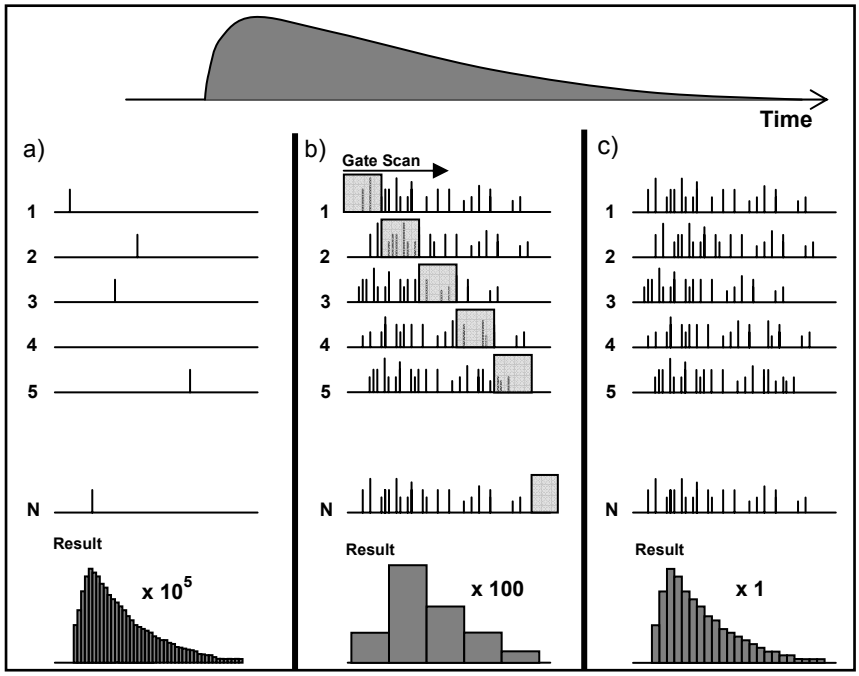

Fig 2: A pictorial representation of (a) time-correlated single photon counting (b) gated photon counting (GPC), and (c) multichannel scaling (MCS). Each row represents the outcome of a single experiment, *i.e.*, a single laser shot. The full shape of the signal could be recovered in a single experiment using the MCS. In TCSPC, (only) one count is obtained generally every 100 experiments. The waveform intensity (*i.e.* histogram height) may be orders of magnitude smaller than that obtained using MSC with an equivalent number of shots. This is the slowest technique for building up the count histogram, but the time resolution can be as high as 1 ps, *i.e.*, 1000-fold better than with MCS. In GPC, the position of the gate must be varied to reconstruct the time profile. The resulting waveform amplitude is, in comparison to MCS, 10- to 1000-fold lower.

Given the considerations above, what is then the best option for photon-counting time-resolved $O_2(a^1\Delta_g)$ phosphorescence detection? GPC detection makes reconstruction of the time profile a tedious task, as the time gate must be scanned. The smaller the gate width, the larger the number of aquisition cycles necessary to reconstruct the whole signal. Likewise, disregarding all photons but one, at most, in TCSPC makes data acquisition unnecessarily long, as there is hardly a need for picosecond time resolution in $O_2(a^1\Delta_g)$ experiments. With emission quantum yields in the 10^{-5}-10^{-7} range, NIR PMTs 20-fold noisier than visible PMTs, and kinetics in the ns-μs range, the best option for $O_2(a^1\Delta_g)$ detection is currently MCS.

B. Emission optics. Two fundamentally different approaches can be used for conditioning the emission signal before sensing it with the detector. The use of a monochromator allows to spectrally resolve the luminescence arising from the sample at

the expense of signal intensity, and therefore of sensitivity. Alternatively, the use of band pass and interference filters provides the highest throughput at the expense of spectral resolution. There are situations which may favour either approach, hence it is not possible to make a single recommendation.

C. Choosing the detector. Currently, Hamamatsu is the only manufacturer marketing NIR PMTs. For the purpose of $O_2(a^1\Delta_g)$ detection, only the series R5509 and H10330 need to be considered, as the high speed of the R3809U NIR microchannel plate provides no advantage for the measurement of lifetimes in the nano- and microsecond time range.

The R5509 family offers two models, the R5509-43 and the R5509-73, corresponding to photocathodes with spectral response ranging from 300 nm to 1.4 μm or to 1.7 μm, respectively. Alternatively, the H10330 series is a family of compact NIR-PMT modules with a convenient internal thermoelectric cooler that eliminates the need for liquid nitrogen and cooling water of the R5509 family. Due to the substrate material (InP) of their transmission-type photocathode, the spectral sensitivity range starts at 950 nm. The longest detectable wavelength is determined by the cathode material itself as follows 1.2 μm (H10330-25), 1.4 μm (H10330-45) and 1.7 μm (H10330-75).

PMTs sensitive up to 1.2 μm are inadequate for $O_2(a^1\Delta_g)$ phosphorescence detection as it peaks at 1270 nm. On the other hand, extending the spectral range to 1.7 μm increases the dark count rate by one order of magnitude in both PMT series, deteriorating the sensitivity of the photon counting system. Therefore, the PMTs R5509-43 and H10330-45 are currently the most suitable ones for $O_2(a^1\Delta_g)$ phosphorescence detection purposes.

In comparing both PMTs, the dark count levels are basically the same, therefore other parameters must be taken into account for making a purchase decision. The most remarkable features of the H10330-45 are its faster time response and the convenience of thermoelectric cooling. The transit time spread (TTS), defined as the time between the absorption of a photon at the photocathode and the output pulse from the anode, is also an advantage: 300 ps for the H10330-45 *vs.* 1.5 ns for the R5509-43. Likewise, the rise time is ~3-fold faster for the H10330-45 (900 ps) than for the R5509-43 (3 ns). Thus, convenience and time resolution point to the H10330-45 PMT as the detector of choice for the dedicated detection of $O_2(a^1\Delta_g)$. On the other hand, the R5509-43 shows a wider spectral response, which may be advantageous for detection of the sensitiser's phosphorescence at the expense of lower time resolution and a less comfortable system to work with.

D. The laser excitation source. Photon counting requires that the individual photons remain distinguishable in the detector output. It is therefore convenient to use lasers delivering energy pulses in the microjoule range to avoid overloading the PMT. In order to reduce the long acquisition times derived from such low-energy laser pulses, high repetition rates are required, the upper limit being given by the inherent $O_2(a^1\Delta_g)$ lifetime, τ_Δ. In order to collect a whole $O_2(a^1\Delta_g)$ signal in biological systems, a time window up to 100 μs is the largest one can need, for which lasers working at 10 kHz repetition rate are best suited.

A typical experimental set-up for time- and spectrally-resolved phosphorescence detection in photon-counting mode is depicted in Fig. 3:

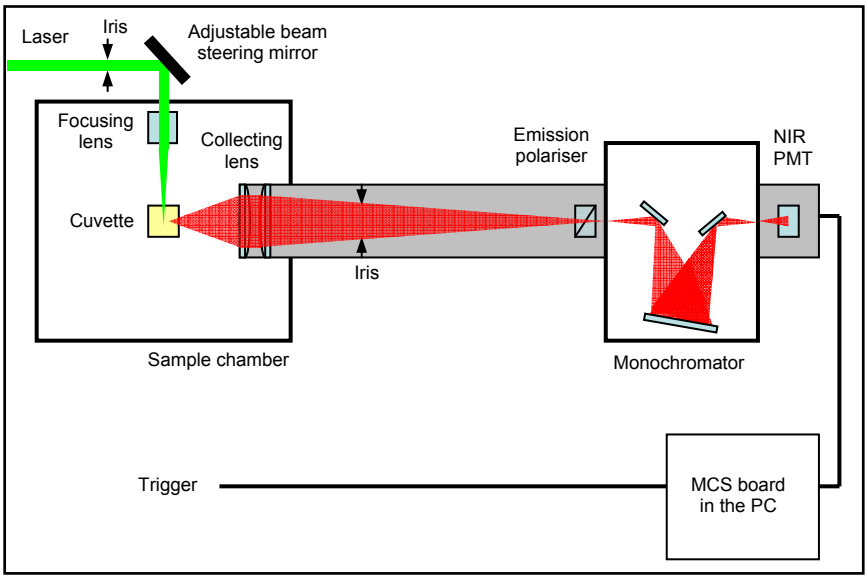

Fig 3: Experimental set-up for the photon-counting time-resolved $O_2(a^1\Delta_g)$ phosphorescence detection.

3.4. ANALOG *vs.* DIGITAL DETECTION: A COMPARISON.

Over the last three decades, much has been learnt about analog time-resolved detection of $O_2(a^1\Delta_g)$ phosphorescence, and the limitations and pitfalls of this approach are now well understood. Three main problems have been identified: (i) lack of time resolution, which precludes obtaining kinetic information in the submicrosecond time range; (ii) lack of sensitivity, which precludes the accurate determination of singlet oxygen production quantum yields below 0.01; and (iii) interference of spurious signals such as sensitiser fluorescence or scattered laser light, which result in “spikes” at the earlier part of the signal that mask $O_2(a^1\Delta_g)$ phosphorescence, particularly when its lifetime is only a few microseconds as in aqueous solvents or even create malfunctions

of the detection system. The following sections address these problems and show how the photon counting approach can be successfully used to overcome them.

A. Time resolution: what is the minimum lifetime that can be measured with analog and photon counting techniques? The lifetime of $O_2(a^1\Delta_g)$ in a particular environment is limited by the presence of physical and chemical quenchers [28]. To the best of our knowledge, the shortest $O_2(a^1\Delta_g)$ lifetime reported to date from analog phosphorescence data is 209 ns, which was obtained by the group of Schmidt using a 3 mm germanium photodiode [29]. As shown in Fig. 4, this value is comparable to the full width at half maximum (FHWM) of the response function of a typical germanium diode (*ca.* 350 ns); hence, even using deconvolution techniques, $O_2(a^1\Delta_g)$ lifetimes below this value can hardly be measured with germanium photodiodes. The use of smaller diodes would improve the time resolution [30], but the cost in sensitivity is unacceptable for most applications. In contrast, the FHWM of the new near-IR photomultipliers is *ca.* 2 ns working in analog mode. When used in photon counting mode, the time resolution is better described by the transit-time-spred (TTS), and is as low as 300 ps for these PMTs. Combined with a 1-ns pulsewidth laser, the FHWM of our instrument's response function (IRF) is *ca.* 7 ns, still 2 orders of magnitude faster than the typical germanium photodiodes (Fig. 4).

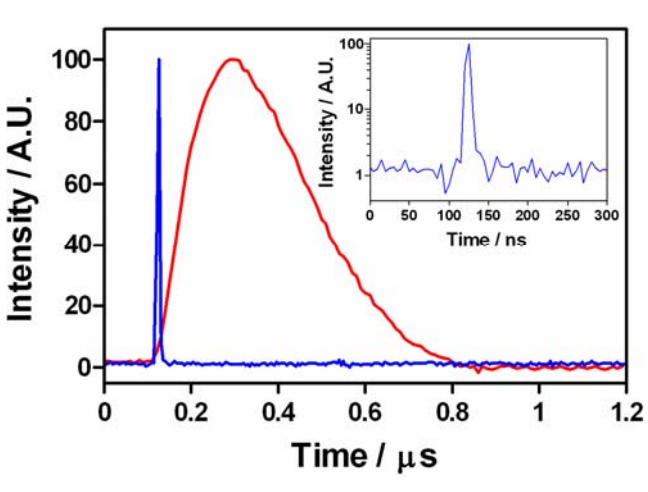

Fig 4: Instrument response function (IRF) recorded with the Hamamatsu H9170-45 PMT (the predecessor of H10330-45 PMT) in photon counting mode (blue) and with the NorthCoast EO-817P Ge diode in analog mode (red). **Inset**: detail of the IRF of the PMT.

In a triplet-photosensitized experiment, the time profile of O_2 ($^1a\Delta_g$) phosphorescence, S_t, is given by Eq. (1) [16]:

$$S_t = A \cdot \left(e^{-t/\tau_1} - e^{-t/\tau_2} \right) \qquad (1)$$

where *A* is an empirical cosntant and τ_1 and τ_2 are the lifetimes of the decay and rise components of the signal, respectively. S_t is proportional to the $O_2(a^1\Delta_g)$ concentration, $[O_2(a^1\Delta_g)]$, as given by Eq. (2) [16]:

$$[O_2(a^1\Delta_g)]_t = [^3\text{sens}^*]_0 \times \frac{k_\Delta^{O_2} \cdot [^3O_2]}{k_d^T + k_q^{O_2} \cdot [^3O_2]} \times \frac{\tau_\Delta}{\tau_T - \tau_\Delta} \times \left(e^{-t/\tau_T} - e^{-t/\tau_\Delta}\right) \qquad (2)$$

where $k_\Delta^{O_2}$ is the rate constant for $O_2(a^1\Delta_g)$ production, k_d^T is the rate constant for the sensitiser's triplet-state decay by oxygen-independent pathways, $k_q^{O_2}$ is the rate constant for oxygen quenching of the sensitiser's triplet state, τ_T is the actual lifetime of the photosensitiser triplet-state ($1/\tau_T = k_d^T + k_q^{O_2} \cdot [^3O_2]$), and τ_Δ is the actual $O_2(a^1\Delta_g)$ lifetime. According to Eq. (2), the $[O_2(a^1\Delta_g)]$ is zero at time t = 0, then grows to a maximum, and finally decays back to zero. The factor $\tau_\Delta/(\tau_T - \tau_\Delta)$ implies that the signal rises with the fastest of the two lifetimes, either τ_T or τ_Δ. In most air-equilibrated neat solvents $\tau_T < \tau_\Delta$ and the *natural* observation is made that the $O_2(a^1\Delta_g)$ phosphorescence grows with the triplet lifetime and decays with the $O_2(a^1\Delta_g)$ own lifetime.

Conversely, under conditions of very strong quenching or low oxygen availability, the counterintuitive observation is made that $O_2(a^1\Delta_g)$ grows with its own lifetime and decays with the lifetime of its precursor, the sensitiser's triplet state (*i.e.*, $\tau_1 = \tau_\Delta$ and $\tau_2 = \tau_T$ in Eq. (1)) [31]. Thus, the unambiguous assignment of τ_1 and τ_2 requires that the triplet lifetime τ_T be determined independently, *e.g.* by transient absorption or by phosphorescence spectroscopy.

Fig. 5 shows the luminescence signals recorded from an air-saturated solution of the photosensitiser platinum(II)-2,3,7,8,12,13,17,18-octaethyl-21*H*,23*H*-porphine, PtOEP, in toluene in the presence of 0.18 M DABCO, a well-known singlet oxygen quencher [28] (k_q = 2.2 x 10^8 $M^{-1}s^{-1}$). Porphine derivatives are well-known, highly efficient $O_2(^1\Delta_g)$ photosensitisers, whose strong phosphorescence provides a convenient means for monitoring their triplet state [32]. Reconvolution fitting of Eq. (1) to the signal at 1275 nm gives two lifetimes τ_1 = 173 ns and τ_2 = 24 ns. When the emission is observed at 645 nm, the wavelength for PtOEP phosphorescence [32], the signal is found to decay monoexponentially with lifetime τ_T = 175 ns. Thus, the lifetime of $O_2(a^1\Delta_g)$ is τ_Δ = 24 ns in our system, which is one order of magnitude below the shortest lifetime ever reported for this reactive oxygen species [29].

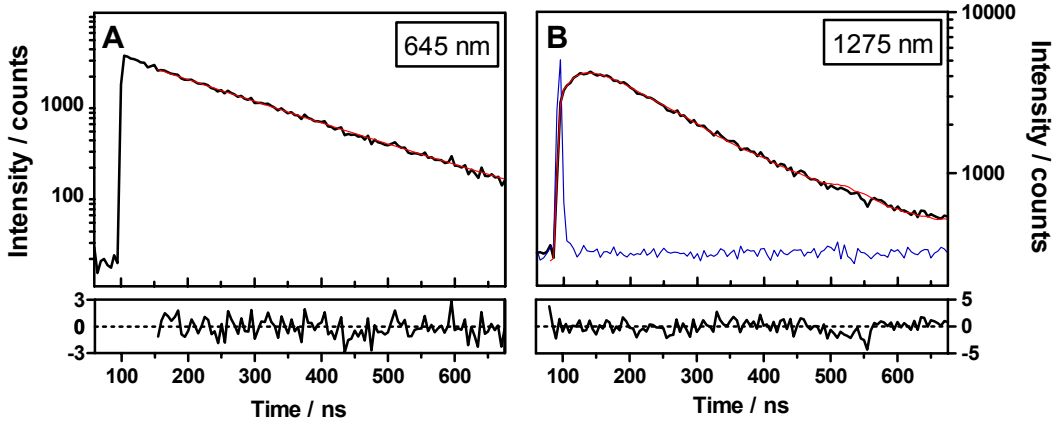

Fig. 5: Phosphorescence of PtOEP solutions in air-saturated toluene containing 0.18 M DABCO, **A:** PtOEP phosphorescence at 645 nm (black). Tail fitting (red) gives τ_T = 175 ns; λ_{exc} = 375 nm. **B:** $O_2(a^1\Delta_g)$ phosphorescence at 1275 nm (black) and instrument response function (blue). Deconvolution fitting (red) gives τ_1 = 173 ns and τ_2 = 24 ns; λ_{exc} = 532 nm.

As a further proof of the validity of the lifetime determinations, the function $\tau_\Delta^0/\tau_\Delta$ is plotted *vs* [DABCO] in Fig. 6. $\tau_\Delta^0/\tau_\Delta$ is expected to increase linearly with [DABCO] according to $\tau_\Delta^0/\tau_\Delta = 1 + k_q^{DABCO}$ [DABCO] [28]. The slope of the straight line is therefore k_q^{DABCO} = (2.3 ± 0.2) x 10^8 $M^{-1}s^{-1}$, in excellent agreement with the rate constant found in literature, k_q = 2.2 x 10^8 $M^{-1}s^{-1}$ [28].

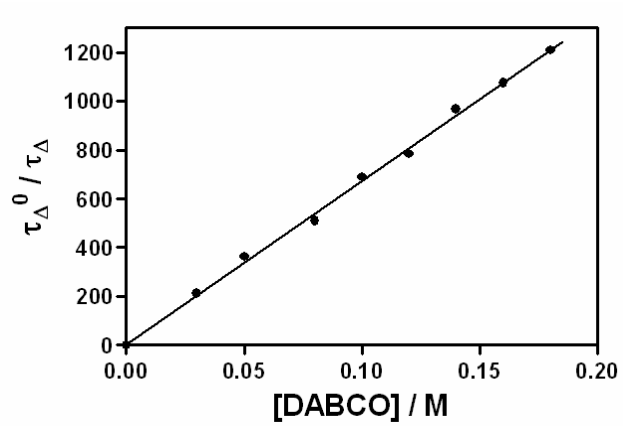

Fig. 6: Stern-Volmer plot of reciprocal $O_2(a^1\Delta_g)$ lifetimes; the slope of the liner least-squares fit is k_q^{DABCO} = (2.3 ± 0.2)·x 10^8 $M^{-1}s^{-1}$.

Clearly, the use of fast photomultiplier tubes as detectors provides the ability to measure $O_2(a^1\Delta_g)$ lifetimes reliably down to a few nanoseconds. Such time resolution paves now the way for unraveling the behaviour of $O_2(a^1\Delta_g)$ in biological systems.

B. Sensitivity: what is the minimum $O_2(a^1\Delta_g)$ quantum yield that can be measured?

The ability of a given photosensitiser to produce $O_2(a^1\Delta_g)$ is quantitatively described by the $O_2(a^1\Delta_g)$ production quantum yield, Φ_Δ [16]. The method for Φ_Δ determination relies on the comparison of signal intensities for solutions of a sample and a reference photosensitiser measured under matched conditions [16].

A question then arises as to which is the fundamental sensitivity of the analog and of the photon counting approach, *i.e.*, which is the minimum signal that can be distinguished from the background noise in either case. In an analog detection system, the output of the detector is fed to a digital oscilloscope, where the signals are digitised, accumulated, and averaged. While in principle the signal-to-noise ratio *SNR* can be indefinitely increased by averaging a large number of independent signals (*N*) according to $SNR \propto \sqrt{N}$, the 8-bit resolution of the ADC converter built in most digital oscilloscopes implies that a signal buried in a noise background 2^8-fold higher (*i.e.*, *SNR* = 0.004) cannot be distinguished from zero, no matter how many signals are averaged (Fig. 7). In practice, the situation is even worse due to baseline fluctuations and other sources of noise.

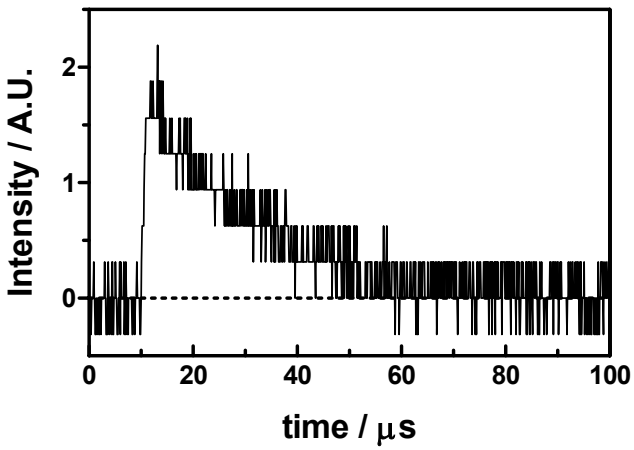

Fig. 7: Effect of analog-to-digital conversion (ADC) in oscilloscopes. Signals smaller than the resolution of the ADC cannot be distinguished from zero.

The intrinsic nature of photon counting, on the contrary, overcomes such problems: as long as there is a signal, *i.e.*, non-random PMT pulses correlated with the laser flash, the improvement in signal-to-noise ratio is limited only by the number of signals acquired, *i.e.*, by the acquisition time. For practical reasons, this should not exceed a few hours. Therefore, photon counting is endowed with the largest intrinsic sensitivity.

To test this conclusion, we assessed the ability to generate $O_2(a^1\Delta_g)$ of substances generally regarded as non-photosensitising. Two such substances are the sunscreens 4-methoxy-2-hydroxybenzophenone (benzophenone-3, BP3) and 2-ethyl-2-cyano-

3,3,diphenylacrylate (octocrylene, OCR) [33]. BP3 and OCR failed to produce any $O_2(a^1\Delta_g)$ signal in methanol. However, when a solution containing either BP3 or OCR was irradiated in air-saturated cyclohexane at 355 nm, clear $O_2(a^1\Delta_g)$ signals could be observed at 1275 nm (Figs. 8A and 8B). The signals disappeared when the emission was monitored at 1150 nm, where $O_2(a^1\Delta_g)$ does not emit, and also when either the sunscreen or oxygen were excluded from the system. Comparison of the signal amplitudes to that recorded for 1*H*-phenalen-1-one (PN), used as a reference sensitiser yielded, Φ_Δ values $(2.7 \pm 0.3) \times 10^{-3}$ for BP3 and $(5.0 \pm 0.1) \times 10^{-4}$ for OCR, respectively, which suggests that these sunscreen may be acting as photosensitisers if localised in non-polar environments [34].

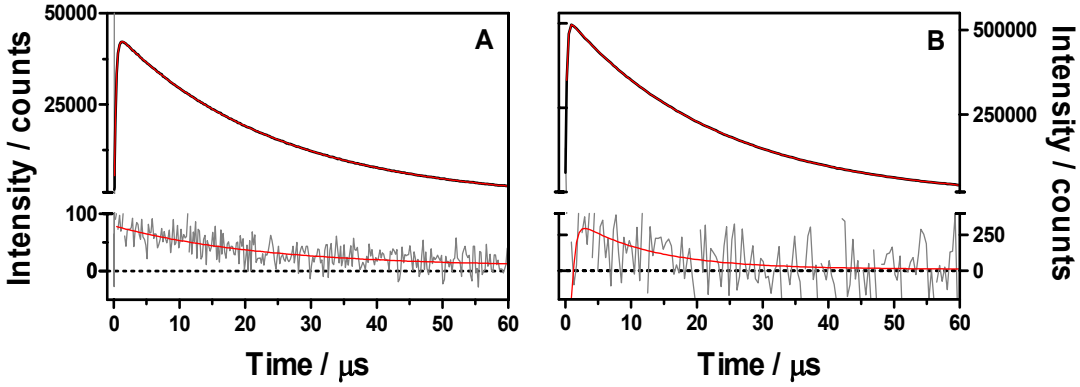

Fig. 8: $O_2(a^1\Delta_g)$transient at 1275 nm sensitized by **A**: BP3 (grey) and PN (black) in cyclohexane, fitted functions (red); **B**: $O_2(a^1\Delta_g)$ transient at 1275 nm sensitized by OCR (grey) and PN (black) in cyclohexane, fitted functions (red). Fitted parameters: BP3, OCR and PN: τ_Δ = 23 μs.

In conclusion, the photon-counting detection technique provides us with the ability to reliably measure Φ_Δ values below 0.001. It might be possible to push this frontier further by observing the signal through long-pass and interference filters rather than through a monochromator. Values below 10^{-4} have been recently measured by Yamaguchi *et al.* [35] by monitoring $O_2(a^1\Delta_g)$ under steady-state conditions. Our approach trades some sensitivity for kinetic information.

C. Effect of sensitiser's fluorescence and scattered laser light. One of the most severe problems in analog $O_2(a^1\Delta_g)$ detection is the presence of background scattered laser light and sensitiser fluorescence. These appear as large spikes in the early stages of the signal that, at the very least, mask the $O_2(a^1\Delta_g)$ signal and, in the worst cases, may even saturate the detection system creating artefacts. The end result is that the $O_2(a^1\Delta_g)$ signal is severely distorted and rendered useless. Spectral isolation of the 1270-nm emission band through a monochromator or a combination of long-pass and interference filters is the simplest and most common approach to minimize this

problem, although it is often still insufficient. Photon counting techniques are less sensitive to this problem: as long as each detector pulse can be counted independently, there is no upper limit for the number of counts in any given channel and the spikes do not lead to artefacts even if they are orders of magnitude larger than the $O_2(a^1\Delta_g)$ component (Fig. 9).

Now, because the detection system is *ca.* 7 ns, the spike vanishes in a few tens of nanoseconds and the growth of the $O_2(a^1\Delta_g)$ signal appears well resolved in most cases (see Fig. 9). In practice, though, highly-scattering samples such as suspensions (e.g. of solids or cells) result in spikes lasting sometimes up to a few hundred nanoseconds, most likely due to long-lived autofluorescence of the optical materials in the detection pathway (filters and lenses) [36] or to the saturation-recovery cycle of the PMT and preamplifier system: Above a certain photon density impinging on the photocathode, single photon pulses are not resolved anymore and a quasi-continuous current flows through the PMT's dynode system. Such current changes the voltage gradients between the dynodes and also saturates the input circuit of the gigahertz preamplifier. Restoring the original voltage gradients, *i.e.*, recovering from saturation, takes a certain time after the decay of the photon burst. The preamplifier's input circuitry also may need some time to recover.

Two examples may serve to illustrate the points above: the first one demonstrates the benefits of the time- and spectral- resolution of the photon counting system to discriminate between the sensitiser's fluorescence, the sensitiser's phosphorescence, and $O_2(a^1\Delta_g)$ phosphorescence; the second one compares the attempts to detect a $O_2(a^1\Delta_g)$ phosphorescence transient from a solution of the green fluorescent protein mutant EGFP usng the analog and the photon counting approaches.

Porphycenes are structural isomers of porphyrins that are under scrutiny for use as photodynamic-therapy photosensitisers [37]. Specifically, the palladium (II) complex of 2,7,12,17-tetraphenylporphycene (PdTPPo) has demonstrated interesting photosensitising potential against a variety of tumour cells [25,38]. This compound is weakly fluorescent though it phosphoresces strongly and exhibits a high $O_2(a^1\Delta_g)$ production quantum yield [39]. Fig. 9 shows the luminescence signals recorded from an air-saturated solution of PdTPPo in toluene: the earliest part of the signals is dominated by the fluorescence decay; at later times a slower, ~200 ns decay component can also be observed, whose spectrum matches that of PdTPPo phosphorescence [39]; concomitant to this decay, the growth of the $O_2(a^1\Delta_g)$ band at 1270 nm is well resolved. Thus, the time and spectral resolution of the photon counting system is able to provide

in information on the kinetics of singlet oxygen photosensitization even in the presence of strong background luminescence signals.

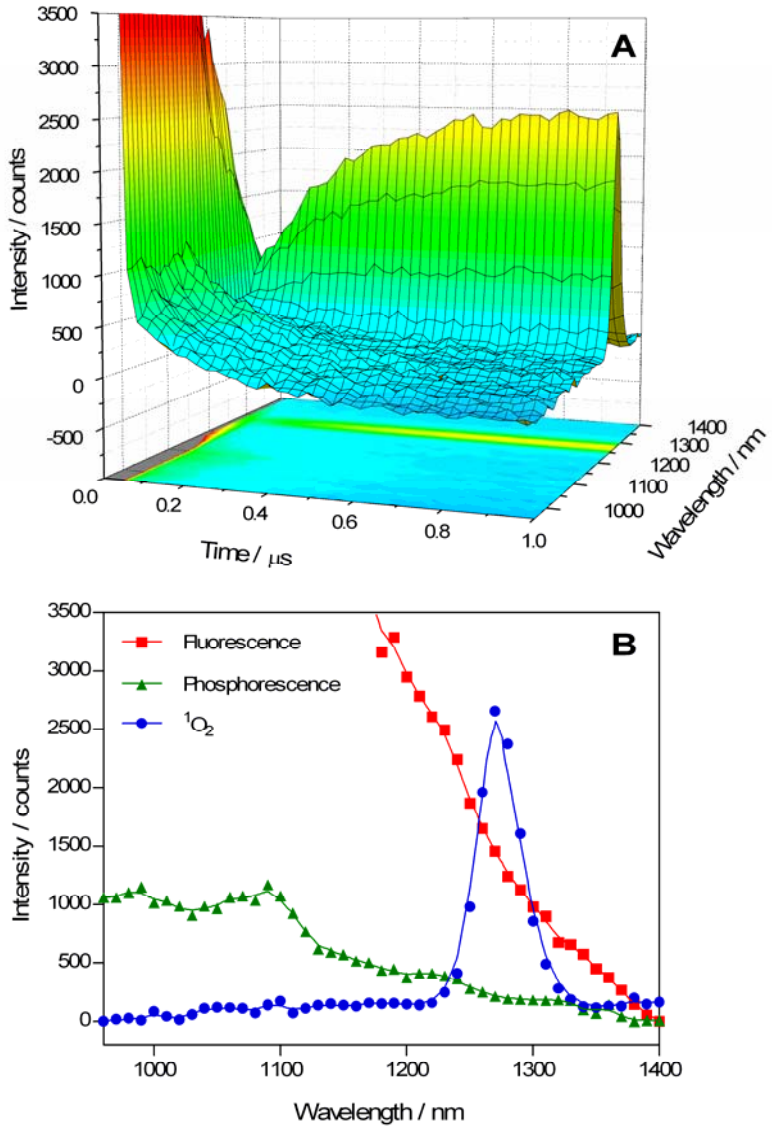

Fig. 9: Time-resolved emission spectra of an air-saturated PdTPPo solution in toluene, λ_{exc} = 532 nm, 20 ns *per* channel, 2 million laser pulses *per* signal.

The second example is provided by green fluorescent proteins, which have become very popular in cell biology for imaging of organelles and processes [40,41]. These proteins tend to bleach upon prolonged irradiation and it has been suggested that $O_2(a^1\Delta_g)$ photosensitized by the protein is the main species responsible for this process [42,43]. When a solution of the enhanced-GFP mutant (EGFP) was irradiated in D_2O with laser pulses above 100 $\mu J \cdot cm^{-2}$, a clear transient could be observed with the germanium photodiode operating in analog mode (Fig. 10A, inset). However, the lifetime of this transient, ca. 200 µs, was not consistent with the reported $O_2(a^1\Delta_g)$

lifetime in D_2O, τ_Δ = 67 μs [28]. Extensive bubbling of the sample with argon had no effect on the signal, suggesting that it was an artifact due to saturation of the detection system rather than a $O_2(a^1\Delta_g)$ transient. Inspection of the early part of the signal revealed the saturation of the detection electronics by the huge EGFP fluorescence burst, a problem well-known to the $O_2(a^1\Delta_g)$ community for highly fluorescent samples [44]. Reducing the laser energy down to 20 μJ·cm^{-2} prevented this problem but then no $O_2(a^1\Delta_g)$ transient could be observed even after averaging 10^3 laser shots (Fig. 10B), likely because it was below the system's sensitivity.

When the EGFP sample was studied with the photon-counting system, a large fluorescence spike of almost 10^6 counts could still be observed, but it did not preclude the detection of an additional 250-counts rise-and-decay $O_2(a^1\Delta_g)$ transient (Figs. 10C and 10D) [45].

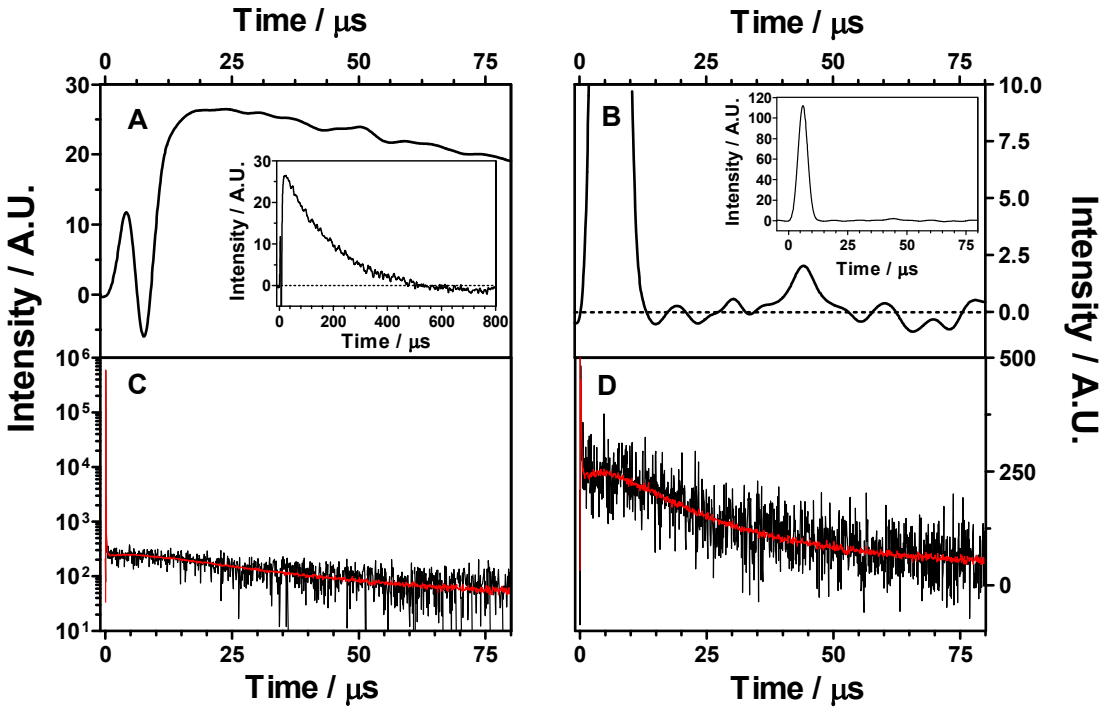

Fig. 10: Detected signals at 1275 nm upon irradiation of a ~200 μM solution of EGFP in deuterated PBS. **A**: Analog mode, 200 μJ·cm^{-2}, detail of the earlier part of the signal, showing an artefact due to saturation of the detection optoelectronics; **inset**: full apparent signal; **B**: analog mode, 20 μJ·cm^{-2}, the detector is not saturated but then the $O_2(a^1\Delta_g)$ signal is below the system's sensitivity; **inset**: detail of the spike of the signal; **C** and **D**: photon-counting mode, 6 μJ·cm^{-2}. Notice the spike in the early channels, more than three orders of magnitude stronger than the $O_2(a^1\Delta_g)$ signal. λ_{exc} = 532 nm.

Clearly, the use of the photon counting approach solves, or at least substantially alleviates, the long-standing problem of the signal spikes precluding the acquisition of clean $O_2(a^1\Delta_g)$ signals in highly scattering and/or highly fluorescent samples. Again, this improvement is judged essential for studying the behavior of $O_2(a^1\Delta_g)$ in biological media. The first results obtained in our as well as in other laboratories are already providing a wealth of novel and highly exciting data [22,24,46,47]. As a final recommendation, it should be noted that lasers with pulsewidth as small as possible should be used to minimize the spike problem.

3.5. CONCLUSIONS AND OUTLOOK

The advantages of photon-counting time-resolved $O_2(a^1\Delta_g)$ phosphorescence detection over the analog technique have been highlighted in the preceding sections. Time resolution in the nanosecond domain, higher sensitivity, and better ability to cope with scattered laser light and sensitiser fluorescence give photon counting detection a clear edge over the analog mode. It can be safely anticipated that progress in optoelectronic technology will eventually provide new NIR PMTs with lower dark-count rates and new lasers with the right balance of energy, repetition rate, and wavelength tunability. Combined with parallel developments is space resolution [38], these advances will push further our ability to temporally and spatially detect $O_2(a^1\Delta_g)$ in systems of ever increasing complexity.

3.6. REFERENCES

[1] Foote, C. S. Photosensitized oxygenations and role of singlet oxygen. *Acc. Chem. Res* **1**:104-&; 1968.

[2] Kanofsky, J. R. Singlet oxygen production by lactoperoxidase - Evidence from 1270-nm chemiluminescence. *J. Biol. Chem.* **258**:5991-5993; 1983.

[3] Kochevar, I. E.; Redmond, R. W. Photosensitized production of singlet oxygen. *Methods in Enzimology*. USA: Academic Press; 2000:20-28.

[4] Foote, C. S.; Valentine, J. S.; Greenberg, A.; Liebman, J. F. e. *Active Oxygen in Biochemistry*: Blackie Academic and Professional; 1995.

[5] Michaeli, A.; Feitelson, J. Reactivity of singlet oxygen toward amino acids and peptides. *Photochem. Photobiol.* **59(3)**:284-289; 1994.

[6] Michaeli, A.; Feitelson, J. Reactivity of singlet oxygen toward large peptides. *Photochem. Photobiol.* **61(3)**:255-260; 1995.

[7] Ravanat, J. L.; Di Mascio, P.; Martinez, G. R.; Medeiros, M. H. G.; Cadet, J. Singlet oxygen induces oxidation of cellular DNA. *J. Biol. Chem.* **275**:40601-40604; 2000.

[8] Zhang, X. S.; Rosenstein, B. S.; Wang, Y.; Lebwohl, M.; Wei, H. C. Identification of possible reactive oxygen species involved in ultraviolet radiation-induced oxidative DNA damage. *Free Radical Biol. Med.* **23**:980-985; 1997.

[9] Dolmans, D. E. J. G.; Fukumura, D.; Jain, R. K. Photodynamic therapy for cancer. *Nat. Rev. Cancer* **3**:380-387; 2003.

[10] Flors, C.; Nonell, S. Light and singlet oxygen in plant defense against pathogens: Phototoxic phenalenone phytoalexins. *Acc. Chem. Res* **39**:293-300; 2006.

[11] Laloi, C.; Apel, K.; Danon, A. Reactive oxygen signalling: the latest news. *Curr. Op. Plant Biol.* **7**:323-328; 2004.

[12] Foyer, C. H.; Noctor, G. Redox sensing and signalling associated with reactive oxygen in chloroplasts, peroxisomes and mitochondria. *Physiologia Plantarum* **119**:355-364; 2003.

[13] Ryter, S. W.; Tyrrell, R. M. Singlet molecular oxygen (O-1(2)): A possible effector of eukaryotic gene expression. *Free Radical Biol. Med.* **24**:1520-1534; 1998.

[14] Schweitzer, C.; Schmidt, R. Physical mechanisms of generation and deactivation of singlet oxygen. *Chem. Rev.* **103**:1685-1757; 2003.

[15] Wilkinson, F.; Helman, W. P.; Ross, A. B. Quantum yields for the photosensitized formation of the lowest electronically excited singlet state of molecular oxygen in solution. *J. Phys. Chem. Ref. Data* **22**:113-262; 1993.

[16] Nonell, S.; Braslavsky, S. E. Time-resolved singlet oxygen detection. In: Packer, L.; Sies, H. eds. *Singlet oxygen, UV-A, and Ozone. Methods in Enzymology, vol.319*. San Diego: Academic Press; 2000:37-49.

[17] Egorov, S. Y.; Kamalov, V. F.; Koroteev, N. I.; Krasnovsky Jr., A. A.; Toleutaev, B. N.; Zinukov, S. V. Rise and decay kinetics of photosensitized singlet oxygen luminescence in water. Measurements with nanosecond time-correlated single photon counting technique. *Chem. Phys. Lett.* **163**:421-424; 1989.

[18] Niedre, M.; Patterson, M. S.; Wilson, B. C. Direct near-infrared luminiscence detection of singlet oxygen generated by photodynamic therapy in cells *in vitro* and tissues *in vivo*. *Photochem. Photobiol.* **75**:382-391; 2002.

[19] Shimizu, O.; Watanabe, J.; Imakubo, K. Photon counting technique facilitates both time- and spectrally-resolved measurements of near-IR emission of singlet oxygen $O_2(^1\Delta_g)$ in aqueous solution. *J. Phys. Soc. Jpn.* **66**:268-269; 1997.

[20] Snyder, J. W.; Skovsen, E.; Lambert, J. D. C.; Ogilby, P. R. Subcellular, time-resolved studies of singlet oxygen in single cells. *J. Am. Chem. Soc.* **127**:14558-14559; 2005.

[21] Dedic, R.; Molnar, A.; Korinek, M.; Svoboda, A.; Psencik, J.; Hala, J. Spectroscopic study of singlet oxygen photogeneration in meso-tetra-sulphonatophenyl-porphin. *J. Lumin.* **108**:117-119; 2004.

[22] Baier, A.; Maier, M.; Engl, R.; Landthaler, M.; Baumler, W. Time-resolved investigations of singlet oxygen luminescence in water, in phosphatidylcholine, and in aqueous suspensions of phosphatidylcholine or HT29 cells. *J. Phys. Chem. B* **109**:3041-3046; 2005.

[23] Tada, D. B.; Vono, L. L. R.; Duarte, E. L.; Itri, R.; Kiyohara, P. K.; Baptista, M. S.; Rossi, L. M. Methylene Blue-containing silica-coated magnetic particles: a potential magnetic carrier for photodynamic therapy. *Langmuir* **23**:8194-8199; 2007.

[24] Postigo, F.; Sagrista, M. L.; De Madariaga, M. A.; Nonell, S.; Mora, M. Photosensitization of skin fibroblasts and HeLa cells by three chlorin derivatives: Role of chemical structure and delivery vehicle. *Biochim. Biophys. Acta* **1758**:583-596; 2006.

[25] Cañete, M.; Ortiz, A.; Juarranz, A.; Villanueva, A.; Nonell, S.; Borrell, J. I.; Teixidó, J.; Stockert, J. C. Photosensitizing properties of palladium-tetraphenylporphycene on cultured tumour cells. *Anti-Cancer Drug Des.* **15**:143-150; 2000.

[26] Becker, W. *Advanced Time-Correlated Single Photon Counting Techniques*: Germany: Springer; 2005.

[27] Lakowicz, J. R. *Principles of fluorescence spectroscopy*: New York: Kluwer Academic/Plenum Publishers; 2006.

[28] Wilkinson, F.; Helman, W. P.; Ross, A. B. Rate constants for the decay and reactions of the lowest electronically excited singlet state of molecular oxygen in solution. An expanded and revised compilation. *J. Phys. Chem. Ref. Data* **24**:663-1021; 1995.

[29] Schmidt, R.; Tanielian, C. Time-resolved determination of the quantum yield of singlet oxygen formation by tetraphenylporphine under conditions of very strong quenching. *J. Phys. Chem.* **104**:3177-3180; 2000.

[30] Iu, K.-K.; Scurlock, R. D.; Ogilby, P. R. The characterization of germanium p-n junction detectors for use in nanosecond time-resolved near-IR spectroscopic studies: the photosensitized formation of singlet molecular oxygen ($1\Delta g$) in solution. *J. Photochem.* **37**:19-32; 1987.

[31] Parker, J. G.; Stanbro, W. D. Dependence of photosensitized singlet oxygen production on porphyrin structure and solvent. In: Doiron, D. R.; Gomer, C. J. eds. *Porphyrin localization and treatment of tumors*. New York: Alan R. Liss; 1984:259-284.

[32] Pan, S. L.; Rothberg, L. J. Enhancement of platinum octaethyl porphyrin phosphorescence near nanotextured silver surfaces. *J. Am. Chem. Soc.* **127**:6087-6094; 2005.

[33] Allen, J. M.; Gossett, C. J.; Allen, S. K. Photochemical formation of singlet molecular oxygen in illuminated aqueous solutions of several commercially available sunscreen active ingredients. *Chem. Res. Toxicol.* **9**:605-609; 1996.

[34] De Sola, L.; Jimenez-Banzo, A.; Nonell, S. Seguridad de los fotoprotectores solares: fotogeneración de oxígeno singlete por los filtros solares benzofenona-3, butilmetoxidibenzoilmetano y octocrileno. *Afinidad* **64**:251-256; 2008.

[35] Yamaguchi, S.; Sasaki, Y. Spectroscopic determination of very low quantum yield of singlet oxygen formation photosensitized by industrial dyes. *J. Photochem. Photobiol. A: Chem.* **142**:47-50; 2001.

[36] Scurlock, R. D.; Iu, K.-K.; Ogilby, P. R. Luminescence from optical elements commonly used in near-IR spectroscopic studies: the photosensitized formation of singlet molecular oxygen (1Dg) in solution. *J. Photochem.* **37**:247-255; 1987.

[37] Stockert, J. C.; Canete, M.; Juarranz, A.; Villanueva, A.; Horobin, R. W.; Borrell, J.; Teixido, J.; Nonell, S. Porphycenes: Facts and prospects in photodynamic therapy of cancer. *Curr. Med. Chem.* **14**:997-1026; 2007.

[38] Cañete, M.; Ortega, C.; Gavalda, A.; Cristobal, J.; Juarranz, A.; Nonell, S.; Teixido, J.; Borrell, J. I.; Villanueva, A.; Rello, S.; Stockert, J. C. Necrotic cell death induced by photodynamic treatment of human lung adenocarcinoma A-549 cells with palladium(II)-tetraphenylporphycene. *Int. J. Oncol.* **24**:1221-1228; 2004.

[39] Rubio, N.; Prat, F.; Bou, N.; Borrell, J. I.; Teixido, J.; Villanueva, A.; Juarranz, A.; Canete, M.; Stockert, J. C.; Nonell, S. A comparison between the photophysical and photosensitising properties of tetraphenyl porphycenes and porphyrins. *New J. Chem.* **29**:378-384; 2005.

[40] Tsien, R. Y. The Green Fluorescent Protein. *Annu. Rev. Biochem.* **67**:509-544; 1998.

[41] Giepmans, B. N. G.; Adams, S. R.; Ellisman, M. H.; Tsien, R. Y. Review - The fluorescent toolbox for assessing protein location and function. *Science* **312**:217-224; 2006.

[42] Bell, A. F.; Stoner-Ma, D.; Wachter, R. M.; Tonge, P. J. Light-driven decarboxylation of wild-type green fluorescent protein. *J. Am. Chem. Soc.* **125**:6919-6926; 2003.

[43] Greenbaum, L.; Rothmann, C.; Lavie, R.; Malik, Z. Green fluorescent protein photobleaching: a model for protein damage by endogenous and exogenous singlet oxygen. *Biol. Chem.* **381**:1251-1258; 2000.

[44] Beeby, A.; Parker, A. W.; Stanley, C. F. Elimination of fluorescence contributions to singlet oxygen measurements using a novel electronic switch. *J. Photochem. Photobiol. B:Biol.* **37**:267-271; 1997.

[45] Jimenez-Banzo, A.; Nonell, S.; Hofkens, J.; Flors, C. Singlet oxygen photosensitization by EGFP and its chromophore HBDI. *Biophys. J.* **94**:168-172; 2008.

[46] Jimenez-Banzo, A.; Sagrista, M. L.; Mora, M.; Nonell, S. The kinetics of singlet oxygen photosensitization in human skin fibroblasts. *Free Radical Biol. Med.* 2008 *(accepted)*.

[47] Snyder, J. W.; Skovsen, E.; Lambert, J. D. C.; Poulsen, L.; Ogilby, P. R. Optical detection of singlet oxygen from single cells. *Phys. Chem. Chem. Phys.* **8**:4280-4293; 2006.

Chapter 4

The Kinetics of Singlet Oxygen Photosensitisation in Human Skin Fibroblasts

The roles played by singlet oxygen ($^1O_2$) in photodynamic therapy are not fully understood yet. In particular, the mobility of $^1O_2$ within cells has been a subject of debate the last two decades. In this chapter, we report on the kinetics of $^1O_2$ formation, diffusion, and decay in human skin fibroblasts. $^1O_2$ has been photosensitized by two water-soluble porphyrins with different subcellular localization, namely in the nucleus and lysosomes, respectively. By recording the time-resolved near-IR phosphorescence of $^1O_2$ and of its precursor the photosensitizer's triplet state, we find that the kinetics of singlet oxygen formation and decay are site-dependent. $^1O_2$ photosensitized in the nucleus is able to escape out of the cells while $^1O_2$ photosensitized in the lysosomes is not. Despite showing a lifetime in the microsecond time domain, $^1O_2$ decay is largely governed by interactions with the biomolecules within the organelle where it is produced. This observation may reconcile earlier views that singlet oxygen-induced photodamage is highly localized, while its lifetime is long enough to diffuse over long distances within the cells.

The work described in this chapter was presented at the XXIII International Conference on Photochemistry, Cologne, Germany (Agost 2007), and it is adapted from: the kinetics of singlet oxygen photosensitisation in human skin fibroblasts, A. Jimenez-Banzo, M.L. Sagristá, M. Mora and S. Nonell; submitted for publication in *Free Radical Biology & Medicine*.

4.1. INTRODUCTION

Oxidative damage to biological systems, either accidental or intended, is a major cause of cell death [1]. In particular, apoptotic or necrotic signaling pathways to cell death can be induced by the combined use of a photoactivatable drug, called the photosensitizer, and *per se* harmless visible light. This process involves the generation of reactive oxygen species (ROS) capable to inflict damage to susceptible cell components such as proteins [2,3], membrane lipids [4], and nucleic acids [5]. This is the basis of the medical treatment photodynamic therapy (PDT) [6,7], increasingly employed in clinical oncology [8], in the treatment of several non-malignant conditions and skin afflictions [9,10] and for virus or bacterial inactivation purposes [11-13].

Singlet oxygen ($^1O_2$) is a member of the general class of ROS that is believed to play a major role in many photooxidation processes, particularly in photodynamic therapy. A common and convenient method to produce $^1O_2$ is *via* photosensitization processes. Thus, the electronically-excited states of the photosensitiser (sens), produced upon light absorption, are efficiently quenched by molecular oxygen, particularly the longer-lived triplet state. Energy transfer between the two species results in the production of $^1O_2$ as illustrated in the following scheme:

$$\begin{aligned} \text{sens} + h\nu &\rightarrow {}^1\text{sens}^* \\ {}^1\text{sens}^* &\rightarrow {}^3\text{sens}^* \\ {}^3\text{sens}^* + {}^3O_2 &\rightarrow \text{sens} + {}^1O_2 \end{aligned}$$

Once produced, $^1O_2$ may diffuse away from the site of production, oxidize biomolecules encountered along its path, or decay back to the ground state within its lifetime. A tiny fraction of $^1O_2$ molecules undergo radiative decay, thereby emitting a photon in the near infrared (NIR). This extremely weak phosphorescence, centered at 1275 nm, provides the means for the most direct and unambiguous method for $^1O_2$ detection. The time-resolved measurement of this NIR emission is now a very well-established method for monitoring $^1O_2$ and determining its lifetime and quantum yield of production [14,15].

A long sought-after goal has been to determine the lifetime of $^1O_2$ within a cell. Early indirect approaches lead to the perception that the cellular $^1O_2$ lifetime was in the nanosecond domain. For instance, Moan and Berg estimated it as 10-40 ns on the basis of the photodegradation rates of porphyrins [16] whereas a lifetime in the range of 170-320 ns was later estimated by Baker and Kanofsky based on experiments using lysed cells [17]. The first direct measurements of $^1O_2$

phosphorescence in actual cell suspensions provided lifetime values in the range 4-80 μs [18,19]. The recent introduction of fast near-infrared sensitive photomultipliers, allowed Niedre *et al.* [20] to determine the $^1O_2$ lifetime in leukemia cells loaded with tetrasulfonated aluminium phthalocyanine. These authors found a value of 600 ± 400 ns, although only 15-19 % of their signals appeared to come from within the cells, the largest fraction being originated from photosensitizer located in the external media. They also confirmed previous findings that the lifetime of the triplet sensitizer increased in the cells relative to the value in aqueous solution, *i.e.*, from 3.2 to 19 μs, and pointed out the value of determining such sensitizer's triplet lifetime in $^1O_2$ photosensitization studies. The latest contributions to this research topic originated from the group of Ogilby, where a novel microscopic method for $^1O_2$ imaging in a single cell was developed, which yielded the striking result that the $^1O_2$ lifetime is in the microsecond range [21-23]. The authors concluded that the lifetime of $^1O_2$ is limited by interactions with the water-based cellular environment, rather than by interactions with biomolecules as assumed for the previous twenty years.

The microscope results are in principle free from ambiguities as to the primary site of $^1O_2$ generation. However, the experiments reported so far have a number of limitations [21-24] which still cast some doubts on the real mobility of $^1O_2$ within the cells and on its implications: 1) the microscope experiments need to be carried out in oxygen-saturated D_2O or H_2O/D_2O mixtures in order to obtain a detectable signal, conditions which do not match the physiological ones, *i.e.*, air-equilibrated H_2O-based systems; 2) the time-resolution of the gated photon counting detection system used, *ca.* 4 μs per point, is too long to differentiate a submicrosecond component such as the 600 ns reported by Niedre *et al.* [20]; 3) only signals generated in the cells' nucleus have been published so far and therefore the fate of $^1O_2$ generated in other organelles remains unknown; 4) finally, values of the sensitizer's triplet lifetime have not been reported and therefore, as pointed out by Niedre *et al.* [20], a sound understanding of the photosensitization process is still incomplete.

In this work we report the results of monitoring the kinetics of both the $^1O_2$ and the sensitizers's phosphorescence in aqueous (H_2O and D_2O) suspensions of human skin fibroblasts. The cells are loaded with photosensitizers displaying clearly different subcellular localization. The two compounds chosen, 5,10,15,20-tetrakis(*N*-methyl-4-pyridyl)-21*H*,23*H*-porphine (TMPyP) and 5,10,15,20-tetrakis-(4-sulfonatophenyl)-21*H*,23*H*-porphine (TPPS, Fig. 1) have been well studied in the

field of PDT and their properties are well established [25,26]. TMPyP is a tetra-cationic porphyrin and an efficient $^1O_2$ photosensitizer (Φ_Δ = 0.77) [27] that localizes mainly in the cell nucleus [28,29]. TPPS, a tetra-anionic porphyrin at physiologic pH, is endowed with a $^1O_2$ quantum yield Φ_Δ = 0.62 in water [27] and localizes mainly in microenvironments with a pH of 5 [30-35], a value which occurs intracellularly only within lysosomes. We show that $^1O_2$ generated in the nucleus is able to diffuse out of the cell, while $^1O_2$ generated in the lysosomes is not.

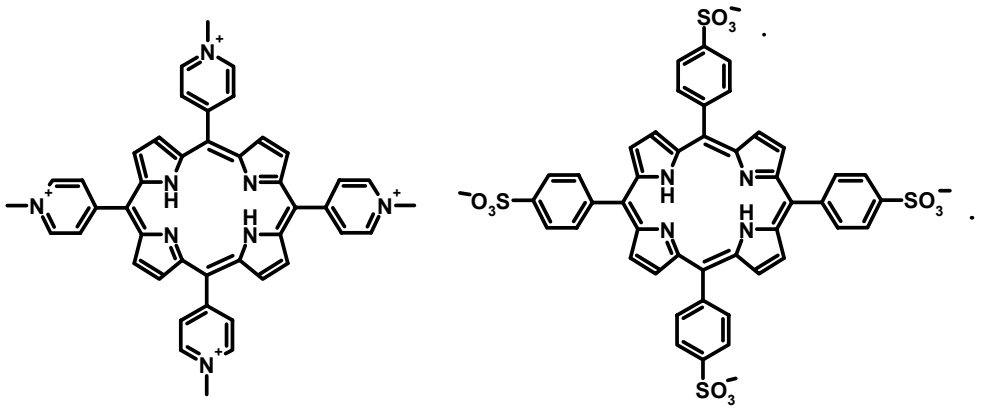

Fig. 1. Chemical structures of 5,10,15,20-tetrakis(*N*-methyl-4-pyridyl)-21*H*,23*H*-porphine (TMPyP) and 5,10,15,20-tetrakis-(4-sulfonatophenyl)-21*H*,23*H*-porphine (TPPS).

4.2. EXPERIMENTAL SECTION

Materials: The porphyrins 5,10,15,20-tetrakis(*N*-methyl-4-pyridyl)-21*H*,23*H*-porphine (TMPyP) and 5,10,15,20-tetrakis-(4-sulfonatophenyl)-21*H*,23*H*-porphine (TPPS) were purchased from Frontier Scientific (Logan, UT, USA), and used as received, had a minimal purity of 99 %. Deuterium oxide (99.9 %) was purchased from Solvents Documentation Synthesis (SDS, Peypin, France).

Dulbecco's Modified Eagle's Medium with 4.5 glucose/l (DMEM), fetal calf serum, penicillin-streptomycin solution and *L*-glutamine solution for biological assays were purchased from Biological Industries (Kibbutz Beit Haemek, Israel). Sterile Dulbecco's phosphate-buffered saline (PBS), dimethyl sulphoxide (DMSO), bovine serum albumin (98%) and 3-[4,5-dimethylthiazol-2-yl]-2,5-diphenyltetrazolium bromide (MTT) were purchased from Sigma-Aldrich Co. (St. Louis, MO, USA). The sterilized material was purchased from Techno Plastic Products (Trasadingen, Switzerland).

4.3. RESULTS AND DISCUSSION

Previous studies have shown that the porphyrins TMPyP and TPPS are good sensitisers for the photoinactivation of several cell lines at concentrations ranging from 0.1 to 10 μM [25,35-37]. Our early attempts to detect $^1O_2$ phosphorescence at these concentrations produced signals too weak to allow us to draw any conclusion. We therefore set out to determine how high we could go in terms of sensitiser uptake to increase the $^1O_2$ signal without compromising the cell's viability. To this end, dark toxicity and uptake experiments were conducted.

A. Dark toxicity. Cell survival fractions after different dark incubation times with TMPyP or TPPS are collected in Table 1. For TPPS, the cell viability decreases to 55% at 200 μM and 22 hours of incubation, while for TMPyP the cell viability was always above 70%. A concentration up to 100 μM and incubation times up to 16 hours were chosen as a good compromise between cellular viability and sensitiser concentration in culture medium, with survival fractions of 89% in the case of TPPS and 73% for TMPyP. We have also chosen to use the same concentration of the two sensitisers to provide a better basis for comparison.

Table 1. Dark toxicity of TMPyP and TPPS in human skin fibroblasts[a].

Sensitiser concentration / μM	Incubation time / h	Cell survival fraction / % ± SD	
		TPPS	TMPyP
1	0.5	101 ± 3	97 ± 3
	3	84 ± 5	81 ± 2
	6	81 ± 2	77 ± 5
	16	80 ± 1	80 ± 2
	22	80 ± 1	80 ± 3
10	0.5	101 ± 6	96 ± 2
	3	85 ± 6	82 ± 2
	6	80 ± 2	80 ± 1
	16	80 ± 2	79 ± 1
	22	85 ± 1	79 ± 1
50	0.5	97 ± 8	97 ± 7
	3	83 ± 1	87 ± 3
	6	86 ± 2	79 ± 2
	16	89 ± 3	71 ± 3
	22	80 ± 8	74 ± 1
100	0.5	95 ± 1	84 ± 3
	3	85 ± 6	75 ± 4
	6	86 ± 1	73 ± 1
	16	89 ± 3	73 ± 4
	22	80 ± 8	73 ± 3
200	0.5	86 ± 7	76 ± 3
	3	74 ± 4	72 ± 1
	6	71 ± 2	68 ± 7
	16	79 ± 7	74 ± 5
	22	55 ± 3	71 ± 1

[a]Mean ± SD values from at least three different experiments are shown.

B. Uptake of the photosensitisers. The uptake of TMPyP and TPPS by human skin fibroblasts was determined measuring the fluorescence of these compounds after lysing the cells with the detergent SDS. The results are shown in Fig. 2. For both compounds, the uptake increases steadily and reaches a plateau after *ca.* 12 hours of incubation. The highest fluorescence increase is observed at 100 μM photosensitiser concentration.

Taking together the results of dark toxicity and cellular uptake, we considered that 100 μM sensitizer concentration and an incubation time between 6 and 16 hours were the most promising conditions for attempting the detection of $^1O_2$ in viable cells. Using the calibration procedure described in the Materials and Methods section, we found that the number of molecules per cell was 1.3 x 10^9 for TMPyP and 1.2 x 10^9 for TPPS, both after incubating a 100 μM solution for 16 hours.

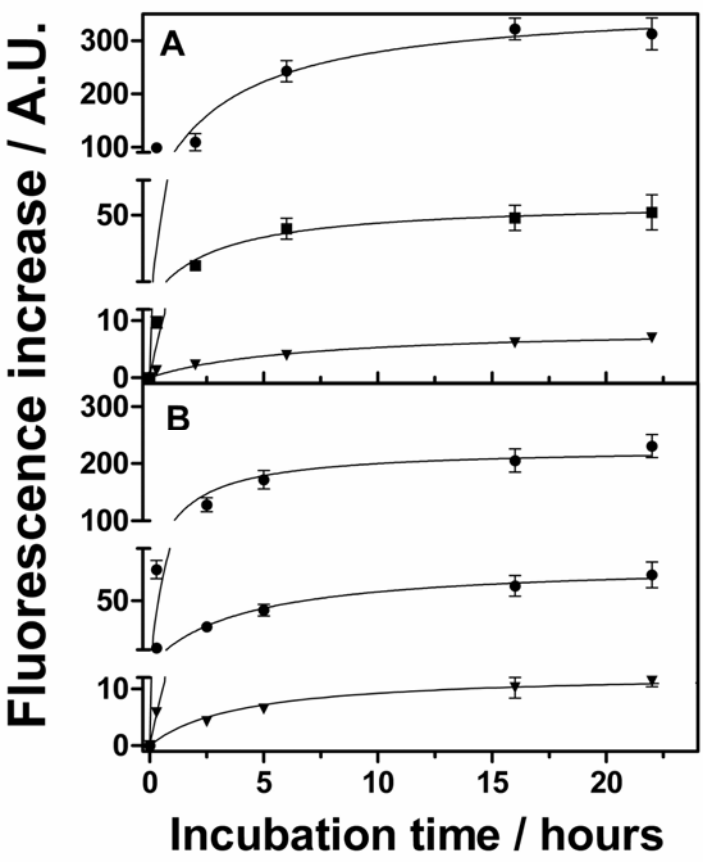

Fig. 2. Photosensitizers uptake by human skin fibroblasts incubated between 30 minutes and 22 hours with 1 μM (▼), 10 μM (■) and 100 μM (•) of TMPyP (A) or TPPS (B) in the dark. Porphyrins were added to the cells dissolved in PBS. At each period of time, cells were washed three times with PBS, trypsinized and centrifuged. The pellet was suspended in a 2% SDS/PBS solution, incubated further for 15 minutes in the dark at room temperature and centrifuged at 10,000 rpm for 10 min. Fluorescence emission from the supernatant were recorded upon excitation at 420 and 412 nm for TMPyP and TPPS, respectively. The fluorescence change plotted is the ratio between the area under the fluorescence emission spectra and the total number of cells in each suspension.

C. Subcellular localisation of the photosensitisers. In cell suspension experiments, it is important to demonstrate that the $^1O_2$ photosensitiser is localized intracellularly and, preferably, in a single organelle. Over the years, several studies have shown that cationic porphyrins penetrate the cell membrane and accumulate mainly in the nucleus due to their high affinity for DNA [38-40]. From *in vitro* experiments it is also well established that the sensitiser TPPS localizes mainly within the lysosomes in various cell lines [31-33,35]. As the intracellular localisation of a photosensitiser might be dependent on the cell line, our first goal was to confirm that TMPyP and TPPS are mainly localized in the nucleus and within the lysosomes, respectively, of human skin fibroblasts.

Phase contrast and fluorescence images of human skin fibroblasts after incubation with 100 μM of TMPyP or TPPS for 14 hours are shown in Fig. 3. Nuclei of the cells previously treated with TMPyP present bright red fluorescence, although a residual fluorescence from the cytoplasm could also be observed. For TPPS, the cellular fluorescence was concentrated to a large degree in spots or granules distributed all over the cells (Fig. 3D). This granular pattern has been attributed to lysosomes in other fibroblasts cell lines [30,32]. It is important to note that no morphological changes were detected in the cells under these conditions.

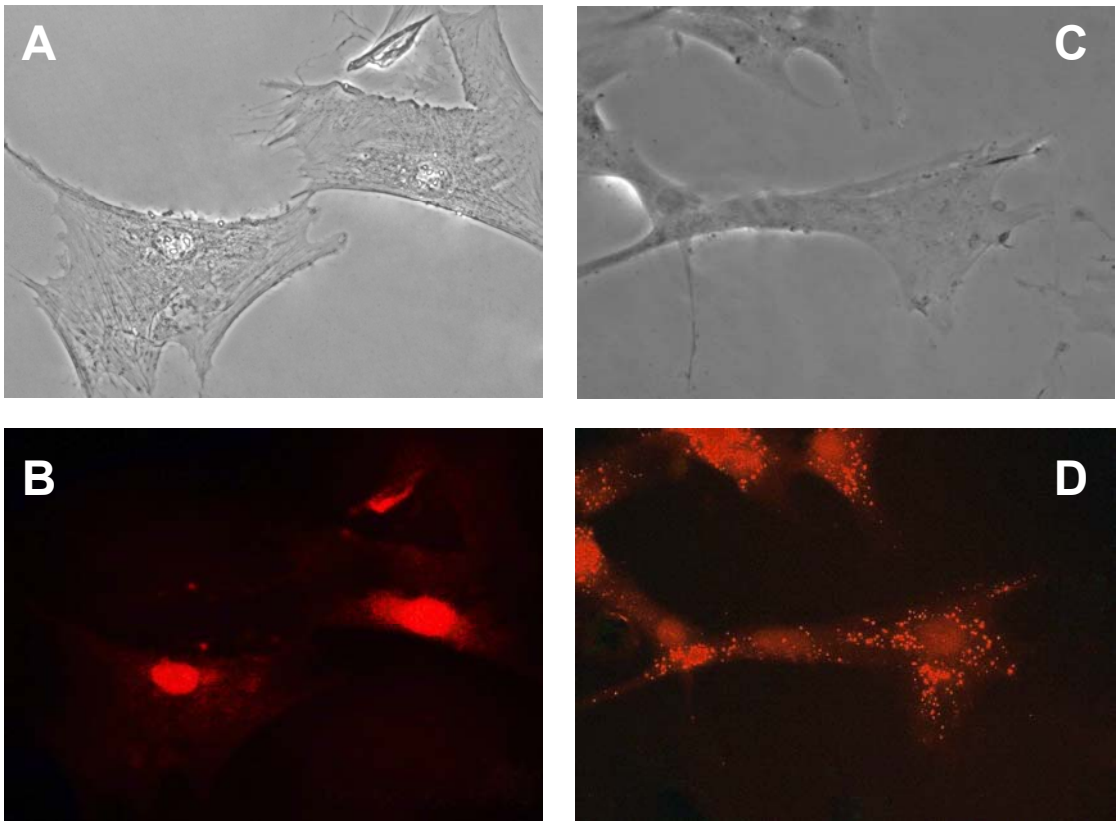

Fig. 3. Phase contrast and fluorescence images of human skin fibroblasts after incubation with 100 μM of TMPyP (A and B) or TPPS (C and D) for 14 hours. Cells were washed three times with PBS cooled at 4ºC and examined immediately thereafter.

On the other hand, the photophysical properties showed remarkable changes in line with previous reports [41]. Fig. 4 shows the absorption and emission spectra of TMPyP measured in buffer solution and in cell suspension at pH 7.4. The Soret band, which peaks at 420 nm for TMPyP in solution, exhibited a pronounced bathochromic shift towards ~ 440 nm when the compound was incorporated into human skin fibroblasts. Likewise, the fluorescence emission spectrum of TMPyP shows a structureless broad band peaking at 680 nm in solution, while the emission is well resolved in the cell

suspension, showing two peaks at 655 and 720 nm corresponding to the (0-0) and (0-1) transitions, respectively. These changes are consistent with the intracellular localization of TMPyP, reflecting a change of polarity of its micro environment [42] as well as the interaction with DNA [43-48].

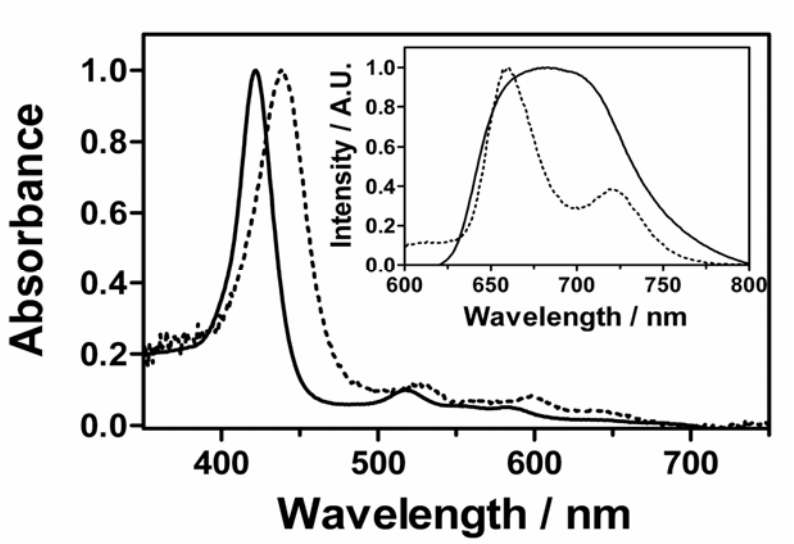

Fig. 4. Absorption spectra of a 0.1 μM TMPyP solution at pH 7.4 (solid line) and from a fibroblasts suspension (dotted line). Absorption values from cell suspension samples were recorded as transmittance and then transformed into absorbance using the following equation: *Abs = 2 – log %T*. Inset: fluorescence emission spectra of TMPyP in solution (solid line) and previously incorporated into human skin fibroblasts (dotted line) (λ_{exc} = 420 nm).

Similar results were found for TPPS. The absorption and emission spectra of TPPS in pH 7.4 and pH 5 solutions, as well as in cell suspension, are depicted in Fig. 5. The Soret band, which is centered at 413 nm for neutral solutions, is 7-nm red shifted when TPPS is incorporated into human skin fibroblasts. The absorption spectrum in the cells matches that of a TPPS solution at pH 5, indicating that the sensitizer is mainly localized in an acidic microenvironment. The same conclusion is arrived at from the fluorescence emission spectra (Fig. 5, inset). Again, the clear differences between TPPS in solution and in the cell suspensions confirm the intracellular localization of this photosensitizer.

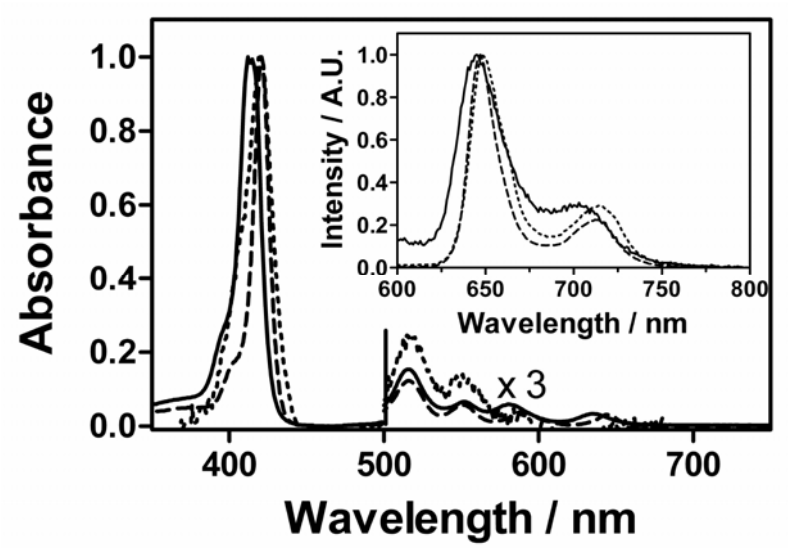

Fig. 5. Absorption spectra of a 0.1 μM TPPS solution at pH 7.4 (solid line), pH 5 (dash line) and from a fibroblasts suspension (dotted line). Absorption values from cell suspension samples were recorded as transmittance and then transformed into absorbance using the following equation: *Abs = 2 – log %T*. Inset: fluorescence emission spectra of TPPS in solution at pH 7.4 (solid line), pH 5 (dash line) and previously incorporated to human skin fibroblasts (dotted line) (λ_{exc} = 413 nm).

In order to get more evidence of the photosensitizer localization, time-resolved fluorescence measurements were carried out on the cell suspensions. As shown in Fig. 6A, the fluorescence of TMPyP in the cells presents a biexponential decay with lifetimes of 1.8 and 11 ns. In contrast, TMPyP decays monoexponentially with a lifetime of 4.6 ns in pH 7.4 aqueous solutions [42]. The absence of such 4.6-ns component in the cell suspension indicates that TMPyP has been taken up by the cells. Several studies have found that TMPyP binds to DNA through intercalation between guanine-cytosine base pairs (GC) and through groove binding at adenine-thymine sites (AT) [40,49], leading to double-exponential fluorescence decays with lifetimes 2 and 11 ns [42,50]. Comparison with our values suggests that, as expected, TMPyP is located in the cell nucleus both intercalated between DNA's GC pairs (1.8 ns) and externally bound to DNA (11 ns), the relative proportions being 75% and 25%, respectively, as determined from the intensities of the two fluorescence decay components.

In the case of TPPS, a single exponential decay with a lifetime of 10 ns was observed in aqueous pH 7.4 solution, whereas a second exponential of 4 ns (20% of the total amplitude) was necessary to fit the decay at pH 5. Values of 3.5 ns and 10-12 ns have been previously assigned to the lifetimes of the dication and unprotonated species of TPPS, respectively [51]. Thus, both the neutral and the dicationic forms of TPPS are present in aqueous pH 5 solutions. Time-resolved fluorescence measurements on human skin fibroblasts incubated with TPPS (Fig. 6B) also showed double exponential

kinetics with lifetimes 3.7 and 14 ns, and relative amplitudes 15% and 85%, respectively. This indicates that TPPS is mainly localized in a environment with a pH around 5, a value which occurs only within the lysosomes [31]. As in the case of TMPyP, these results make us confident that TPPS is localized within the cells and mostly in a single organelle, the lysosomes in this case. Therefore, $^1O_2$ will also be generated mostly in the nucleus when TMPyP is used as sensitizer and in the lysosomes when the sensitizer is TPPS.

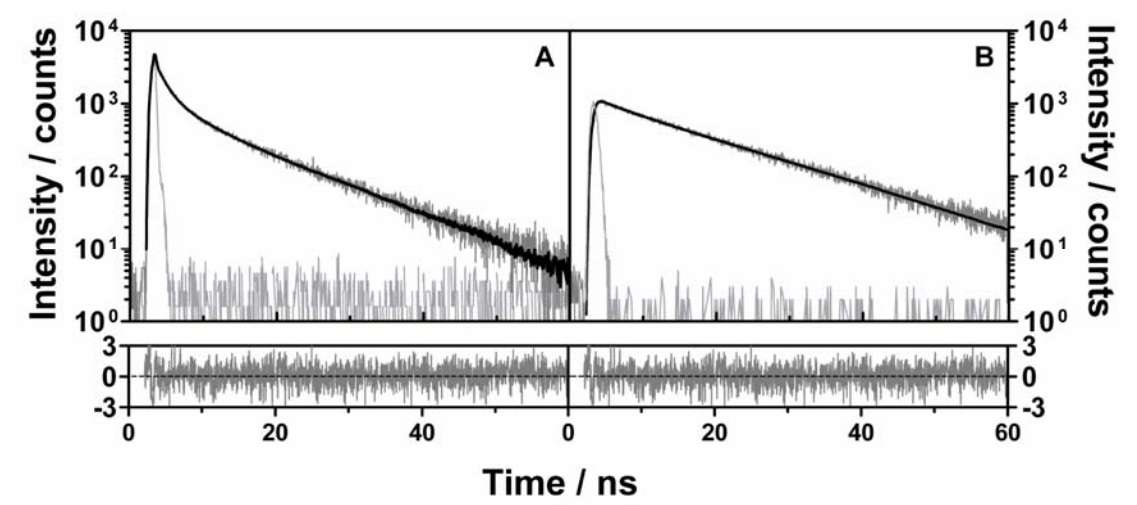

Fig. 6. Fluorescence decays of TMPyP (A) and TPPS (B) incorporated into human skin fibroblasts: decay (dark grey), fit (black) and IRF (light grey). Samples were excited at 405 and 457 nm, respectively, and fluorescence was observed at 650 nm. Solution decays are not shown for the sake of clarity. Fitted parameters: TMPyP, 1.8 ns (75%) and 11 ns (25%). TPPS, 3.7 ns (15%) and 14 ns (85%)

D. Time-resolved $^1O_2$ detection in human skin fibroblasts incubated with TMPyP. In a typical experiment, a 1-ml cell suspension containing ~50 x 10^6 cells was irradiated with 25 million laser pulses at 532 nm with a fluence of ~0.1 J·m^{-2}, *i.e.*, each cell received *ca.* 0.5 μJ of laser energy. Irradiation of TMPyP-loaded cells in D_2O-based PBS (D-PBS) produced the 1275-nm time-resolved luminescence signal shown in Fig. 7A. Only two exponentials were needed to fit the data, yielding τ_1^{D2O} = 13 ± 1 μs and τ_2^{D2O} = 24 ± 2 μs for the rise and decay of the signal, respectively. Control experiments demonstrated that $^1O_2$ was the species responsible for the luminescence in this experiment: 1) the signal disappeared when 35 mM NaN_3 was added to the cell suspension. NaN_3 is a well-known quencher of $^1O_2$ [52] that readily enters the cell from the extracellular medium [20,21]. 2) No signal could be detected at 1200 nm, where $^1O_2$ does not emit [15]. 3) Finally, the lifetime of $^1O_2$ decreased significantly when D_2O was replaced with H_2O, in agreement with the well-known isotope effects [15]. Having established that $^1O_2$ was responsible for the emission observed, we also tested whether it was produced in the cell or in the extracellular aqueous buffer by a TMPyP

molecule that might have leaked from the cell [20]. To this end, we centrifuged the cells and analyzed the supernatant fluid at 1275 nm. The absence of signal in this case makes us confident that our signals in the cell suspensions reflect the behavior of $^1O_2$ generated within the cells. This and the above control experiments were performed for all sets of experiments.

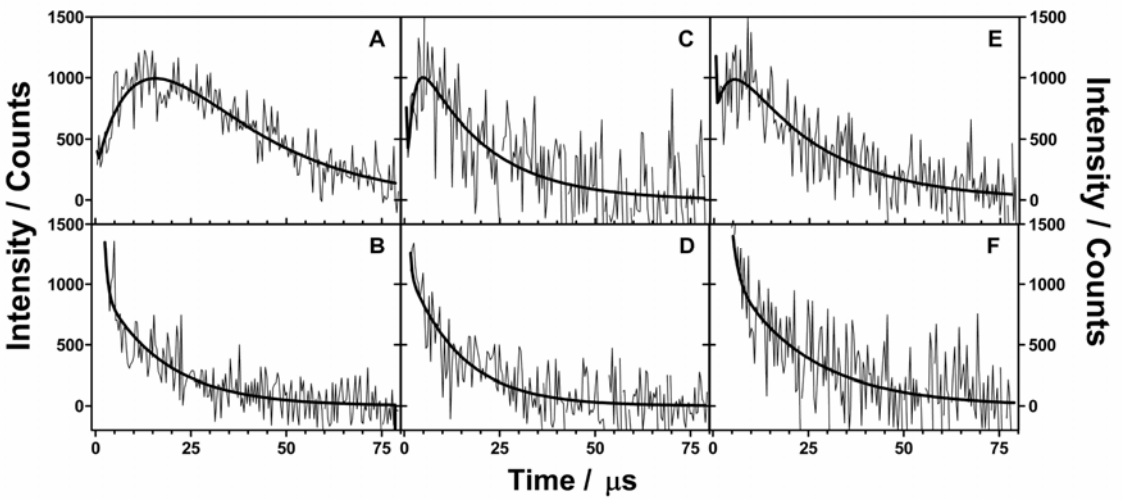

Fig. 7. Time-resolved luminescence decays recorded upon 532 nm excitation of a human fibroblast suspension, previously incubated with 100 μM TMPyP during 16 hours in the dark. **A**: 1275 nm, D_2O, fitted parameters: τ_1 = 13 ± 1 μs, τ_2 = 24 ± 2 μs; **B**: 960 nm, D_2O, fitted parameter: τ_1 = 14 ± 2 μs; **C**: 1275 nm, H_2O, fitted parameters: τ_1 = 1.7 ± 1 μs, τ_2 = 15 ± 2 μs; **D**: 960 nm, H_2O, fitted parameter: τ_1 = 14 ± 2 μs; **E**: 1275 nm, 0.77 mM BSA in D_2O, fitted parameters: τ_1 = 6 ± 2 μs, τ_2 = 13 ± 3 μs and **F**: 960 nm, 0.77 mM BSA in D_2O, fitted parameter: τ_1 = 14 ± 2 μs.

Fig. 7C shows the time-resolved $^1O_2$ phosphorescence decay of an H_2O-based cell suspension. The biexponential fit of the data yielded τ_1^{H2O} = 1.7 ± 1 μs and τ_2^{H2O} = 15 ± 2 μs, which must be compared to the values found in D_2O, τ_1^{D2O} = 13 ± 1 μs and τ_2^{D2O} = 24 ± 2 μs. In a triplet-photosensitized experiment, the time profile of $^1O_2$ phosphorescence (S_t) is given by Eq. (2) [14]:

$$S_t = S_0 \cdot \frac{\tau_\Delta}{\tau_T - \tau_\Delta} \cdot \left[\exp\left(-t/\tau_T\right) - \exp\left(-t/\tau_\Delta\right)\right], \qquad (2)$$

where S_0, a quantity proportional to the amount of $^1O_2$ formed upon pulse excitation, τ_T is the actual lifetime of the photosensitizer's triplet-state, and τ_Δ is the actual $^1O_2$ lifetime. Because the pre-exponential factor $\tau_\Delta/(\tau_T - \tau_\Delta)$ can be positive or negative depending on the sign of the difference $(\tau_T - \tau_\Delta)$, the signal rises with the shortest of the two lifetimes, be it τ_T or τ_Δ. Assuming that the rate of $^1O_2$ production is insensitive to solvent isotope effects, we identify the photosensitizer's triplet state lifetime as τ_T~ 14

μs = $\tau_1^{D2O} \approx \tau_2^{H2O}$, and therefore, $\tau_\Delta^{H2O} = \tau_1^{H2O}$ = 1.7 ± 1 μs and $\tau_\Delta^{D2O} = \tau_2^{D2O}$ ~24 μs. We thus see an inversion of the kinetics on passing from D_2O to H_2O [53]. Our $^1O_2$ lifetime in H_2O, τ_Δ^{H2O} = 1.7 ± 1 μs is comparable to the value of 600 ± 400 ns reported by Niedre *et al.* [20] and is substantially shorter than the value observed in neat H_2O, 3.2 μs [52], suggesting that a fraction of $^1O_2$ molecules are quenched by cellular components (*vide infra)*.

E. Time-resolved photosensitiser phosphorescence. A further confirmation of the lifetime assignments was obtained from phosphorescence spectroscopy taking advantage of the porphyrins' phosphorescence in the near infrared region. The luminescence of a D_2O-cell suspension, recorded at 960 nm upon 532 nm irradiation, is shown in Fig. 7B. A single exponential was enough to fit the data, yielding a lifetime of 14 ± 2 μs that matches the risetime of the $^1O_2$ emission at 1275 nm. Likewise, the phosphorescence lifetime observed in H_2O suspensions is $\tau_T^{H_2O}$ = 14 ± 2 μs, also confirming the results derived from the $^1O_2$ experiments and further supporting the assumption that the buffer change has no significant effect on the kinetics of $^1O_2$ formation.

The lifetime of the sensitizer's triplet state is significantly longer than that in air-equilibrated aqueous systems (~2 μs) [54]. Similar increases have been reported previously for several photosensitizers taken up by cells [55-57], bacteria [58] and particularly for TMPyP bound to DNA in solution [54,59], reflecting some degree of shielding of the sensitizer from oxygen quenching. Indeed, using Eq. (3):

$$k_q = \frac{1/\tau_T - 1/\tau_T^0}{[O_2]} \qquad (3)$$

where τ_T and τ_T^0 are the triplet state lifetimes in the cell suspension and in deoxygenated solution, respectively, together with $[O_2]$ = 2.8 x 10^{-4} M [60] and τ_T^0 = 165 μs [61], a value of k_q ~3 x 10^8 $M^{-1}s^{-1}$ is calculated for the rate constant of oxygen quenching of the TMPyP triplet state. This value is an order of magnitude smaller than that observed in solution and close to that published by Kruk *et al.* for TMPyP bound to DNA and various synthetic polynucleotides [54,59].

F. Singlet oxygen production quantum yield. Binding to DNA and lower oxygen accessibility to the sensitizer's triplet state may lead to a lower production of $^1O_2$. To verify this hypothesis, we measured the $^1O_2$ quantum yield of TMPyP incorporated into the cells, Φ_Δ. The S_0 parameter in Eq. (2*)*, a quantity proportional to Φ_Δ [14],

was determined by fitting Eq. (2) to the 1275 nm time-resolved phosphorescence signal. It was then compared to that produced by a reference sensitizer under the same conditions. The reference sensitizer chosen was TMPyP added to a sensitizer-free cell suspension and measured before any significant uptake by the cells could take place, as assessed by absorbance and fluorescence experiments. This recreated the same light-scattering conditions in the sample and reference suspensions. The biexponential fit of the reference signal at 1275 nm yielded lifetimes of ~4 and 67 μs for the formation and decay of $^1O_2$, respectively. These values are close to those measured for TMPyP in homogeneous D_2O solution, thus ruling out any significant quenching of $^1O_2$ by the cells in these experiments. Under the assumption that the $^1O_2$ radiative rate constant in the cells was essentially equal to that in the aqueous buffer [62], the Φ_Δ value for TMPyP incorporated into human skin fibroblasts was determined as $\Phi_\Delta = 0.3 \pm 0.1$, significantly smaller than the value in water solution ($\Phi_\Delta = 0.77$) but in agreement with values reported for TMPyP bound to DNA [54,59].

G. Diffusion of $^1O_2$ in the cells. A single lifetime τ_Δ ~24 μs was obtained for $^1O_2$ decay in a D_2O suspension of human skin fibroblasts loaded with TMPyP, similar to the lifetime τ_Δ ~ 20 μs found for TMPyP taken up by the nuclei of neurons [23]. The fact that this value is shorter than that observed in the external aqueous phase (67 μs, see the previous section *Singlet oxygen production quantum yield*) indicates that some quenching is taking place in the cell. The fact that the decay is monoexponential suggests that there is a fast diffusional exchange of $^1O_2$ between the cell and the external aqueous phase, leading to a common decay rate constant inside and outside the cells. Then, the measured lifetime of τ_Δ = 24 μs is an average between the intracellular and external buffer lifetimes.

The rate constant of $^1O_2$ decay in microheterogeneous systems under exchange equilibrium conditions, k_d, is appropriately described by Eq. (4) [63]:

$$k_d = \frac{1}{\tau_\Delta} = \frac{K_{eq} f_m k_{d,cell} + (1 - f_m) k_{d,water}}{K_{eq} f_m + (1 - f_m)} \qquad (4)$$

where $K_{eq} = \left[^1O_2\right]_{cell} / \left[^1O_2\right]_{water}$ is the partition equilibrium of $^1O_2$ between the two phases, f_m and (1-f_m) are the volume fractions of the cell and aqueous phase, respectively, and $k_{d,cell}$ and $k_{d,water}$ are the decay rate constants inside and outside the cell, respectively.

Using Eq. (4) and assuming K_{eq} ~ 1 and f_m ~ 0.15 for our suspensions with 10^7 cells/ml, the lifetime of $^1O_2$ within the cell can be estimated as $\tau_{\Delta cell}$ ~ 5 μs.

To test if $^1O_2$ produced in the nucleus is able to diffuse out the cell, we added bovine serum albumin (BSA) to the extracellular aqueous phase. BSA is an efficient $^1O_2$ quencher [52] but it is too large (~65 kDa) to penetrate the cell membrane [22]. Another popular $^1O_2$ quencher, sodium azide, could not be used for this experiment: although we found that sodium azide quenched the $^1O_2$ luminescence, it penetrates the cell membrane [20] and therefore one cannot be sure whether the quenching has taken place inside or outside the cells.

Upon addition of 0.77 mM BSA to the extracellular D_2O-based medium, a biexponential fit to the 1275 nm signal yielded τ_1 = 13 ± 3 μs and τ_2 = 6 ± 2 μs (Fig. 7E). The data recorded at 960 nm yielded a single lifetime of 14 ± 2 μs for the sensitizer triplet state, close to the value observed in the absence of BSA (Fig. 7F), thereby confirming that TMPyP and BSA are well separated [64]. The decrease of the $^1O_2$ lifetime from 24 to 6 μs confirms that $^1O_2$ molecules are able to diffuse out of the cell where they are quenched by BSA. A summary of the lifetimes recorded in all experiments is given in Table 2.

The value $\tau_{\Delta, ,cell}$ ~ 5 μs calculated above is in agreement with the $^1O_2$ lifetime measured in the presence of BSA, τ_Δ = 6 ± 2 μs, and indicates that the quenching in the cell is taking place with a pseudo-first order rate constant $k_q[Q]$ ~ 2.5 x 10^5 s^{-1}.

The efficiency of $^1O_2$ quenching, η, can be calculated by means of Eq. (5):

$$\eta = \frac{k_q[Q]}{k_q[Q] + 1/\tau_\Delta^0} \cdot 100 \qquad (5)$$

The values found are ~ 93% and ~ 42% for D_2O (τ_Δ^0 = 68 μs) and H_2O (τ_Δ^0 = 3.2 μs) cell suspensions, respectively. This indicates a substantial degree of interaction with nucleus components in the case of D_2O suspensions, and a more balanced contribution of solvent interactions for H_2O suspensions. It is remarkable that 93% quenching by cellular constituents is nevertheless compatible with $^1O_2$ diffusion outside the cell. This observation may reconcile earlier views that singlet oxygen damage is confined within short distances of its site of production [65], with the recently-proposed notion that $^1O_2$ is able to diffuse over long distances within the cells [21-24].

H. Time-resolved $^1O_2$ detection in human skin fibroblasts incubated with TPPS. The same series of experiments was repeated on a cell suspension previously incubated with TPPS, a photosensitizer that is localized mainly in the lysosomes. The results are shown in Fig. 8 and Table 2.

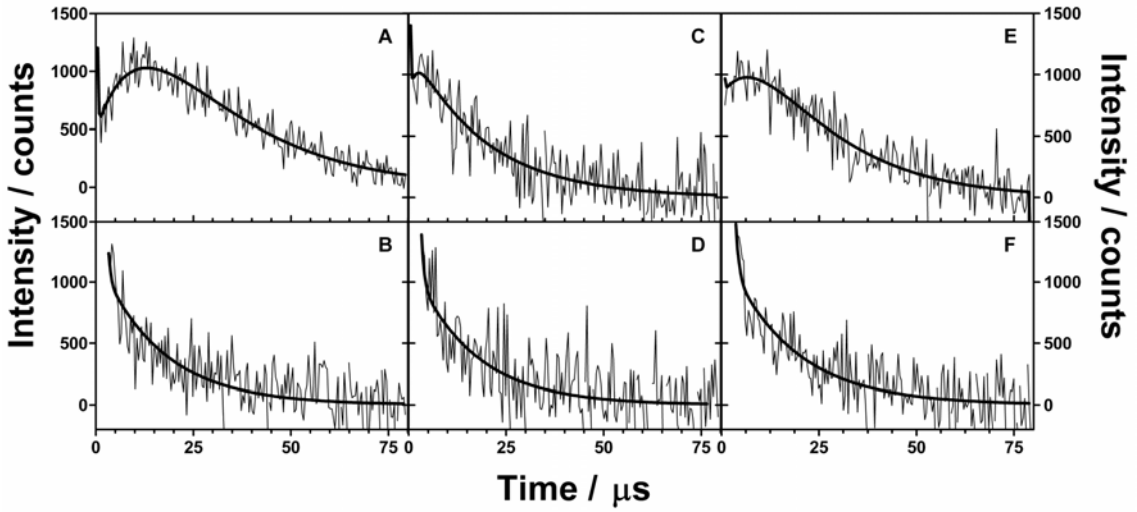

Fig. 8. Time-resolved luminescence decays recorded upon 532 nm excitation of a human fibroblast suspension previously incubated with 100 μM TPPS during 16 hours in the dark. **A**: 1275 nm, D_2O, fitted parameters: τ_1 = 14 ± 2 μs, τ_2 = 21 ± 1 μs; **B**: 960 nm, D_2O, fitted parameter: τ_1 = 19 ± 2 μs; **C**: 1275 nm, H_2O, fitted parameters: τ_1 = 1.5 ± 1 μs, τ_2 = 20 ± 1 μs and **D**: 960 nm, H_2O, fitted parameter: τ_1 = 19 ± 1 μs; **E**: 1275 nm, 0.77 mM BSA in D_2O, fitted parameters: τ_1 = 13 ± 2 μs, τ_2 = 20 ± 1 μs, and **F**: 960 nm, 0.77 mM BSA in D_2O, fitted parameter: τ_1 = 17 ± 3 μs.

In D_2O, the signal at 1275 nm showed, as in the case of TMPyP, a biexponential behavior, although in this case with $\tau_1^{D_2O}$ = 14 ± 2 μs and $\tau_2^{D_2O}$ = 21 ± 1 μs (Fig. 8A). The sensitizer's phosphorescence recorded at 990 nm (Fig. 8B) yielded a lifetime of 19 ± 2 μs for the triplet state of TPPS, therefore τ_Δ = 14 ± 2 μs under these conditions, significantly shorter than the value observed using TMPyP as photosensitizer (24 μs). The experiments performed in an H_2O-based suspensions (Fig. 8C and 8D) yielded a $^1O_2$ lifetime $\tau_\Delta^{H_2O}$ = 1.5 ± 1 μs and confirmed the lifetime of ~20 μs for the triplet state of TPPS, ten-fold longer than that observed in neat H_2O, τ_T = 1.9 μs [26]. The rate constant of triplet state quenching by molecular oxygen is now calculated as $k_q \sim 1.7 \times 10^8$ M^{-1} s^{-1} assuming τ_T^0 = 420 μs for TPPS [61]. This indicates a low accessibility of oxygen to the sensitizer's triplet state also in the lysosomes. The ability of TPPS to photoproduce $^1O_2$ in human skin fibroblasts is found to be Φ_Δ = 0.4 ± 0.1, smaller than the value in solution (Φ_Δ = 0.62) but still in the range of those for typical PDT photosensitizers.

Table 2. $^1O_2$ kinetic parameters in air-equilibrated aqueous suspensions of human skin fibroblasts[a].

Sensitizer	Solvent	τ_T / μs	τ_Δ / μs
TMPyP	D_2O	14 ± 2	24 ± 2
	D_2O / 0.77 mM BSA	14 ± 2	6 ± 2
	H_2O	15 ± 2	1.7 ± 1
TPPS	D_2O	20 ± 2	14 ± 2
	D_2O / 0.77 mM BSA	20 ± 1	13 ± 2
	H_2O	20 ± 2	1.5 ± 1

[a]Mean ± SD values from three to eight different experiments are shown.

Upon addition of a 0.77 mM BSA solution (Fig. 8E and 8F), and in contrast to TMPyP-loaded cells, both lifetimes remained essentially constant, *i.e.*, τ_Δ = 13 ± 2 μs and τ_T = 20 ± 1 μs, which indicates that $^1O_2$ is not able to diffuse out of the cell when it is photosensitized in the lysosomes. Thus, the measured lifetime τ_Δ = 13 ± 2 μs indeed reflects the $^1O_2$ lifetime within the cell. The fact that it is different from that observed with TMPyP indicates that the actual lifetime of $^1O_2$ within a cell is an average of those of the different cell compartments through which it diffuses. Quenching in the cell occurs now with a rate constant k_q'[Q'] ~ 7 x 10^4 s^{-1}, and the effcicieny of $^1O_2$ quenching is ~83% and ~20% for for D_2O and H_2O cell suspensions, respectively.

Using the Einstein-Smoluchowski Eq. (6) and a diffusion coefficient D = 2·x 10^{-5} cm^2 s^{-1} for oxygen in water [65], assumed to be valid for $^1O_2$ as well, one can roughly estimate that $^1O_2$ may diffuse a distance up to δ ~0.4 – 0.9 μm in D_2O-based cells before being completely deactivated (t = 5τ_Δ).

$$\delta = \sqrt{6Dt} \qquad (6)$$

Considering a human skin fibroblast cell diameter of 10-30 μm, one should expect that $^1O_2$ generated inside the cells should stay within the cells. Moreover, taking into account the dimensions of typical cell organelles (lysosomes, 50-500 nm; mitochondria, ~500 nm; nucleus, ~5 μm), $^1O_2$ is expected to spend most of its lifetime within the organelle where it has been generated. Only if $^1O_2$ is photosensitized near the outer membrane of the cell (typical membrane thickness <10 nm), it can be expected to diffuse into the extracellular medium. As shown in Fig. 3, the nucleus of the human skin fibroblasts is clearly located close to the

plasma membrane whereas lysosomes are distributed throughout the cytoplasm. This may explain why $^1O_2$ produced in the nucleus can leave the cells while $^1O_2$ produced in the lysosomes cannot.

4.4. CONCLUSIONS

Data obtained with an ultrasensitive near-infrared spectrometer with submicrosecond time resolution show that the lifetime of $^1O_2$ within human skin fibroblasts is in the microsecond range under physiological conditions and that it strongly depends on the organelle where $^1O_2$ has been generated. Notwithstanding, $^1O_2$ is mostly deactivated by cellular constituents, particularly when it is generated in the lysosomes. This reconciles the apparently conflicting observations that $^1O_2$-induced damage is highly localized, while its lifetime is long enough to diffuse up to 1 μm across the cell.

4.5. REFERENCES

[1] Martindale, J. L.; Holbrook, N. J. Cellular response to oxidative stress: Signaling for suicide and survival. *J. Cell. Physiol.* **192**:1-15; 2002.

[2] Michaeli, A.; Feitelson, J. Reactivity of singlet oxygen toward amino acids and peptides. *Photochem. Photobiol.* **59(3)**:284-289; 1994.

[3] Michaeli; A.; Feitelson, J. Reactivity of singlet oxygen toward large peptides. *Photochem. Photobiol.* **61(3)**:255-260; 1995.

[4] Stark, G. Functional consequences of oxidative membrane damage. *J. Membr. Biol.* **205**:1-16; 2005.

[5] Ravanat, J. L.; Di Mascio, P.; Martinez, G. R.; Medeiros, M. H. G.; Cadet, J. Singlet oxygen induces oxidation of cellular DNA. *J. Biol. Chem.* **275**:40601-40604; 2000.

[6] Dougherty, T. J.; Gomer, C. J.; Henderson, B. W.; Jori, G.; Kessel, D.; Korbelik, M.; Moan, J.; Peng, Q. Photodynamic therapy. *J. Natl. Cancer Inst.* **90**:889-905; 1998.

[7] Dougherty, T. J. An update on photodynamic therapy applications. *J. Clin. Laser. Med. & Surg.* **20**:3-7; 2002.

[8] Dolmans, D. E. J. G.; Fukumura, D.; Jain, R. K. Photodynamic therapy for cancer. *Nat. Rev. Cancer* **3**:380-387; 2003.

[9] Kalka, K.; Merk, H.; Mukhtar, H. Photodynamic therapy in dermatology. *J. Am. Acad. Dermatol.* **42**:389-413; 2000.

[10] Fritsch, C.; Goerz, G.; Ruzicka, T. Photodynamic therapy in dermatology. *Arch. Dermatol.* **134**:207-214; 1998.

[11] Allen, C. M.; Weber, J. M.; Van Lier, J. E. Sulfophthalocyanines for photodynamic inactivation of viruses in blood products: effect of structural modification. *Photochem. Photobiol.* **62**:184-189; 1995.

[12] Malik, Z.; Hanania, J.; Nitzan, Y. Bactericidal effects of photoactivated porphyrins - an alternative approach to antimicrobial drugs. *J. Photochem. Photobiol. B:Biol.* **5**:281-293; 1990.

[13] Gaspard, S.; Tempête, C.; Werner, G. H. Studies on photoinactivation by various phthalocyanines of a free or replicating non-enveloped virus. *J. Photochem. Photobiol. B:Biol.* **31**:159-162; 1995.

[14] Nonell, S.; Braslavsky, S. E. Time-resolved singlet oxygen detection. In: Packer, L.; Sies, H. eds. *Singlet oxygen, UV-A, and Ozone. Methods in Enzymology, vol.319*. San Diego: Academic Press; 2000:37-49.

[15] Schweitzer, C.; Schmidt, R. Physical mechanisms of generation and deactivation of singlet oxygen. *Chem. Rev.* **103**:1685-1757; 2003.

[16] Moan, J.; Berg, K. The photodegradation of porphyrins in cells can be used to estimate the lifetime of singlet oxygen. *Photochem. Photobiol.* **53**:549-553; 1991.

[17] Baker, A.; Kanofsky, J. R. Quenching of singlet oxygen by biomolecules from L1210 leukemia cells. *Photochem. Photobiol.* **55**:523-528; 1992.

[18] Baker, A.; Kanofsky, J. R. Direct observation of singlet oxygen phosphorescence at 1270 nm from L1210 leukemia cells exposed to polyporphyrin and light. *Arch. Biochem. Biophys.* **286**:70-75; 1991.

[19] Baker, A.; Kanofsky, J. R. Time-resolved studies of singlet-oxygen emission from L1210 leukemia cells labelled with 5-(*N*-hexadecanoyl)amino eosin. A comparison with a one-dimensional model of singlet-oxygen diffusion and quenching. *Photochem. Photobiol.* **57**:720-727; 1993.

[20] Niedre, M.; Patterson, M. S.; Wilson, B. C. Direct near-infrared luminiscence detection of singlet oxygen generated by photodynamic therapy in cells *in vitro* and tissues *in vivo*. *Photochem. Photobiol.* **75**:382-391; 2002.

[21] Skovsen, E.; Snyder, J. W.; Lambert, J. D. C.; Ogilby, P. R. Lifetime and diffusion of singlet oxygen in a cell. *J. Phys. Chem. B* **109**:8570-8573; 2005.

[22] Snyder, J. W.; Skovsen, E.; Lambert, J. D. C.; Ogilby, P. R. Subcellular, time-resolved studies of singlet oxygen in single cells. *J. Am. Chem. Soc.* **127**:14558-14559; 2005.

[23] Snyder, J. W.; Skovsen, E.; Lambert, J. D. C.; Poulsen, L.; Ogilby, P. R. Optical detection of singlet oxygen from single cells. *Phys. Chem. Chem. Phys.* **8**:4280-4293; 2006.

[24] Hatz, S.; Lambert, J. D. C.; Ogilby, P. R. Measuring the lifetime of singlet oxygen in a single cell: addressin the issue of cell viability. *Photochem. Photobiol. Sci.* **6**:1106-1116; 2007.

[25] Villanueva, A.; Caggiari, L.; Jori, G.; Milanesi, C. Morphological aspects of an experimental tumor photosensitized with a mesosubstituted aationic porphyrin. *J. Photochem. Photobiol. B:Biol.* **23**:49-56; 1994.

[26] Dedic, R.; Molnar, A.; Korinek, M.; Svoboda, A.; Psencik, J.; Hala, J. Spectroscopic study of singlet oxygen photogeneration in meso-tetra-sulphonatophenyl-porphin. *J. Lumin.* **108**:117-119; 2004.

[27] Wilkinson, F.; Helman, W. P.; Ross, A. B. Quantum yields for the photosensitized formation of the lowest electronically excited singlet state of molecular oxygen in solution. *J. Phys. Chem. Ref. Data* **22**:113-262; 1993.

[28] Villanueva, A.; Juarranz, A.; Díaz, V.; Gómez, J.; Cañete, M. Photodynamic effects of a cationic mesosubstituted porphyrin in cell cultures. *Anti-Cancer Drug Des.* **7**:297-303; 1992.

[29] Juarranz, A.; Villanueva, A.; Cañete, M.; Stockert, J. C. Fluorescent porphyrin counterstaining of chromatin DNA in conjunction with immunofluorescence methods using FITC-labelled antibodies. *J. Microsc.* **182**:46-49; 1996.

[30] Berg, K.; Western, A.; Bommer, J. C.; Moan, J. Intracellular-localization of sulfonated meso-tetraphenylporphines in a human carcinoma cell-line. *Photochem. Photobiol.* **52**:481-487; 1990.

[31] Wessels, J. M.; Strauss, W.; Seidlitz, H. K.; Ruck, A.; Schneckenburger, H. Intracellular-localization of meso-tetraphenylporphine tetrasulfonate probed by time-resolved and microscopic fluorescence spectroscopy. *J. Photochem. Photobiol. B:Biol.* **12**:275-284; 1992.

[32] Strauss, W. S. L.; Gschwend, M. H.; Sailer, R.; Schneckenburger, H.; Steiner, R.; Ruck, A. Intracellular fluorescence behavior of meso-tetra(4-sulphonatophenyl)porphyrin during photodynamic treatment at various growth phases of cultured-cells. *J. Photochem. Photobiol. B:Biol.* **28**:155-161; 1995.

[33] Schneckenburger, H.; Gschwend, M. H.; Sailer, R.; Ruck, A.; Strauss, W. S. L. Time-resolved pH-dependent fluorescence of hydrophilic porphyrins in solution and in cultivated cells. *J. Photochem. Photobiol. B:Biol.* **27**:251-255; 1995.

[34] Malik, Z.; Amit, I.; Rothmann, C. Subcellular localization of sulfonated tetraphenyl porphines in colon carcinoma cells by spectrally resolved imaging. *Photochem. Photobiol.* **65**:389-396; 1997.

[35] Noodt, B. B.; Berg, K.; Stokke, T.; Peng, Q.; Nesland, J. M. Different apoptotic pathways are induced from various intracellular sites by tetraphenylporphyrins and light. *Br. J. Cancer* **79**:72-81; 1999.

[36] Juarranz, A.; Villanueva, A.; Díaz, V.; Cañete, M. Photodynamic effects of the cationic porphyrin, meso-tetra-4-(*N*-methylpyridyl)porphine, on microtubules of HeLa cells. *J. Photochem. Photobiol. B:Biol.* **27**:47-53; 1995.

[37] Santoro, O.; Bandieramonte, G.; Melloni, E.; Marchesini, R.; Zunino, F.; Lepera, P.; Depalo, G. Photodynamic therapy by topical meso-tetraphenylporphinesulfonate tetrasodium salt administration in superficial basal-cell carcinomas. *Cancer Res.* **50**:4501-4503; 1990.

[38] Fiel, R. J. Porphyrin - nucleic-acid interactions: a review. *J. Biomol. Struct. Dyn.* **6**:1259-1275; 1989.

[39] Pasternack, R. F.; Gibbs, E. J.; Villafranca, J. J. Interactions of porphyrins with nucleic-acids. *Biochemistry* **22**:5409-5417; 1983.

[40] Pasternack, R. F.; Gibbs, E. J.; Villafranca, J. J. Interactions of porphyrins with nucleic-acids. *Biochemistry* **22**:2406-2414; 1983.

[41] Borissevitch, I. E.; Tominaga, T. T.; Schmitt, C. C. Photophysical studies on the interaction of two water-soluble porphyrins with bovine serum albumin. Effects upon the porphyrin triplet state characteristics. *J. Photochem. Photobiol. A:Chem.* **114**:201-207; 1998.

[42] Chirvony, V. S. Primary photoprocesses in cationic 5,10,15,20-meso-tetrakis(4-*N*-methylpyridiniumyl)porphyrin and its transition metal complexes bound with nucleic acids. *J. Porphyrins Phthalocyanines* **7**:766-774; 2003.

[43] Lee, S.; Jeon, S. H.; Kim, B. J.; Han, S. W.; Jang, H. G.; Kim, S. K. Classification of CD and absorption spectra in the Soret band of H_2TMPyP bound to various synthetic polynucleotides. *Biophys. Chem.* **92**:35-45; 2001.

[44] Pasternack, R. F.; Bustamante, C.; Collings, P. J.; Giannetto, A.; Gibbs, E. J. Porphyrin assemblies on DNA as studied by a resonance light-scattering technique. *J. Am. Chem. Soc.* **115**:5393-5399; 1993.

[45] Sari, M. A.; Battioni, J. P.; Dupre, D.; Mansuy, D.; Lepecq, J. B. Interaction of cationic porphyrins with DNA: importance of the number and position of the charges and minimum structural requirements for intercalation. *Biochemistry* **29**:4205-4215; 1990.

[46] Pasternack, R. F.; Garrity, P.; Ehrlich, B.; Davis, C. B.; Gibbs, E. J.; Orloff, G.; Giartosio, A.; Turano, C. The influence of ionic-strength on the binding of a water-soluble porphyrin to nucleic-acids. *Nucleic Acids Res.* **14**:5919-5931; 1986.

[47] Borissevitch, I. E.; Gandini, S. C. M. Photophysical studies of excited-state characteristics of meso-tetrakis (4-*N*-methyl-pyridiniumyl) porphyrin bound to DNA. *J. Photochem. Photobiol. B:Biol.* **43**:112-120; 1998.

[48] Lee, S.; Lee, Y. A.; Lee, H. M.; Lee, J. Y.; Kim, D. H.; Kim, S. K. Rotation of periphery methylpyridine of meso-tetrakis(n-*N*-methylpyridiniumyl)porphyrin (n=2, 3, 4) and its selective binding to native and synthetic DNAs. *Biophys. J.* **83**:371-381; 2002.

[49] Ford, K.; Fox, K. R.; Neidle, S.; Waring, M. J. DNA-sequence preferences for an intercalating porphyrin compound revealed by footprinting. *Nucleic Acids Res.* **15**:2221-2234; 1987.

[50] De Paoli, V. M.; De Paoli, S. H.; Borissevitch, L. E.; Tedesco, A. C. Fluorescence lifetime and quantum yield of $TMPyPH_2$ associated with micelles and DNA. *J. All. Comp.* **344**:27-31; 2002.

[51] Harriman, A.; Richoux, M. C. Luminescence of porphyrins and metalloporphyrins VIII. Luminescence and hydrogen photogeneration from porphyrin conjugate diacids. *J. Photochem.* **27**:205-214; 1984.

[52] Wilkinson, F.; Helman, W. P.; Ross, A. B. Rate constants for the decay and reactions of the lowest electronically excited singlet state of molecular oxygen in solution. An expanded and revised compilation. *J. Phys. Chem. Ref. Data* **24**:663-1021; 1995.

[53] Parker, J. G.; Stanbro, W. D. Dependence of photosensitized singlet oxygen production on porphyrin structure and solvent. In: Doiron, D. R.; Gomer, C. J. eds. *Porphyrin localization and treatment of tumors*. New York: Alan R. Liss; 1984:259-284.

[54] Kruk, N. N.; Shishporenok, S. I.; Korotky, A. A.; Galievsky, V. A.; Chirvony, V. S.; Turpin, P.-Y. Binding of the cationic 5,10,15,20-tetrakis(4-*N*-methylpyridyl)porphyrin at 5'CG3' and 5'GC3' sequences of hexadeoxyribonucleotides: triplet-triplet transient absorption, steady-state and time-resolved fluorescence and resonance Raman studies. *J. Photochem. Photobiol. B:Biol.* **45**:67-74; 1998.

[55] Aveline, B. M.; Hasan, T.; Redmond, R. W. The effects of aggregation, protein binding and cellular incorporation on the photophysical properties of benzoporphyrin derivative monoacid ring A (BPDMA). *J. Photochem. Photobiol. B:Biol.* **30**:161-169; 1995.

[56] Truscott, T. G.; McLean, A. J.; Phillips, A. M. R.; Foulds, W. S. Detection of hematoporphyrin derivative and hematoporphyrin excited-states in cell environments. *Cancer Lett.* **41**:31-35; 1988.

[57] Firey, P. A.; Jones, T. W.; Jori, G.; Rodgers, M. A. J. Photoexcitation of zinc phthalocyanine in mouse myeloma cells: the observation of triplet states but not of singlet oxygen. *Photochem. Photobiol.* **48**:357-360; 1988.

[58] Maisch, T.; Baier, J.; Franz, B.; Maier, M.; Landthaler, M.; Szeimies, R. M.; Baumler, W. The role of singlet oxygen and oxygen concentration in photodynamic inactivation of bacteria. *Proc. Natl. Acad. Sci. USA* **104**:7223-7228; 2007.

[59] Kruk, N. N.; Dzhagarov, B. M.; Galievsky, V. A.; Chirvony, V. S.; Turpin, P.-Y. Photophysics of cationic 5,10,15,20-tetrakis-(4-*N*-methylpyridyl)porphyrin bound to DNA, [poly (dA-dT)]$_2$ and [poly(dG-dC)]$_2$: interaction with molecular oxygen studied by porphyrin triplet-triplet absorption and singlet oxygen luminiscence. *J. Photochem. Photobiol. B:Biol.* **42**:181-190; 1998.

[60] Murov, S. L.; Carmichael, I.; Hug, G. L. *Handbook of Photochemistry*: New York: Marcel Dekker; 1993.

[61] Kalyanasundaram, K.; Neumann-Spallart, M. Photophysical and redox properties of water-soluble porphyrins in aqueous media. *J. Phys. Chem.* **86**:5163-5169; 1982.

[62] Scurlock, R. D.; Nonell, S.; Braslavsky, S. E.; Ogilby, P. R. Effect of solvent on the radiative decay of singlet molecular oxygen ($^1\Delta_g$). *J. Phys. Chem.* **99**:3521-3526; 1995.

[63] Lee, P. C.; Rodgers, M. A. J. Singlet molecular-oxygen in micellar systems: distribution equilibria between hydrophobic and hydrophilic compartments. *J. Phys. Chem.* **87**:4894-4898; 1983.

[64] Davila, J.; Harriman, A. Photoreactions of macrocyclic dyes bound to human serum albumin. *Photochem. Photobiol.* **51**:9-19; 1990.

[65] Moan, J. On the diffusion length of singlet oxygen in cells and tissues. *J. Photochem. Photobiol. B:Biol.* **6**:343-347; 1990.

Chapter 5

Singlet Oxygen Photosensitisation by GFP-like Proteins

The photosensitisation of reactive oxygen species, in particular singlet oxygen ($^1O_2$), by proteins from the green fluorescent protein (GFP) family influences important processes such as photobleaching and genetically-targeted chromophore-assisted light inactivation (CALI). In this chapter, an investigation of $^1O_2$ photoproduction by several GFPs using time-resolved detection of the NIR phosphorescence of $^1O_2$ is reported. The results are compared with those obtained for the model compound of the enhanced-GFP fluorophore to provide important information about the role played by the tertiary structure of the protein.

The work described in this chapter is adapted from A. Jimenez-Banzo, S. Nonell, J. Hofkens and C. Flors in *Biophys. J.* **2008**, *94* (1), 1-5, and was presented at the 12th Congress of the European Society for Photobiology, Bath (England), September 2007, and at the 52nd Biophysical Annual Meeting and 16th International Biophysics Congress, Long Beach (USA), February 2008.

5.1. INTRODUCTION

Green Fluorescent Protein (GFP) was discovered by Shimomura *et al.* [1] as a companion protein to aequorin, the famous chemiluminescent protein from *Aequorea victoria* jellyfish. In a footnote to their account of aequorin purification, they noted that "*a protein giving solutions that look slightly greenish in sunlight through only yellowish under tungsten lights, and exhibiting a very bright, greenish fluorescence in the ultraviolet of a Mineralite, has also been isolated from squeezates*". GFPs exist in a variety of coelenterates, both hydrozoa such as *Aequorea*, *Obelia*, and *Phialidium*, and anthozoa such as *Renilla* [2], but unfortunately, *Aequorea* GFP genes are the only GFP genes that have been cloned nowadays.

GFP has a unique can-like shape consisting of an 11-strand β-barrel with a single α-helical strand containing the chromophore almost perfectly buried in the centre of the β-can (Fig. 1). The chromophore is a *p*-hydroxybenzylideneimidazolinone [3,4] formed from residues 65–67, which are Ser-Tyr-Gly in the native protein. Fig. 2 shows the currently accepted mechanism [5-7] for chromophore formation, which occurs in a series of discrete steps, referred as *maturation*.

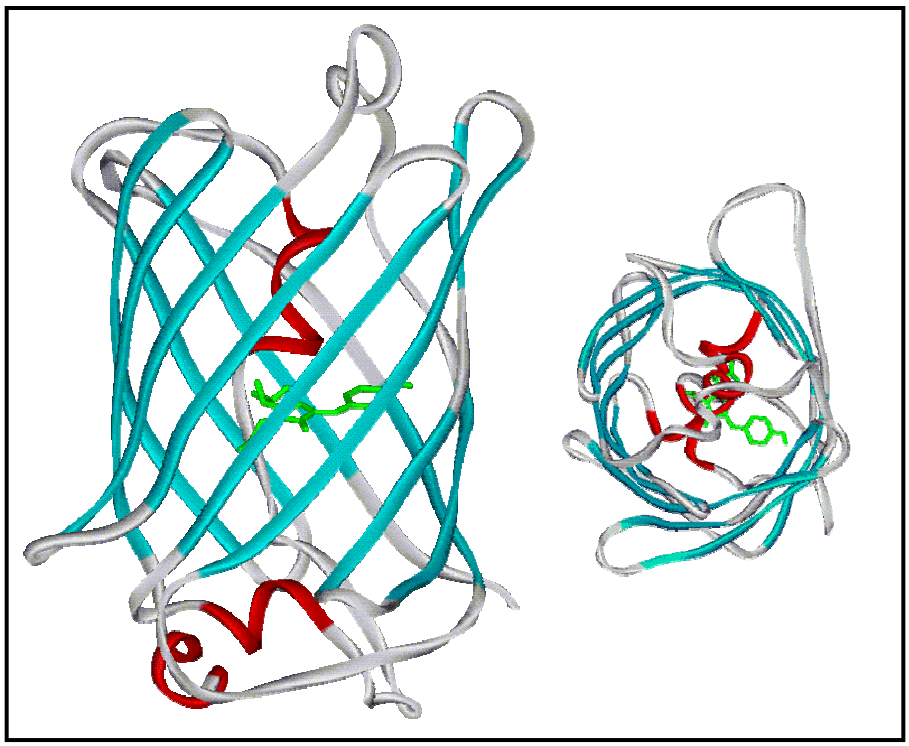

Fig. 1: Three-dimensional structure of GFP, showing 11 β-strands forming a hollow cylinder through which is threaded a helix bearing the chromophore (light green).

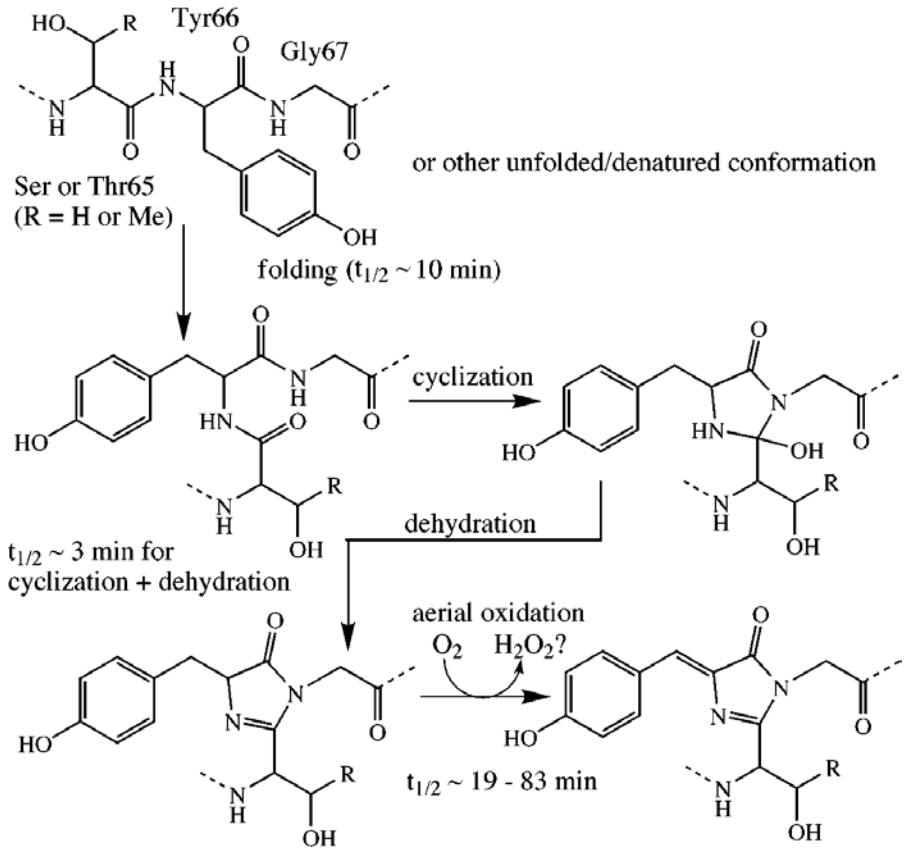

Fig. 2: proposed mechanism for the intramolecular biosynthesis of the GFP chromophore [8].

Since its discovery, the green fluorescent protein from the jellyfish *Aequorea Victoria* has vaulted from obscurity to become one of the most widely studied and exploited proteins in biochemistry and cell biology. Indeed, GFPs have become popular as genetically encoded reporters for intracellular dynamics, protein expression and protein-protein interaction studies based on fluorescence microscopy [9,10]. However, extended observation of GFPs is limited by photobleaching/photoconversion of the chromophore or light-induced damage of the surrounding biological medium. Photoproduction of reactive oxygen species (ROS) can play a role in this limitation [11]. Photosensitized singlet oxygen ($^1O_2$) has indeed been detected in GFP-expressing *E.coli* bacteria and kidney cells by means of electron spin resonance [12]. $^1O_2$ is a highly reactive ROS that is potentially damaging to biological systems. In proteins, damage is mainly directed to cysteine, histidine, methionine and tryptophan residues [13]. The photoinduced formation of $^1O_2$ mainly involves energy transfer from a photosensitiser with a suitable triplet energy level. Although photooxidation by $^1O_2$ is not the main photobleaching pathway in GFPs, its influence in the process has been evidenced [14].

Photosensitisation of $^1O_2$ by GFP-like proteins is not only regarded as a negative factor affecting its performance in fluorescence microscopy, but it can also be of great use in genetically-targeted chromophore-assisted light inactivation (CALI) [15]. CALI consists in the illumination of a photosensitiser-tagged molecule to produce $^1O_2$ and specifically inactivate a target. It has been shown that it is possible to use GFP derivatives for this purpose [16-18]. Moreover, GFPs have been mutated with the particular goal of generating ROS for photodestruction of cells. Very recently, Lukyanov *et al.* have developed KillerRed, a fully genetically encoded photosensitiser derived from the GFP-like hydrozoan chromoprotein anm2CP [19]. According to the authors, KillerRed inactivates efficiently *E. coli* and eukaryotic cells, and $^1O_2$ has been identified as the main species responsible for its phototoxicity.

Despite the interest generated by the capability of GFPs to act as photosensitisers [9,10], very few studies have addressed this topic. In this chapter, the investigation of $^1O_2$ photosensitisation by GFP-like proteins by means of time-resolved detection of the NIR phosphorescence (TRPD) of $^1O_2$ at 1275 nm [20] is reported. The results with those on the fluorophore 4-hydroxybenzylidene-1,2-dimethylimidazoline (HBDI) [21] are compared. This comparison may assist in the estimation of the effect of the protein scaffold on the photosensitisation properties.

5.2. EXPERIMENTAL SECTION

***Materials*:** HBDI was synthesized as described previously (purity > 95%) (14). The EGFP vector was purchased from Clontech Laboratories Inc (Mountain View, CA) and KillerRed vector was from Evrogen (Moscow, Russia). GFPmut2 and H148G proteins were kindly provided by Prof. Viappiani from Parma University. The measurements were performed in D_2O (SdS, Solvents Documentation Synthesis, Peypin, France) buffered solutions, since deuterium greatly enhances the $^1O_2$ lifetime and thus makes its detection easier. Thus, all the HBDI experiments were carried out in D_2O buffered solutions, while all the GFPs experiments were performed in 1:2 or 1:3 mixtures of PBS and deuterated PBS (D-PBS) or deuterated CHES (D-CHES).

HBDI samples were contained in squared 1 cm optical path fused silica cuvettes (Hellma 101-QS) whereas protein solutions were contained in rectangular 1x0.4x3.5 cm fused silica cuvettes (Hellma QS-117.104F), and were centrifuged before use. The concentration of the samples was adjusted to produce an absorbance at the excitation wavelength close to 0.1.

5.3. RESULTS AND DISCUSSION

A. HBDI chromophore. After the GFP chromophore was identified as *p*-hydroxybenzylideneimidazolodinone, the synthetic analog HBDI has been the subject of study of many groups. This compound is essentially non-fluorescent in solution, presumably due to effective internal conversion processes [22-25], but a ~10^4 enhancement in its fluorescence quantum yield is observed when the chromophore is attached to the protein and buried in the centre of the β-can.

The absorption spectra of HBDI in NaOH 1M (anionic form) and phosphate-citrate buffer 50 mM pH 5.0 (neutral form) are shown in Fig. 3.

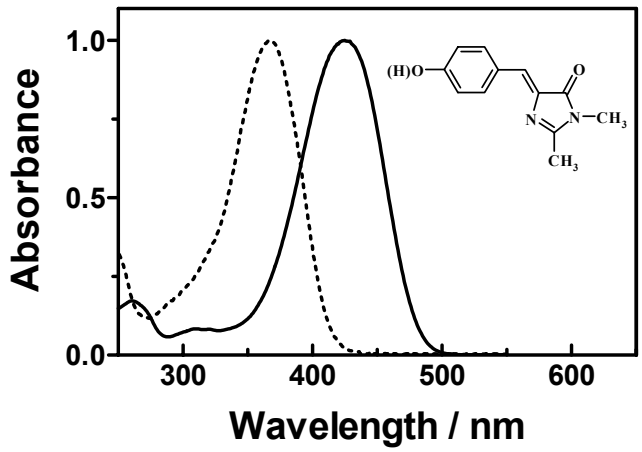

Fig. 3: Normalized absorption spectra of the anionic form of HBDI in NaOH 1M (*continuous line*) and neutral form in phosphate-citrate buffer pH 5.0 (*dotted line*).

Upon irradiation at 355 nm of the model compound HBDI in anionic form, we were able to detect a signal at 1275 nm, which grows with a lifetime of around 3 μs and decays in 20 μs (Fig. 4). The spectrum of the 20-μs component matches that of $^1O_2$ phosphorescence (inset Fig. 4), which strongly suggests that this component represents the $^1O_2$ lifetime. Upon addition of the $^1O_2$ quencher sodium azide (6 mM), the lifetime decreased from 20 to ~5 μs, consistent with a quenching constant, k_q, of 5-$9 \cdot 10^7$ $M^{-1} \cdot s^{-1}$ in basic pH [26], which further supports its assignment to the decay of $^1O_2$ phosphorescence.

The 20 μs lifetime is shorter than the natural lifetime of $^1O_2$ in D_2O (67 μs, [26]), suggesting partial quenching by HBDI. We attribute the 3-μs rise to the formation of $^1O_2$ with the lifetime of the triplet state of anionic HBDI. Irradiation of the neat solvent in the same conditions did not produce any signal at 1275 nm which further supports that singlet oxygen is produced by the HBDI sample.

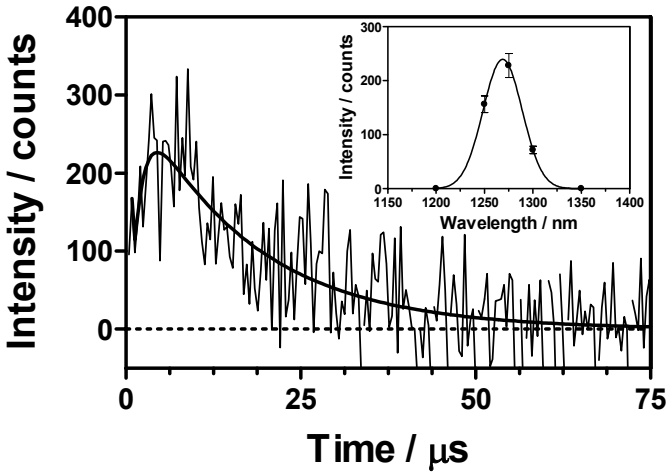

Fig. 4: $^1O_2$ signal photosensitized by HBDI in the anionic form. A solution of HBDI in NaOH 1M was irradiated with 20 million laser pulses at 355 nm and the concomitant phosphorescence of $^1O_2$ was detected at 1275 nm (100 ns per channel). The signal was fitted by Eq. (1) with lifetimes of 2 μs and 17 μs for the rise and decay, respectively. **Inset:** $^1O_2$ phosphorescence spectra obtained from the intensity of the signal at different wavelengths.

We cannot rigorously exclude the possibility of an impurity in the sample being the actual photosensitiser; however that impurity should compete effectively with HBDI for the incoming photons and have the same pH behaviour as HBDI. As the purity of the HBDI sample was higher than 95%, we judge this combination of factors unlikely. It is worth noting that basic HBDI solutions are very unstable and experiments were performed on freshly prepared samples. Furthermore, we verified that the degradation product(s) did not contribute to the signal at 1275 nm by carrying out the following two experiments: in the first one, we monitored the intensity of the signal with time and upon extended irradiation of the solution. After light doses 10-fold larger than those used in the previous experiments, the variations of intensity were below 20%. In the second series of experiments, we repeated the measurements in a mixture of acetonitrile/methanol (4:1) with 10 mM NaOH added. This produced better $^1O_2$ signals, owing to the larger radiative rate constant in this medium, and allowed us to decrease the number of laser pulses by a factor of 5. The stability of HBDI was also higher in this less-polar and less-protic solvent. The extent of sample degradation was now less than 10% and under these conditions we measured a quantum yield of singlet oxygen Φ_Δ= 0.003 ± 0.001, close to the value in D_2O (Φ_Δ= 0.004, see below). Thus, we can safely rule out a degradation product as the actual $^1O_2$ photosensitiser.

To quantify the quantum yield of $^1O_2$ photosensitisation (Φ_Δ), defined as the number of photosensitized $^1O_2$ molecules per absorbed photon, the phosphorescence intensity at time zero, *S(0)*, was compared to that produced by an optically-matched reference in

the same solvent and at the same excitation wavelength and intensity. *S*(0), a quantity proportional to Φ_Δ was determined by fitting Eq. 1 to the time-resolved phosphorescence intensity at 1270 nm.

$$S(t) = S(0)\left(e^{-t/\tau_T} - e^{-t/\tau_\Delta}\right)\tau_\Delta/(\tau_T - \tau_\Delta) \qquad (1)$$

For the isolated anionic chromophore HBDI (in NaOH 1M in D_2O), Φ_Δ = 0.004 ± 0.001 (*vs* sulfonated phenalenone in the same solvent, Φ_Δ = 1 [27]). The value of Φ_Δ not only provides information about the efficiency of $^1O_2$ photosensitisation, but also represents a lower limit for the intersystem crossing quantum yield in HBDI. We found the same Φ_Δ value in acetonitrile/methanol (4:1) with 10 mM NaOH added.

For neutral HBDI, we found biexponential decaying signals (3 and 0.6 μs) in the range 950-1350 nm. However, the spectra of none of the components resembled that of $^1O_2$ phosphorescence, and neither their lifetime nor their intensity was affected by saturation with Ar or O_2. Thus, no $^1O_2$ was detected in this case.

B. Enhanced Green Fluorescent Protein (EGFP). Mutation of Ser 65 in wt-GFP by Thr stabilises the phenolate anion of the chromophore, resulting in the suppression of the neutral phenol 395-nm excitation peak and the five- to six fold amplitude enhancement, as well as a red shift to 490 nm, for the anionic peak. The most relevant protein from this family of GFPs (class 2 mutants) is EGFP.

The absorption spectra of EGFP in PBS 50 mM buffer pH 7.4 is shown in Fig. 5. (Note that respect to HBDI in solution, the chromophore in the protein environment exhibits a ~ 40 nm bathochromic shift).

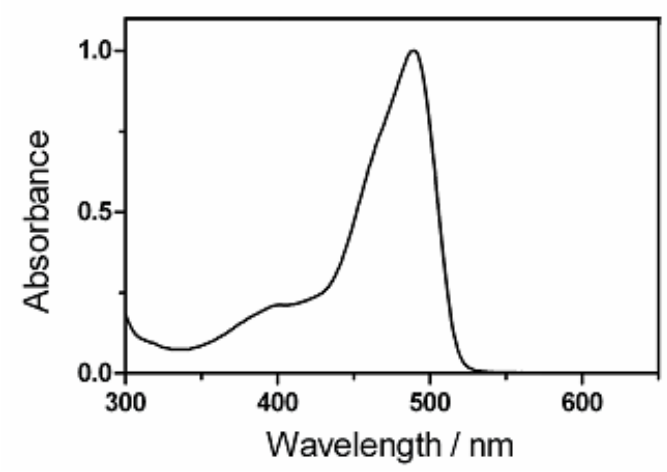

Fig. 5: Normalized absorption spectra of EGFP in PBS buffer pH 7.4.

Irradiation of EGFP in a mixture of PBS and D-PBS (1:3) required a high protein concentration (~0.2 mM) in order to get the appropriate signal to noise ratio for $^1O_2$ detection in time-resolved mode. This might induce some protein aggregation. The signal at 1275 nm shows, as in the case of anionic HBDI, a rise followed by a decay, with components of about τ_1 = 4 μs and τ_2 = 25 μs, respectively (Fig. 6A). It is tempting to directly assign these lifetimes to the formation and decay of $^1O_2$, as above. However, it is worth noting that the pre-exponential factors of both components were different, *i.e.*, the signal could not be fitted by Eq. (1), and that the spectrum of the long component does not match that of the phosphorescence of $^1O_2$. On the other hand, the 4-μs component only appeared at 1275 nm, suggesting that it is indeed related to $^1O_2$.

Experiments performed in 1100-1300 nm region revealed the presence of a kinetic component of 25 μs, which also contributes to the detected signal at 1275 nm. In an attempt to isolate the $^1O_2$ signal, our approach was to normalize the signals at 1275 and 1100 nm (Figs. 6A and 6B) and subtract the latter from the former (see the Annex of this chapter). The resulting signal could then be fitted by Eq. (1), and rises in 4 μs and decays in 25 μs (Fig. 6C). Note that, according to Eq. (1), the signal rises with the lifetime τ_Δ when $\tau_T > \tau_\Delta$, as the pre-exponential factor is positive in this case.

The addition of azide (7 mM), which should affect the $^1O_2$ lifetime and amplitude but not the EGFP triplet lifetime neither its amplitude (see the Annex), eliminated the rise component of the signal at 1275 nm, confirming its attribution to $^1O_2$ phosphorescence. The presumably smaller amplitude of the rise and its faster kinetics precluded a reliable determination of its time constant (Fig. 6D and Annex). As to the nature of the 25-μs component observed in the range 1100-1300 nm, we tentatively attribute it to the protein phosphorescence, since saturation with oxygen resulted in a decrease of this component to 3-6 μs (Fig. 5E). Our triplet-state lifetime value of 25 μs for EGFP would confirm a previous proposed value of ~30 μs, extracted from FCS measurements on this protein [28]. The exceptionally long triplet lifetime of EGFP in air-saturated solution may be explained by the low accessibility of O_2 to the chromophore due to its screening by the β-can [8]. Indeed, using Eq. (2):

$$k_q = \frac{1/\tau_T^{O_2} - 1/\tau_T^{air}}{[O_2]^{O_2} - [O_2]^{air}} \qquad (2)$$

where τ_T^{O2} = 3-6 μs and τ_T^{air} = 25 μs are the triplet state lifetimes in oxygen- and in air-saturated solutions, respectively, together with $[O_2]^{O2}$ = 1 x 10^{-3} M and $[O_2]^{air}$ = 2 x 10^{-4} M, a value of k_q ~2 x 10^8 $M^{-1}s^{-1}$ is calculated for the rate constant of oxygen quenching

of the EGFP triplet state. This value is an order of magnitude smaller than those observed in solution, supporting the notion that the β-can effectively shields the chromophore from oxygen.

As to the $^1O_2$ lifetime, which we would expect as ~11 μs given the proportion of H_2O/D_2O used [29], the shorter value observed, ~4 μs, probably reflects quenching either by the aminoacids near the chromophore and/or by the chromophore itself, as found for anionic HBDI.

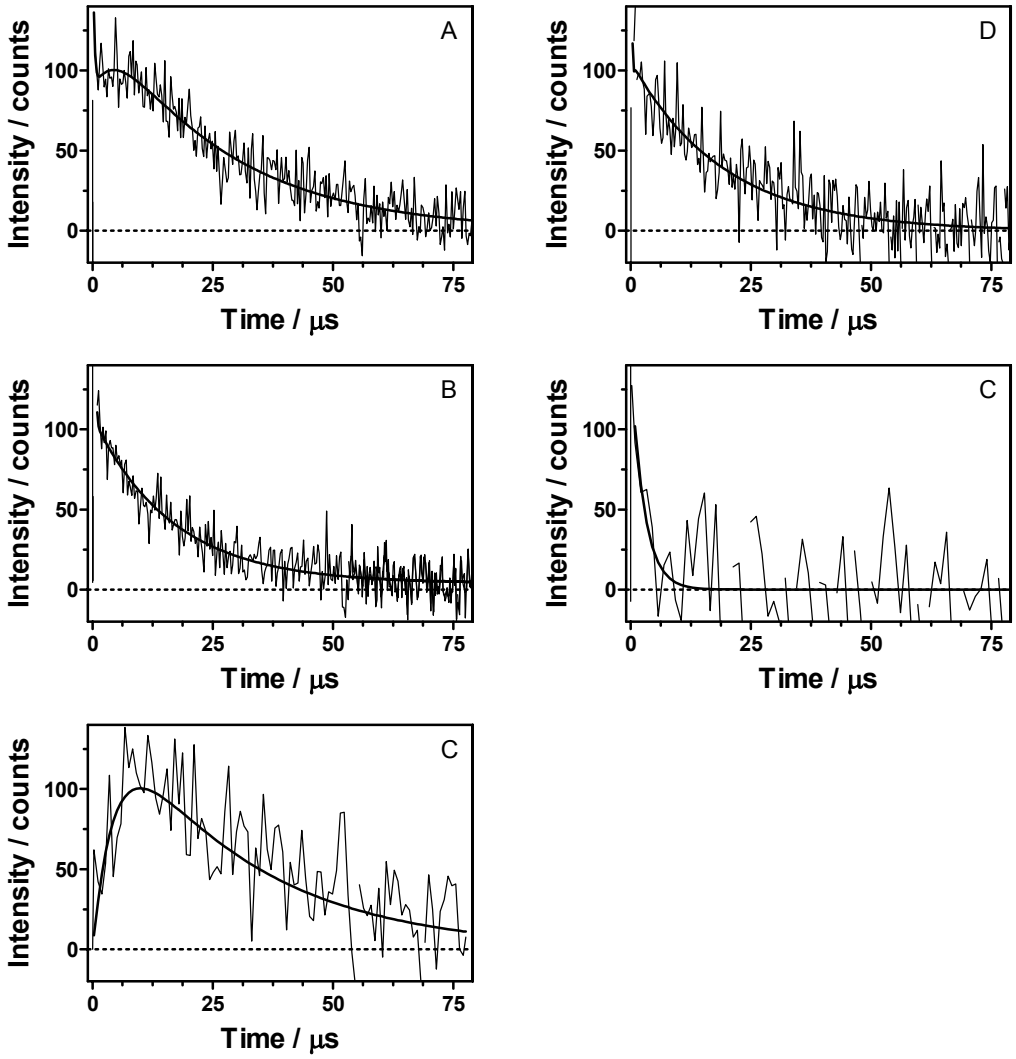

Fig. 6: Normalized emission signals of EGFP in D-PBS irradiated at 532 nm and detected at: **A:** 1275 nm, 40 million laser pulses, 20 ns per channel, fitted parameters: τ_1 = 4.4 ± 1μs, τ_2 = 26 ± 1 μs; **B:** 1100 nm, 40 million laser pulses, 20 ns per channel, fitted parameter: τ = 20 ± 2 μs; **C:** signal resulting from (*A*)-(*B*), fitted parameters: τ_Δ = 4.5 μs, τ_T = 28 μs. **D:** 1275 nm, [NaN_3] = 7 mM, 40 million laser pulses, 20 ns per channel, fitted parameters: τ_1 = 0.2 μs, τ_2 = 23 ± 1 μs. **E:** 1275 nm, oxygen-saturated D-PBS, 30 million laser pulses, 200 ns per channel, fitted parameter: τ = 3-6 μs.

We have attempted to record the steady-state emission spectrum of EGFP up to 1000 nm at room temperature and also at 77 K (the latter to reduce radiationless deactivation) using a Fluorolog 1500 fluorimeter (Spex Industries, Metuchen, NJ). Unfortunately, this spectrometer lacks the sensitivity to detect the EGFP phosphorescence. Also, we have attempted to extend our time-resolved emission measurements down to 1000 nm (the lower limit of our apparatus) but no maximum could be located in that range either. We must conclude that the phosphorescence maximum must be below 1000 nm, *i.e.*, the triplet energy of EGFP is higher than 120 $kJ \cdot mol^{-1}$.

Due to the presence of an additional signal at 1275 nm, we are not able to quantify the photosensitisation ability of EGFP in terms of Φ_Δ, but we have shown that this value is 0.004 for HBDI, providing the first estimation or lower limit for the triplet yield of this model compound. In any case, our above results show that the β-can indeed provides shielding of the chromophore and reduces its ability to sensitize $^1O_2$, as judged from the different triplet lifetimes in HBDI and EGFP.

C. GFPmut2. The most commonly used mutation to favour ionisation of the phenol of the chromophore is the replacement of Ser65 by Thr, as in EGFP, though several other aliphatic residues such as Gly, Ala, Cys, and Leu have roughly similar effects [8]. GFPmut2, the triple mutant S65A, V68L and S72A, while showing very similar spectroscopic features to those of EGFP, offers some advantages, like higher folding and chromophore formation efficiencies at 37 ºC [30].

The absorption spectrum of GFPmut2 in 50 mM PBS at pH 7.4 is shown in Fig. 7. As for EGFP, the wt-GFP neutral phenol peak at ~395 nm is suppressed and a ~15-nm bathochromic shift in the peak corresponding to the anion is observed. In addition, the more noticeable shoulder at ~475 nm for GFPmut2 than for EGFP suggests that some additional rigidity in the chromophore environment has been introduced in GFPmut2 [30]. In contrast to wt-GFP, kinetic studies have shown that there is no efficient proton-transfer mechanism in the excited state, so the neutral or anionic forms of the GFPmut2 chromophore can be independently excited as a function of the pH [30].

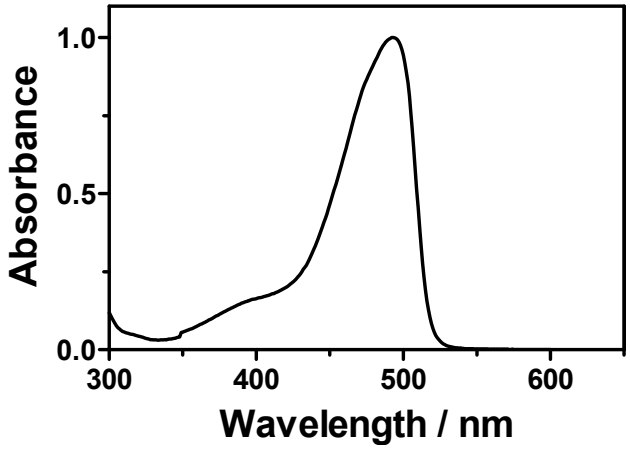

Fig. 7: Normalized absorption spectra of a ~0.1 mM GFPmut2 solution in PBS buffer.

Irradiation at 355 nm of GFPmut2 in a mixture of PBS and D-PBS (1:2) revealed the presence of a signal in the 1200-1300 nm range that could be fitted with a single exponential of τ_1 ~ 18 μs (Fig. 8). However, the spectrum of this component did not resemble that of $^1O_2$ (Fig. 8, inset) and neither its lifetime nor its intensity was affected by saturation with Ar or O_2. On the basis of the aforementioned experiments with EGFP, we tentatively assign the 18-μs component to the GFPmut2 phosphorescence. The fact that this component was not affected by saturation with Ar or O_2 is in line with studies on the protein GFP-S65T which indicate that its bleaching rate is insensitive to O_2 or to the addition of triplet state quenchers due to the shielding effect of the chromophore by the β-can [31]. Other studies pointed out that the accessibility of the chromophore to the solvent is very similar for both GFPmut2 and GFP-S65T [30].

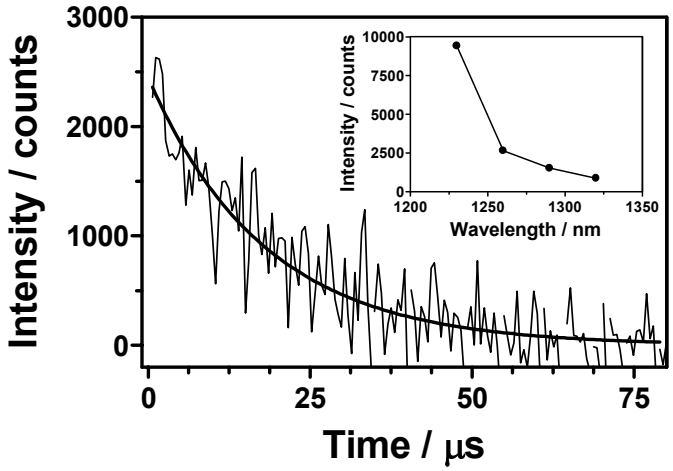

Fig. 8: Signal detected at 1275 nm upon 355-nm irradiation of a ~0.1 mM GFPmut2 sample in PBS / D-PBS (1:2), 100 million laser pulses, 256 ns *per* pulse. Fitted parameter: τ_1 = 18 ± 3 μs. **Inset**: spectrum obtained from the intensity of the signal at different wavelengths.

Taking into account the similarities between GFPmut2 and EGFP one should expect comparable photosensitising properties for both proteins. It is worth noting that a single mutation can affect not only the chromophore but also the whole protein structure. For example, the replacement of Ser65 by the bulkier residue Thr in EGFP favours ionisation of the chromophore [8] but likely also distorts the protein structure. The resulting looser β-can could provide poorer chromophore shielding for EGFP than for those proteins where Ser65 has been mutated with the smaller aminoacid Ala, as in the case of GFPmut2. Our hypothesis is therefore that the mutations in GFPmut2, particularly S65A, lead to a tighter β-can, effectively shielding the chromophore from oxygen. This might explain why we are unable to detect $^1O_2$ photosensitised by GFPmut2 despite the similarities with EGFP.

Assuming the validity of this hypothesis, we tried to induce a floppier β-can for GFPmut2. It is well documented that the flexibility of the protein structure can be increased without inducing significant unfolding (<10%) adding guanidinium chloride (GdnHCl) 1.5 M [32]. Irradiation at 355 nm of an oxygen-saturated GFPmut2 sample in PBS / D-PBS (1:2) with 1 M GdnHCl yielded however a signal at 1275 nm that was fitted with a single exponential of τ_1 = 16 ± 3 μs, as in the absence of GdnHCl. Thus, not significant changes were observed upon addition of GdnHCl. We are lead to conclude that GFPmut2 does not produce $^1O_2$, at least as efficient as EGFP. The most likely reason is the extremely low oxygen accessibility to the chromophore due to a tighter β-can, evidenced by the long triplet state lifetime measured under oxygen saturation even in the presence of GdnHCl.

D. GFPmut2-H148G. The influence of His148 on the accessibility of the chromophore to the solvent has been shown previously [30]. Mutation of His148 by Gly, *i.e.*, substitution of the imidazole with a less bulky aliphatic group, creates a hole in the β-can that should allow an easier entrance way for O_2 molecules and also eliminate a well-known $^1O_2$ quencher from the chromophore surroundings. The combination of both effects should favour the production of $^1O_2$ by this mutant. To test this hypothesis, the additional mutation H148G has been introduced to GFPmut2. This mutation substantially affected the pK_a value of the protein, shifting it from 6.1 to 7.6, and introduced some additional rigidity in the chromophore environment [30]. Such enhanced rigidity might, in principle, act against the accessibility of oxygen to the chromophore.

In order to maximize the chances to observe $^1O_2$ in this protein we stabilised its anionic form by using a pH 8.5 D-CHES 25 mM buffer, as the experiments with HBDI showed

that the anionic form of the chromophore is the photosensitising one and that no efficient excited-state proton transfer mechanism has been observed for this protein either. Likewise, we added 1.5 M GdnHCl to increase the protein flexibility and, finally, we saturated the solution with oxygen. The absorption spectra of GFPmut2-H148G in pH 7.4 D-PBS buffer and in pH 8.5 D-CHES buffer containing 1.5 M GdnHCl are shown in Fig 10. The absence of changes in the absorption spectra in the presence of 1.5 M GdnHCl indicates that no significant unfolding has taken place under these conditions.

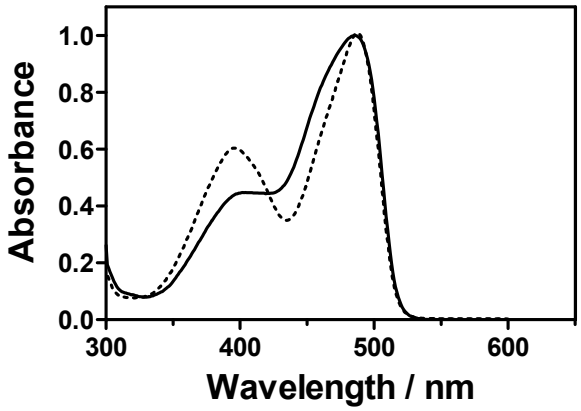

Fig. 10: Normalized absorption spectra of a ~0.1 mM GFPmut2-H148G solution in pH 8.5 CHES buffer (continuos line) and in pH 7.4 D-PBS buffer (dotted line).

Irradiation of an oxygen-saturated GFPmut2-H148G sample in PBS / D-CHES (1:3) in the presence of 1.5 M GdnHCl yielded a signal at 1275 nm that rises with a lifetime of about τ_1 = 2 μs and decays with τ_2 = 10 μs (Fig. 11A). The signal disappeared upon addition of 20 mM NaN_3 to the solution, confirming that the emission detected at 1275 nm was indeed due exclusively to $^1O_2$ phosphorescence. Experiments performed at 1100 nm revealed the presence of a kinetic component of 10 μs (Fig 11B) that we tentatively attribute to protein phosphorescence, since argon saturation resulted in its lifetime increase up to 20 μs (Fig. 11C).

The exceptionally long triplet state lifetime of GFPmut2-H148G in oxygen-saturated solution indicates, as in the case of EGFP, a low accessibility of O_2 to the chromophore due to screening by the β-can. The triplet lifetime measured for GFPmut2-H148G is longer than for EGFP under oxygen saturation (3-6 μs), pointing to an even higher degree of shielding for GFPmut2-H148G. Indeed, the calculated value of k_q ~6 x 10^7 $M^{-1}s^{-1}$ for the rate constant of oxygen quenching of the GFPmut2-H148G triplet state is an order of magnitude smaller than that calculated for EGFP (*vide supra*), supporting the idea of a more effective shielding for GFPmut2-H148 than for EGFP.

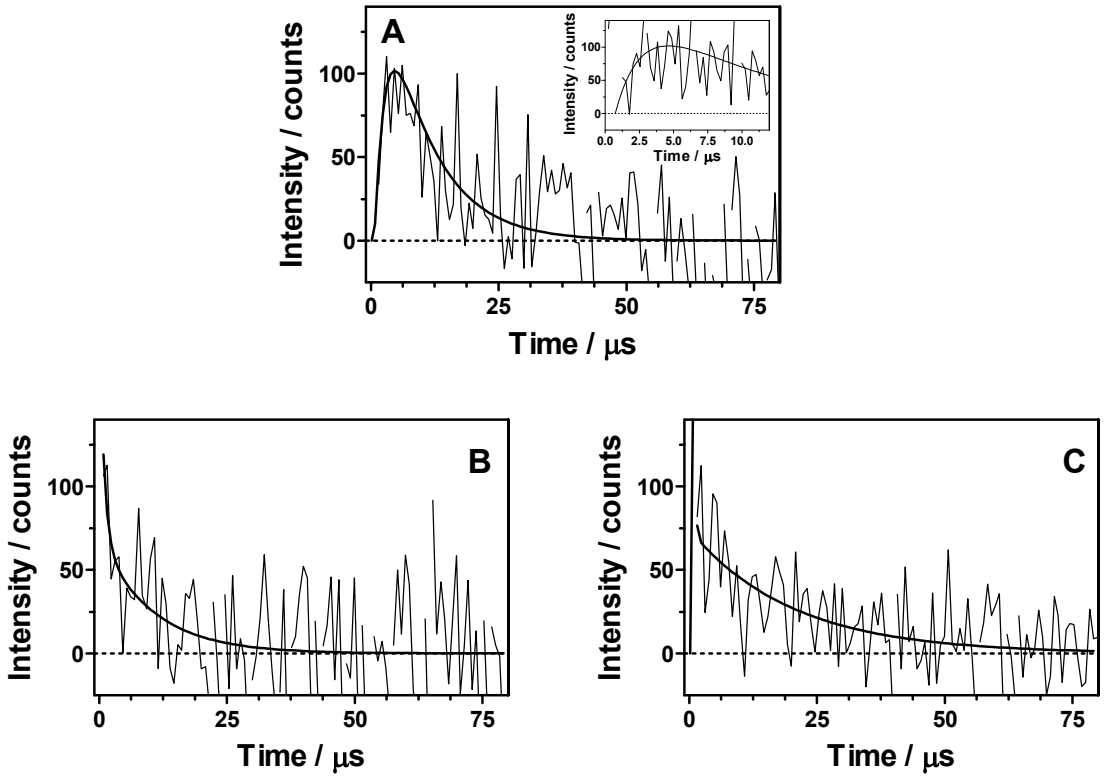

Fig. 11: Normalized emission signals of GFPmut2-H148G in PBS/D-CHES (1:3) in the presence of 1.5 M GdnHCl, irradiated at 355 nm and detected at: **A:** 1275 nm, O_2-saturated, 100 million laser pulses, 256 ns *per* channel, fitted parameters: τ_1 = 2 ±1 μs, τ_2 = 11± 2 μs; **B:** 1100 nm, O_2-saturated, 100 million laser pulses, 256 ns *per* channel, fitted parameter: τ = 10 ± 2 μs; **C:** 1100 nm, Ar-saturated, 100 million laser pulses, 256 ns *per* channel, fitted parameter: τ = 20 ± 2 μs.

As to the $^1O_2$ lifetime, we would expect to be close to 10 μs given the proportion of H_2O/D_2O used and taking into account the presence of 1.5 M GdnHCl (k_q ~10^4 $M^{-1}s^{-1}$). The value found τ_Δ = 2 μs indicates quenching by the chromophore itself, as in the case of HBDI, and/or its reaction with the aminoacids near the chromophore. This behaviour is similar to that found in EGFP, suggesting aminoacids other than His148 contribute to $^1O_2$ quenching. In fact, wt-GFP contains 240 aminoacids out of which the 10% are potential $^1O_2$ quenchers: 9 tyrosines (k_q = 8 x 10^6 $M^{-1}s^{-1}$), 9 histidines (k_q = 3 x 10^7 $M^{-1}s^{-1}$), 4 methionines (k_q = 1 x 10^7 $M^{-1}s^{-1}$), 2 cysteines (k_q = 4 x 10^8 $M^{-1}s^{-1}$) and 1 triptophan (k_q = 5 x 10^7 $M^{-1}s^{-1}$) [26]. It is expected therefore that the replacement of His 148 by Gly should have only a marginal effect on the $^1O_2$ lifetime.

In comparison to GFPmut2, the lower sensitivity of the triplet state lifetime to oxygen concentration indicates that the GFPmut2-H148G chromophore is less screened, confirming the shielding role of H148. Our results indicate that the photosensitising properties of the protein are very sensitive to those mutations that alter its flexibility.

E. KillerRed. This red-fluorescent mutant from an homolog of GFP contains several mutations respective to wt-GFP, being T145N and C161A those spatially closer to the chromophore and reported indispensable for KillerRed phototoxic effect. Other substitutions affecting the folding and brightness seem to be also important [19].

The phototoxic activity of KillerRed was characterised by Bulina *et al*. [19]. KillerRed was able to kill bacteria and cultured eukaryotic cells in a light-mediated manner that resulted in almost complete inactivation of the cells upon green light irradiation (540-580 nm). On the basis of oxygen concentration experiments, as well as the addition of specific quenching compounds, such as azide and imidazole for $^1O_2$, superoxide dismutase for $O_2^{-\bullet}$, and mannitol for $O_2^{-\bullet}$ and $OH^\bullet$, it was proposed that $^1O_2$ was the main phototoxic agent involved in KillerRed phototoxicity.

The absorption spectra of the KillerRed sample used by Bulina *et al.* [19] and that in our experiments are depicted in Figs. 12A and 12B, respectively. It is worth noting that our fresh sample already exhibits a ~50% bleaching at 584 nm as deduced from the absorption spectrum reported by Bulina *et al.* [19].

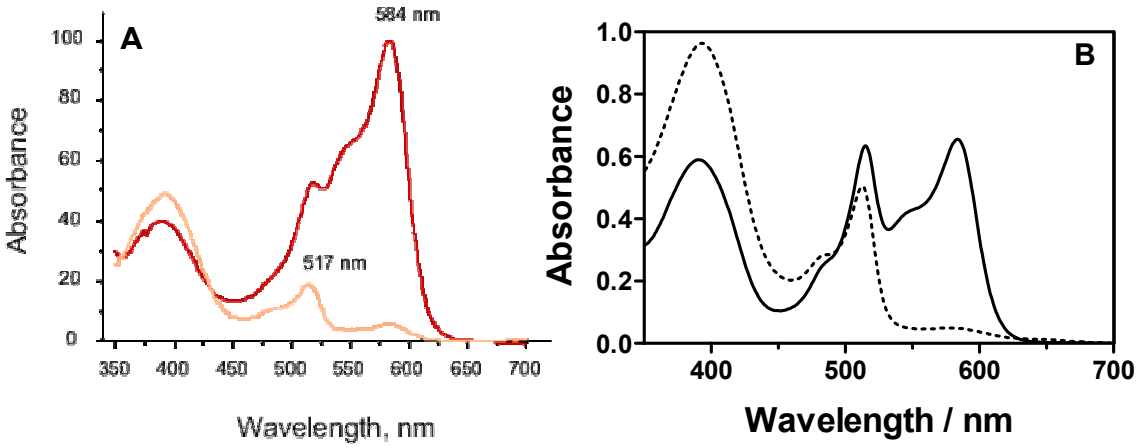

Fig. 12: A: Absorption spectra of intact (red line) and pre-bleached (yellow line) KillerRed. From Bulina *et al.* [19], supporting information. **B:** Absorption spectra of a KillerRed solution in D-PBS before (*continuous line*) and upon prolonged irradiation at 532 nm (*dotted line*).

Upon 532 nm irradiation of a sample containing 5 μL of KillerRed in 400 μL of pH 7.4 D-PBS, we were unable to detect any signal at 1275 nm (Figure 13). Further increases in protein and/or oxygen concentration did not produce any signal either, although bleaching of the sample was observed during the time course of the measurements, in agreement with the report by Bulina *et al*. [19]. These authors stated that pre-bleaching of KillerRed is mandatory for $O_2^{\bullet-}$ production but were not as precise in establishing which protein form is the responsible for $^1O_2$ formation. In our case, the protein was not

as bleached as that of Bulina *et al*. [19], hence our negative results suggest that the bleached form is the photosensitising one.

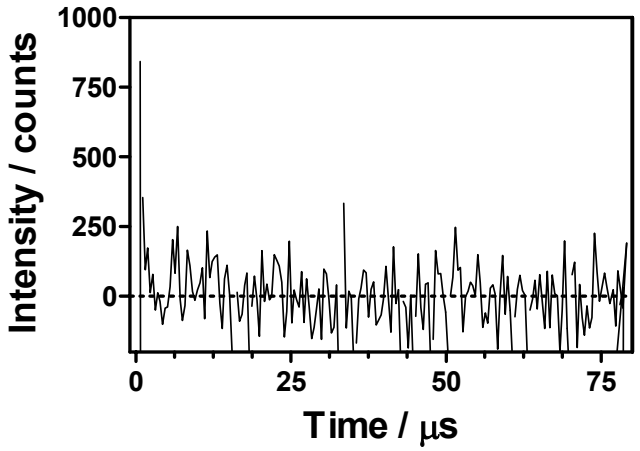

Fig. 13: signal detected at 1275 nm upon 532-nm irradiation of a KillerRed sample in D-PBS, 180 million laser pulses, 200 ns *per* pulse.

To test this hypothesis, KillerRed in D-PBS was irradiated at 532 nm with a diode-pumped solid-state Q-switched Nd:YAG laser (CryLas, FTQ355-QS, 12 mW, 1.2 μJ *per* pulse) until its absorption spectrum resembled that of the bleached KillerRed (Figs. 12A and 12B). Even then, we were still unable to detect any signal at 1275 nm in at O_2-saturated solution.

Our failure to detect $^1O_2$ from KillerRed agrees with the results from other laboratories. Specifically, $^1O_2$ detection has been attempted in Prof. Chignell's lab (NIEHS, USA) using ESR and a Ge-diode based $^1O_2$ steady-state spectrophotometer, also with negative results for both the intact and bleached form of KillerRed [33].

Additional reasons why we were unable to observe $^1O_2$ may stem from the fact that the KillerRed samples used in our experiments already showed ~50% bleaching at 584 nm (Figs. 12A and 12B), probably due to light exposure during isolation of the protein from *E. Coli* bacteria. In addition, KillerRed's phototoxicity was assessed by Bulina *et al.* [19] on living cells, whereas our experiments were conducted in solution. To minimize the handling time and to test if the photosensitising properties of this protein were associated to any compound present in living cells, we irradiated D-PBS suspensions with different concentrations of *E. Coli*-expressing KillerRed, in air- and oxygen-saturated solutions. Once again, no $^1O_2$ was detected in either case, ruling out both possibilities as the actual reasons for the absence of positive results. Altogether, the results reported herein fail to confirm that KillerRed sensitises the production of $^1O_2$.

5.4. CONCLUSIONS

Irradiation of EGFP and GFPmut2-H148G results in the formation of $^1O_2$, confirming earlier results obtained with indirect methods [12,14]. Our results provide, for the first time, unequivocal direct evidence for $^1O_2$ production derived from its specific phosphorescence at 1275 nm. In addition, they have revealed the kinetics of formation and decay of $^1O_2$. The low efficiency for $^1O_2$ photosensitisation by GFPs is possibly the reason why little was known to date about the kinetic parameters involved in these processes.

The triplet state of the GFP mutants are quite long lived (~10-30 μs), which indicates a low oxygen accessibility to the chromophore in the β-can. Likewise, the lifetime of $^1O_2$ photosensitized by either EGFP or GFPmut2-H148G (~ 2-4 μs) is substantially shorter than that in solution, which suggests that it is partially quenched by the β-can aminoacids and/or by the chromophore itself.

On the other hand, we have not been able to detect any $^1O_2$ signal from GFPmut2 nor from the red fluorescent protein KillerRed, reported as the first genetically-encoded photosensitiser [19].

It is unclear at this point which features govern the ability of GFPs to photosensitize $^1O_2$, though the accessibility of molecular oxygen to the chromophore seems to play a major role. The accessibility of oxygen to the chromophore can be related to the maturation time of the GFPs [34], so confirmation of our hypothesis could be obtained from comparing maturation times and $^1O_2$ photosensitisation properties. Also, the availability of the crystal structures of these proteins might shed additional light onto this issue, and help understand the origin of the different phototoxicity in GFP-like proteins.

Taken together, our results indicate that the study of $^1O_2$ photosensitisation by proteins can be helpful in designing genetically-encoded CALI agents, as well as more photostable GFPs for single molecule spectroscopy.

5.5. REFERENCES

[1] Shimomura, O.; Johnson, F. H.; Saiga, Y. Extraction, purification and properties of *Aequorin*, a bioluminescent protein from *Luminous Hydromedusan, Aequorea*. *J. Cell. Comp. Physiol.* **59**:223-&; 1962.

[2] Morin, J. G.; Hastings, J. W. Biochemistry of bioluminescence of colonial hydroids and other coelenterates. *J. Cell. Physiol.* **77**:305-&; 1971.

[3] Cody, C. W.; Prasher, D. C.; Westler, W. M.; Prendergast, F. G.; Ward, W. W. Chemical-structure of the hexapeptide chromophore of the *Aequorea* Green-Fluorescent Protein. *Biochemistry* **32**:1212-1218; 1993.

[4] Prasher, D. C.; Eckenrode, V. K.; Ward, W. W.; Prendergast, F. G.; Cormier, M. J. Primary structure of the *Aequorea*-Victoria Green-Fluorescent Protein. *Gene* **111**:229-233; 1992.

[5] Heim, R.; Prasher, D. C.; Tsien, R. Y. Wavelength mutations and posttranslational autoxidation of Green Fluorescent Protein. *Proc. Natl. Acad. Sci. USA* **91**:12501-12504; 1994.

[6] Heim, R.; Cubitt, A. B.; Tsien, R. Y. Improved Green Fluorescence. *Nature* **373**:663-664; 1995.

[7] Reid, B. G.; Flynn, G. C. Chromophore formation in green fluorescent protein. *Biochemistry* **36**:6786-6791; 1997.

[8] Tsien, R. Y. The Green Fluorescent Protein. *Annu. Rev. Biochem.* **67**:509-544; 1998.

[9] Giepmans, B. N. G.; Adams, S. R.; Ellisman, M. H.; Tsien, R. Y. Review - The fluorescent toolbox for assessing protein location and function. *Science* **312**:217-224; 2006.

[10] Remington, S. J. Fluorescent proteins: maturation, photochemistry and photophysics. *Curr. Opin. Struct. Biol.* **16**:714-721; 2006.

[11] Dixit, R.; Cyr, R. Cell damage and reactive oxygen species production induced by fluorescence microscopy: effect on mitosis and guidelines for non-invasive fluorescence microscopy. *Plant J.* **36**:280-290; 2003.

[12] Greenbaum, L.; Rothmann, C.; Lavie, R.; Malik, Z. Green fluorescent protein photobleaching: a model for protein damage by endogenous and exogenous singlet oxygen. *Biological Chemistry* **381**:1251-1258; 2000.

[13] Halliwell, B.; Gutteridge, J. M. C. *Free Radicals in Biology and Medicine*: New York: Oxford University Press; 1999.

[14] Bell, A. F.; Stoner-Ma, D.; Wachter, R. M.; Tonge, P. J. Light-driven decarboxylation of wild-type green fluorescent protein. *J. Am. Chem. Soc.* **125**:6919-6926; 2003.

[15] Tour, O.; Meijer, R. M.; Zacharias, D. A.; Adams, S. R.; Tsien, R. Y. Genetically targeted chromophore-assisted light inactivation. *Nature Biotechnol.* **21**:1505-1508; 2003.

[16] Surrey, T.; Elowitz, M. B.; Wolf, P. E.; Yang, F.; Nedelec, F.; Shokat, K.; Leibler, S. Chromophore-assisted light inactivation and self-organization of microtubules and motors. *Proc. Natl. Acad. Sci. USA* **95**:4293-4298; 1998.

[17] Rajfur, Z.; Roy, P.; Otey, C.; Romer, L.; Jacobson, K. Dissecting the link between stress fibres and focal adhesions by CALI with EGFP fusion proteins. *Nat. Cell Biol.* **4**:286-293; 2002.

[18] Tanabe, T.; Oyamada, M.; Fujita, K.; Dai, P.; Tanaka, H.; Takamatsu, T. Multiphoton excitation-evoked chromophore-assisted laser inactivation using green fluorescent protein. *Nature Methods* **2**:503-505; 2005.

[19] Bulina, M. E.; Chudakov, D. M.; Britanova, O. V.; Yanushevich, Y. G.; Staroverov, D. B.; Chepurnykh, T. V.; Merzlyak, E. M.; Shkrob, M. A.; Lukyanov, S.; Lukyanov, K. A. A genetically encoded photosensitizer. *Nat. Biotechnol.* **24**:95-99; 2006.

[20] Nonell, S.; Braslavsky, S. E. Time-resolved singlet oxygen detection. In: Packer, L.; Sies, H. eds. *Singlet oxygen, UV-A, and Ozone. Methods in Enzymology, vol.319*. San Diego: Academic Press; 2000:37-49.

[21] Kojima, S.; Ohkawa, H.; Hirano, T.; Maki, S.; Niwa, H.; Ohashi, M.; Inouye, S.; Tsuji, F. I. Fluorescent properties of model chromophores of tyrosine-66 substituted mutants of *Aequorea* green fluorescent protein (GFP). *Tetrahedron Lett.* **39**:5239-5242; 1998.

[22] Mandal, D.; Tahara, T.; Webber, N. M.; Meech, S. R. Ultrafast fluorescence of the chromophore of the green fluorescent protein in alcohol solutions. *Chem. Phys. Lett.* **358**:495-501; 2002.

[23] Mandal, D.; Tahara, T.; Meech, S. R. Excited-state dynamics in the green fluorescent protein chromophore. *J. Phys. Chem. B* **108**:1102-1108; 2004.

[24] Webber, N. M.; Litvinenko, K. L.; Meech, S. R. Radiationless relaxation in a synthetic analogue of the green fluorescent protein chromophore. *J. Phys. Chem. B* **105**:8036-8039; 2001.

[25] Litvinenko, K. L.; Webber, N. M.; Meech, S. R. Internal conversion in the chromophore of the green fluorescent protein: temperature dependence and isoviscosity analysis. *J. Phys. Chem. A* **107**:2616-2623; 2003.

[26] Wilkinson, F.; Helman, W. P.; Ross, A. B. Rate constants for the decay and reactions of the lowest electronically excited singlet state of molecular oxygen in solution. An expanded and revised compilation. *J. Phys. Chem. Ref. Data* **24**:663-1021; 1995.

[27] Nonell, S.; González, M.; Trull, F. R. 1H-Phenalen-1-one-2-sulfonic acid: an extremely efficient singlet molecular oxygen sensitizer for aqueous media. *Afinidad* **50**:445-450; 1993.

[28] Haupts, U.; Maiti, S.; Schwille, P.; Webb, W. W. Dynamics of fluorescence fluctuations in green fluorescent protein observed by fluorescence correlation spectroscopy. *Proc. Natl. Acad. Sci. USA* **95**:13573-13578; 1998.

[29] Schweitzer, C.; Schmidt, R. Physical mechanisms of generation and deactivation of singlet oxygen. *Chem. Rev.* **103**:1685-1757; 2003.

[30] Abbruzzetti, S.; Grandi, E.; Viappiani, C.; Bologna, S.; Campanini, B.; Raboni, S.; Bettati, S.; Mozzarelli, A. Kinetics of acid-induced spectral changes in the GFPmut2 chromophore. *J. Am. Chem. Soc.* **127**:626-635; 2005.

[31] Swaminathan, R.; Hoang, C. P.; Verkman, A. S. Photobleaching recovery and anisotropy decay of green fluorescent protein GFP-S65T in solution and cells: Cytoplasmic viscosity probed by green fluorescent protein translational and rotational diffusion. *Biophys. J.* **72**:1900-1907; 1997.

[32] Campanini, B.; Bologna, S.; Cannone, F.; Chirico, G.; Mozzarelli, A.; Bettati, S. Unfolding of Green Fluorescent Protein mut2 in wet nanoporous silica gels. *Protein Sci.* **14**:1125-1133; 2005.

[33] Chignell, C. F. Personal Communication. 2007.

[34] Evdokimov, A. G.; Pokross, M. E.; Egorov, N. S.; Zaraisky, A. G.; Yampolsky, I. V.; Merzlyak, E. M.; Shkoporov, A. N.; Sander, I.; Lukyanov, K. A.; Chudakov, D. M. Structural basis for the fast maturation of *Arthropoda* green fluorescent protein. *EMBO Rep.* **7**:1006-1012; 2006.

5.6. ANNEX

Process for recovering the singlet oxygen decay from data at 1270 and 1100 nm.

It is often found that the emission signal at 1270 nm has two components, one due to the triplet sensitizer phosphorescence $S_T(t,1270)$, and one from singlet oxygen, $S_\Delta(t,1270)$:

$$S(t,1270) = S_T(t,1270) + S_\Delta(t,1270) \qquad \text{(S1)}$$

Thus, it is possible to obtain the "pure" singlet oxygen transient by subtracting the triplet component from the total signal. We do this using the transient at 1100 nm as the "pure" triplet component and multiplying it by the necessary factor α to match the triplet component amplitude in the composite signal at 1270 nm:

$$S_T(t,1270) \approx \alpha \cdot S_T(t,1100). \qquad \text{(S2)}$$

Therefore,

$$S_\Delta(t,1270) = S(t,1270) - S_T(t,1270) \approx S(t,1270) - \alpha \cdot S_T(t,1100). \qquad \text{(S3)}$$

The standard kinetic model for singlet oxygen photosensitisation and decay, as given in eq. 1 of the text,

$$S_\Delta(t,1270) = S_\Delta(0,1270) \times \frac{\tau_\Delta}{\tau_T - \tau_\Delta} \times \left[\exp(-t/\tau_T) - \exp(-t/\tau_\Delta)\right], \qquad (1)$$

requires that the amplitude of the rise and decay components of the "pure" singlet oxygen signal be identical. We thus vary the factor α until the fit of Eq. (1) to the resulting data is satisfactory.

Chapter 6

Tetraphenylporphycenes as Photosensitisers for Two-Photon Photodynamic Therapy

Porphycenes are structural isomers of porphyrins that have many unique properties and features. Since the synthesis of the first porphycene in 1986, a variety of substituted derivatives have been prepared. Our group has focused its interest in the family of the 2,7,12,17-tetraphenylporphycenes and its metal-ion complexes.

In this chapter, the resonant two-photon absorption properties of TPPo and its palladium (II) complex are reported. The data obtained are compared to those of the isomeric compound *meso*-tetraphenylporphyrin. These results promote tetraphenylporphycenes as promising photosensitisers for two-photon initiated photodynamic therapy.

The work described in this chapter is adapted from J. Arnbjerg, A. Jimenez-Banzo, M.J. Paterson, S. Nonell, J.I. Borrell, O. Christiansen and P.R. Ogilby in *J. Am .Chem. Soc.* **2007**, *129*, 5188-5199, and was presented at the IV Simposium de Investigadores Jóvenes, Burgos (Spain), November 2007.

6.1. INTRODUCTION

The porphycene macrocycle is an isomer of the naturally-occurring porphyrin macrocycle. Since the synthesis of the first porphycene in 1986 [1], a variety of substituted derivatives have been prepared, including 2,7,12,17-tetraphenylporphycene, TPPo, which is an isomer of *meso*-tetraphenylporphyrin, TPP (Chart 1) [2,3]. Likewise, several metal-ion complexes of porphycenes have been prepared, including the palladium (II) complex of tetraphenylporphycene, PdTPPo [4].

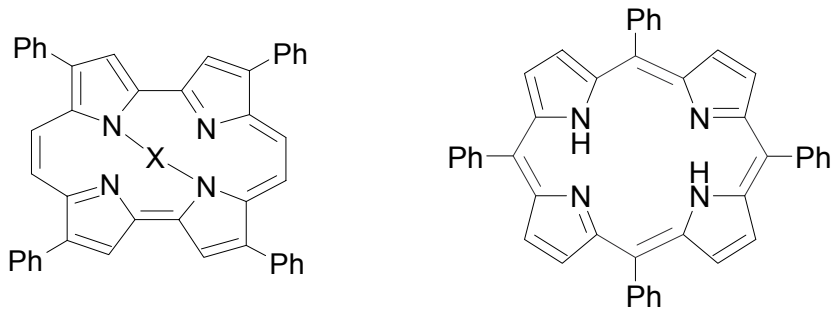

Chart 1. Structures of 2,7,12,17-tetraphenylporphycene, TPPo, its palladium (II) complex, PdTPPo, and *meso*-tetraphenylporphyrin, TPP.

Porphyrin derivatives have arguably been the most studied class of molecules for application as sensitizers in photodynamic therapy, PDT [5-7]. Indeed, one of the few compounds approved for medical use in this regard, Photofrin®, is a composite of porphyrin derivatives [5]. Given the structural similarities between porphycenes and porphyrins, it is reasonable to consider that porphycenes would likewise be viable sensitizers for PDT. In this regard, it is important to note that, upon irradiation, porphycenes generally produce singlet molecular oxygen, $^1O_2$, in moderate to high yields [8,9]. This is pertinent in that $^1O_2$ plays a critical role in the mechanisms of cell death associated with PDT [5,10]. Several studies have examined the behaviour of TPPo, PdTPPo, and other porphycenes in cells, and it has been demonstrated that these molecules are indeed PDT photosensitisers [4,11-13]. It has specifically been shown, for example, that TPPo is effective in mediating lysosome destruction [12], which is a pathway to induce apoptotic cell death [14].

Linear photophysical and photosensitizing parameters for TPPo and PdTPPo have been quantified and compared with corresponding values for the much studied naturally occurring porphyrin isomer TPP [9,15,16]. For the porphycenes, one-photon absorption in the so-called Q region is significantly enhanced and shifted towards longer wavelengths in comparison with their porphyrin counterparts (*vide infra*).

Nevertheless, despite this red-shift, direct one-photon absorption of the porphycene in the wavelength range ~700-900 nm still does not occur. The latter is pertinent from the perspective of one interested in PDT simply because 700-900 nm is the wavelength range over which tissue is most transparent [5,17]. This wavelength-dependent limitation in both porphyrins and porphycenes, however, can potentially be overcome via nonlinear, two-photon excitation of the PDT sensitizer over the range 700-900 nm. Although the absorbance of tissue is comparatively large over the range ~ 900-1050 nm due to a water absorption band with λ_{max} at 970 nm [17], one could also potentially excite a PDT sensitizer at a wavelength slightly longer than 1050 nm. As such, we set out to study the two-photon absorption properties of the porphycenes TPPo and PdTPPo in the spectral region 750-850 nm and also at 1100 nm, and to compare the results obtained to those obtained from the porphyrin TPP.

From a fundamental perspective, we first note that a comparatively large number of studies have focused on the nonlinear optical properties of porphyrins and porphyrin derivatives [18-26]. To our knowledge, however, corresponding nonlinear studies have not been performed on the isomeric porphycenes. As such, a simple comparison between the data sets obtained from these respective isomers should provide unique insight into the effect that molecular structure has on defining nonlinear optical properties. Such insight is a prerequisite in any attempt to exert control over these chromophores in the design, for example, of a viable drug for PDT.

In recent years, the level of sophistication applied to experimental studies of nonlinear optical phenomena has increased dramatically. Much of this derives from the relative ease with which well-characterized femtosecond laser pulses can now be obtained. The development and application of independent techniques to quantify two-photon absorption cross sections has also been a boon to the field [27,28]. With respect to the latter, we have established the viability and advantages of using the intensity of the photosensitized $O_2(a^1\Delta_g) \rightarrow O_2(X^3\Sigma_g^-)$ phosphorescence signal as a tool to characterize nonlinear light absorption by a given molecule [24,29,30], and it is this approach we use in the present study on porphycenes. Finally, and perhaps most importantly, it is now established that two-photon excitation of a sensitizer can be advantageous, not only in PDT but in studying the mechanisms of cell death pertinent to PDT [31,32].

Although the level of sophistication with which computational methods can be applied to model electronic excitations is likewise constantly improving, the calculation of nonlinear phenomena such as two-photon absorption has been a significant challenge to the theoretical community. Almost all of the approaches that have been used thus far on molecules of this size have relied on explicit sum-over-states methods that are

generally limited by problems such as slow convergence when considering a large number of states [18,33-35]. Nevertheless, significant improvements in the calculation of two-photon absorption cross sections and transition energies have recently become possible due to advances in response theory, and this newer methodology has been applied to comparatively large molecular systems with reasonable success [24,36-38]. Although the characteristic features of response theory are described in detail elsewhere [39-41], one issue pertinent for molecules of the size considered here is that response theory implicitly sums over all states in the system without explicitly constructing these states. This is particularly important for the problem at hand because the two-photon transition proceeds through a virtual state which is a linear combination of all real eigenstates in the system. Furthermore, recent advances in density functional theory (DFT), higher-order density functional response theory, and functionals for use in response theory [42-44], mean it is now possible to more readily perform accurate response computations of both one- and two- photon absorption spectra for molecules as large as TPP and TPPo. In the present report, we show that this DFT methodology can be used to compute two-photon parameters of comparatively large molecules that agree well with those experimentally obtained. Our quantum chemical approach thus represents progress in the application of theory to nonlinear optical problems.

6.2. EXPERIMENTAL SECTION

***Materials*:** TPPo and PdTPPo were synthesized and purified as described previously [2-4], while TPP was purchased from Porphyrin Systems. Concentrations of these compounds used in the two-photon experiments (~$2 \cdot 10^{-4}$ M) were calculated from known molar extinction coefficients (Table 1). It was confirmed that, over the course of our experiments, laser irradiation caused no photodegradation of the sensitizers. Spectroscopic grade toluene was purchased from Aldrich and used as received. Experiments were performed using air-equilibrated samples.

Computational Details: Computational calculations were performed by Dr. Paterson from Heriot-Watt University (England) and are included in this chapter to go beyond the qualitative arguments derived from one- and two-photon experiments. A detailed description of the computational methodology is given in the original manuscript. Very briefly, ground state geometries of both TPP and TPPo were optimized using density functional theory with the B3LYP functional and the 6-31G* basis set, as implemented in the *Gaussian 03* program (revision C.02, 2004). At each of the minimum energy

geometries, one- and two-photon absorption spectra and associated absorption cross sections were computed using density functional response theory as implemented in a local version of the Dalton program. For further information see: http://www.kjemi.uio.no/software/dalton/dalton.html.

In the response calculations, Coulomb-attenuated version of the B3LYP functional, CAM-B3LYP, was used because this has been shown to give reliable two-photon results compared to high accuracy coupled-cluster response calculations [45]. In the response theory calculations, the one-photon spectra were obtained from the linear response function whereas the two-photon spectra were obtained from the quadratic response function, the poles giving the excitation energies and the residues the transition moments [39].

The calculated two-photon absorption cross sections are reported in atomic units (au), not in the so-called Göppert-Mayer units (GM) pertinent to experimental results (1 GM = 10^{-50} cm^4 s $photon^{-1}$ $molecule^{-1}$). A more complete discussion of the conversion from atomic units to GM is presented elsewhere [36].

6.3. RESULTS AND DISCUSSION

Because porphycenes and porphyrins are both tetrapyrrolic systems, they have many common electronic-structure-based properties. This is readily seen in the one-photon absorption spectra, which for the three molecules considered in this study, TPPo, PdTPPo and TPP, are shown in Fig. 1.

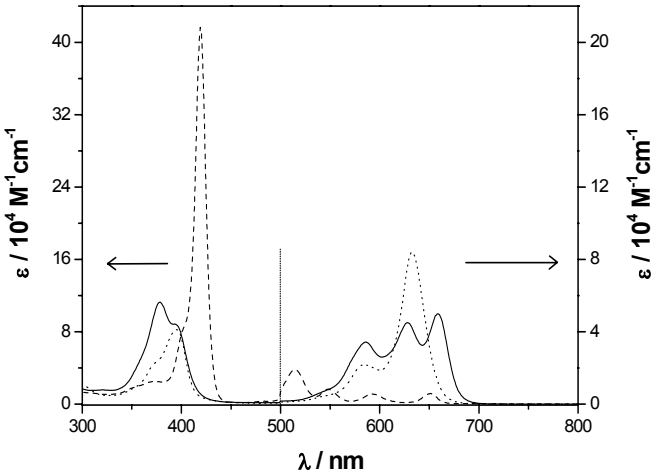

Fig. 1. Absorption spectra of TPPo (—), PdTPPo (···) and TPP (---) in toluene. Note the change of scale in the ordinate for wavelengths longer than 500 nm.

Briefly, all molecules show strong one-photon absorption in the Soret region (~ 350-430 nm). For the porphycenes, however, the Soret band is less intense, broadened and blue-shifted in comparison with the Soret band for TPP. Also, for both porphycenes, one-photon transitions in the Q region between ~ 500-700 nm are significantly enhanced compared with those for TPP. Moreover, of the bands in the Q region, the 0-0 transition is the weakest in TPP whereas this transition is the strongest for TPPo and PdTPPo.

A more detailed discussion of these spectroscopic features is presented elsewhere, along with a discussion of the significant photophysical properties of these molecules [9,16]. One point to be noted here is that data from a number of sources, including our own computations (*vide infra*), indicate that the macrocycle in TPPo is not planar and is characterized by an appreciable amount of flexibility. This is reflected, for example, in a quantum yield for TPPo internal conversion, Φ_{ic} = 0.52, that is much larger than that for TPP, Φ_{ic} = 0.05 (Table 1) [9]. For PdTPPo, the introduction of the metal has other consequences on the photophysical behaviour of the porphycene. Of greatest interest here is the effect of the metal on intersystem crossing, resulting in a comparatively large triplet yield, Φ_T, and, in turn, a large quantum yield of $^1O_2$ production, Φ_Δ (Table 1).

Table 1. Selected photophysical parameters for TPPo, PdTPPo and TPP in toluene.[a]

	$\log \varepsilon_{Soret}$[b] (λ_{max})	$\log \varepsilon_{Q}$[b] ($\lambda_{max,\ 0\text{-}0}$)	Φ_{ic}	Φ_T	Φ_Δ	δ / GM[c]	(λ)
TPPo	5.05 (378 nm)	4.70 (659 nm)	0.52 ± 0.07	0.33 ± 0.04	0.23 ± 0.02	2280 ± 350 14 ± 3[d]	(770 nm) (1100 nm)
PdTPPo	4.92 (395 nm)	4.92 (632 nm)	0.22 ± 0.06	0.78 ± 0.06	0.78 ± 0.04	1750 ± 265 19 ± 3[d]	(770 nm) (1100 nm)
TPP	5.62 (419 nm)	3.60 (648 nm)	0.05 ± 0.10	0.82 ± 0.10	0.66 ± 0.08[e]	24[f] 6[g]	(760 nm) (1100 nm)

a) One-photon parameters for TPPo and PdTPPo taken from Rubio et al.[9] Singlet oxygen quantum yields, Φ_Δ, were independently verified in the present study. b) ε values in M^{-1} cm^{-1}. c) 1 GM = 10^{-50} cm^4 s $photon^{-1}$ $molecule^{-1}$. d) These numbers are based on a value of 6 GM for TPP at 1100 nm reported by Kruk *et al*.[21] (see discussion in text). e) From Wilkinson et al.[46] f) Value published by Kruk *et.al*.[21] Error limits for their number were not reported. g) Value reported by Kruk *et al*.[21], and used as a reference for the TPPo and PdTPPo experiments at 1100 nm.

A. Two-photon absorption spectra. As already outlined, two-photon absorption parameters for a given molecule were obtained by monitoring the phosphorescence intensity of $^1O_2$ produced by energy transfer from that molecule. Experiments were performed using, as a reference standard, the $^1O_2$ signal obtained from a molecule for which two-photon parameters had been independently quantified.

Upon irradiation of TPPo and PdTPPo at wavelengths longer than 740 nm, the intensity of the $^1O_2$ signal observed scaled quadratically with the incident laser power, as required for a two-photon process (eq. (1)). This is illustrated in Fig. 2 for TPPo in a double logarithmic plot of the observed $^1O_2$ emission intensity as a function of incident laser power for irradiation at 800 nm.

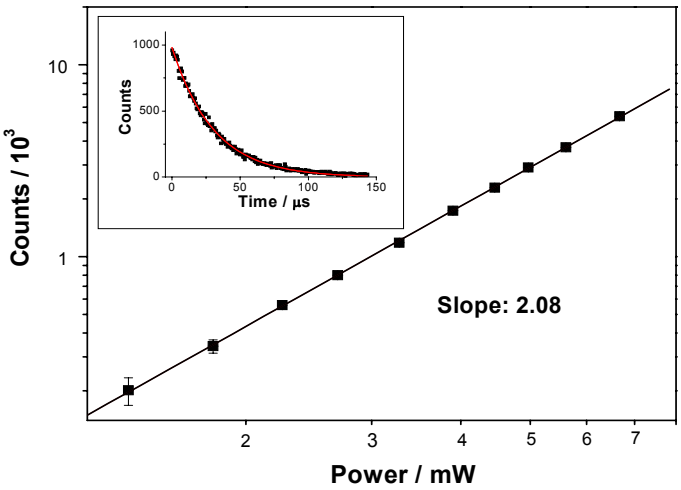

Fig. 2. Double logarithmic plot of the $^1O_2$ phosphorescence intensity (data from a photon counting experiment) as a function of the incident laser power used to irradiate TPPo at 800 nm in air-saturated toluene. A linear fit to the data yields a slope of 2 as expected for a two-photon process. Inset: time-resolved trace of the $^1O_2$ phosphorescence signal. A single exponential decay function was fitted to the data, resulting in a lifetime of $\tau = 30.4 \pm 0.2$ µs. With the exception of the data points for the two lowest powers, the error on each point falls within the mark used to denote that point.

Upon irradiation of TPPo and PdTPPo at 740 nm and shorter wavelengths, however, plots of the $^1O_2$ signal intensity against the incident laser power deviated from this quadratic dependence and approached a linear dependence instead. Keeping in mind that the spectral profile of a fs laser pulse is comparatively broad (*i.e.*, fwhm of ~10-15 nm), this observation is consistent with the onset of the more dominant one-photon transitions in the Q region that competitively absorb the incident light (see Fig. 1). The masking of two-photon transitions by interfering one-photon absorption is a common phenomenon observed in many molecules, including TPP and other porphyrins [20,21].

For all experiments, the time-resolved $^1O_2$ signal observed followed first-order decay kinetics, yielding a lifetime consistent with that expected for an experiment performed in toluene [τ_Δ(toluene) ≈ 30 μs [47], inset of Fig. 2]. This result demonstrates the absence of competing photo-induced processes that result in the creation of transients that, in turn, can quench any $^1O_2$ produced [48-51]. Finally, and arguably most importantly, it was verified that irradiation of neat toluene under our conditions did not give rise to a $^1O_2$ signal, a phenomenon which can adversely influence similar two-photon experiments [30].

Two-photon excitation spectra for TPPo and PdTPPo, obtained through the use of equation 1, are shown in Fig. 3. These data, recorded over the spectral range 750-850 nm, are plotted together with the corresponding one-photon spectra. Note that these spectra are plotted as a function of both the total transition energy (in eV) and total transition wavelength (in nm), an approach that facilitates comparison with calculated spectra (*vide infra*). Thus, it is important to recognize that the two-photon experiments were actually performed at wavelengths twice as long as those shown in the plots.

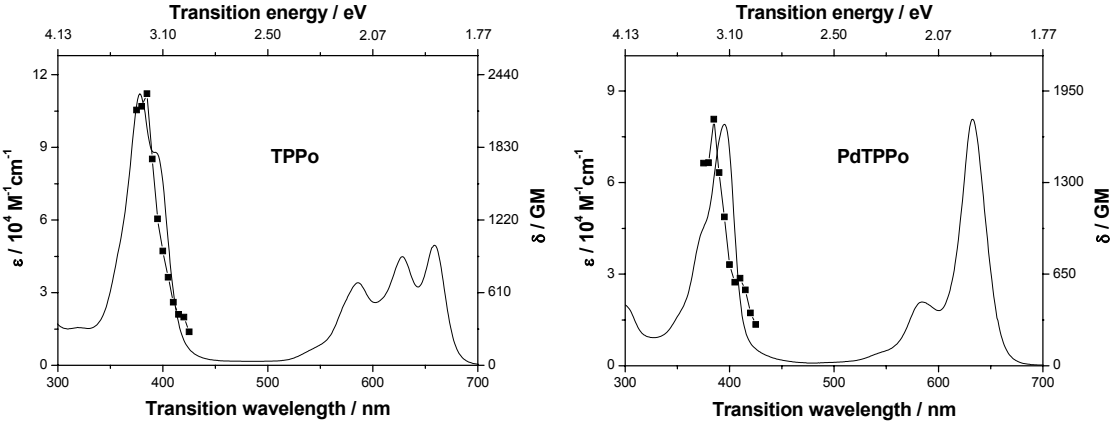

Fig. 3. Two-photon absorption spectra for TPPo and PdTPPo in toluene (■, right axes). As outlined in the text, the data were recorded as singlet oxygen excitation spectra through the use of Eq. (1). The corresponding one-photon spectra are also plotted (—, left axes). The *x*-axes display the total transition energy and wavelength and, as such, it is important to recognize that the two-photon experiments were performed at wavelengths twice as long as those shown. The scale for the two-photon absorption cross section, δ, was established using values independently determined for the reference compound CNPhVB in toluene [30]. The error on each data point (not shown for clarity) is estimated to be 15 %.

Corresponding one- and two-photon absorption spectra for TPP are shown in Fig. 4. In this case, we have re-plotted the two-photon fluorescence excitation profile originally published by Kruk *et al.* [21] (It is important to note here that, in the report of Kruk *et al.* [21], the scale published for the TPP molar extinction coefficient is incorrect in their Fig. 1a. The published scale should indicate a value of ~ 4.7 × 10^5 M^{-1} cm^{-1} for the extinction coefficient at the 419 nm maximum of the TPP Soret band [52]. This latter

extinction coefficient is consistent with a value of 4.2×10^5 M^{-1} cm^{-1} obtained in our own experiments and with published data [53]. However, the scale published by Kruk *et al.* [21] for the TPP two-photon cross sections in their Fig. 1a is correct [52].

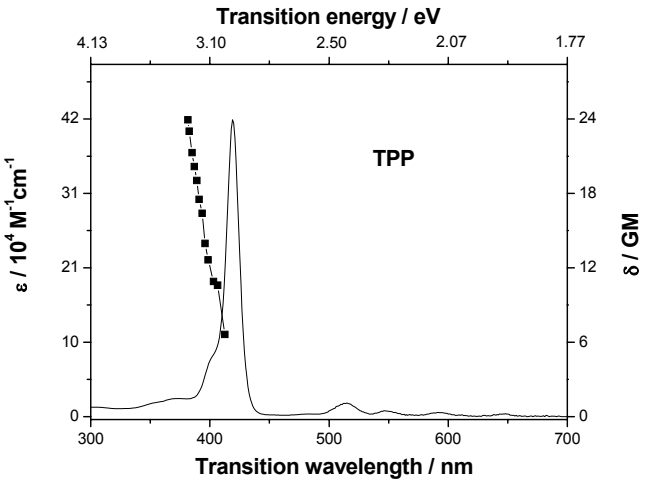

Fig. 4. Two-photon excitation spectrum (■, right axis) and one-photon absorption spectrum (—, left axis) of TPP in toluene. The two-photon spectrum uses data published by Kruk *et al.* [21] using an average for the individual data sets reported at a given wavelength. The *x*-axes display the total transition energy and wavelength and, as such, it is important to recognize that the two-photon experiments were performed at wavelengths twice as long as those shown. Two-photon data could not be collected at wavelengths shorter than those shown due to competing absorption by one-photon transitions (see text).

For TPPo, it is clear from Fig. 3 that the spectral profile for two-photon absorption matches the corresponding one-photon absorption profile for experiments performed in the region of the Soret band. Specifically, the two-photon spectrum has a band maximum at twice the wavelength of the band maximum observed in the one-photon spectrum. Thus, the data indicate that, for the porphycene TPPo, (a) the state initially populated upon two-photon excitation is nearly degenerate with the state initially populated upon one-photon excitation, or (b) the two-photon transition, in fact, populates the same state as the one-photon transition. These data are in stark contrast to those observed from the isomeric porphyrin, TPP (Fig. 4). In this latter case, although one is unable to discern a band maximum in the two-photon spectrum of TPP, the data clearly indicate that this maximum will occur at a transition energy that is significantly higher than that observed in the one-photon spectrum. Thus, for TPP, the state initially populated upon two-photon excitation is higher in energy than that initially populated upon one-photon excitation.

The one- and two-photon data in TPP have been discussed in terms of parity selection rules applied to a centrosymmetric molecular geometry wherein transitions allowed as one-photon electric dipole processes are forbidden as two-photon processes [21]. On

this same basis, one would thus expect that the one- and two-photon spectra recorded for TPPo would likewise show the same behaviour as that observed for TPP. The data obtained, however, clearly show otherwise. Indeed, the similarity between the one- and two-photon spectra shown in Fig. 3 suggests that, on the basis of these selection rules, the equilibrium geometry of TPPo does not have a center of inversion. In part, this phenomenon could reflect the increased flexibility of the porphycene macrocycle (*vide supra*) through which, due to state mixing mediated by vibronic coupling, two-photon character could be imparted into a transition that would otherwise contain only one-photon character. I will return to these issues when discussing our calculations on these systems (Section D, *vide infra*).

B. Two-photon absorption cross sections. Pertinent values of the two-photon absorption cross section, δ, are listed in Table 1. At their band maxima, both TPPo and PdTPPo have comparatively large absorption cross sections: δ(770 nm) = 2280 ± 350 and 1750 ± 265 GM, respectively. These data indicate that incorporation of the metal into the porphycene macrocycle has only a minor effect on the two photon transition probability. On the other hand, the porphycene δ values are significantly larger than the maximum value reported for TPP in the same spectral region, ~ 24 GM. Admittedly and as clearly seen in Fig. 4, this δ value for TPP may not represent the value at the maximum of the two-photon absorption band. Nevertheless, given the spectra shown, it is fairly safe to surmise that the maximum δ values for the porphycenes will be significantly larger than that for TPP. This issue is discussed further in Section C, *vide infra*.

To further study the nonlinear optical behaviour of TPPo and PdTPPo, and to compare this behaviour to that of TPP, two-photon absorption into the Q region was performed by tuning the excitation wavelength to 1100 nm. Upon irradiation of these respective molecules at this wavelength, we indeed observed a $^1O_2$ phosphorescence signal that scaled quadratically with incident power. To quantify δ values for the porphycenes at this wavelength, experiments were performed using TPP as the two-photon reference. Specifically, Kruk *et al.* have reported that δ = 6 GM for irradiation of TPP at 1100 nm in toluene [21]. Against this δ value for TPP, we ascertained that δ = 14 ± 3 and 19 ± 3 GM for TPPo and PdTPPo, respectively.

First, it is clear that, for all three molecules, values for the absorption cross section at 1100 nm are significantly smaller than those recorded upon irradiation in the Soret region (*vide supra*, Table 1). Moreover, and as with the data recorded upon irradiation in the Soret region, these data obtained upon irradiation in the Q-region indicate that

the two-photon absorption cross sections for the porphycenes are larger than that for the corresponding porphyrin. However, care must be exercised in this latter assessment simply because data were only recorded at one wavelength. Rather, one should ideally record data over a range of wavelengths to accommodate molecule-dependent spectral shifts. Unfortunately, upon irradiation of these molecules at wavelengths longer than 1100 nm, we observed a large near IR emission signal that scaled linearly with the incident power. Although this observation might reflect direct absorption by oxygen (*i.e.*, $O_2(X^3\Sigma_g^-)_{v=0} \rightarrow O_2(a^1\Delta_g)_{v=1}$) [54], it more likely derives from the increased transmittance of the silicon-based optics used to isolate the 1270 nm $^1O_2$ phosphorescence. As such, our detector may be responding to light from a number of different sources. It is also important to note that, in this spectral region, toluene has an appreciable one-photon absorption band that is assigned to a second vibrational overtone (Fig. 5) [55]. We have previously demonstrated that both overtone and two-photon excitation of toluene itself can cause appreciable interference when performing two-photon experiments on a sensitizer dissolved in this solvent [30]. (Indeed, in a private communication, we have been told that δ values for TPP at wavelengths longer than ~ 1100 nm in toluene published by Kruk *et al.* [21] may be incorrect due to the interfering effects of solvent in their measurement [52])

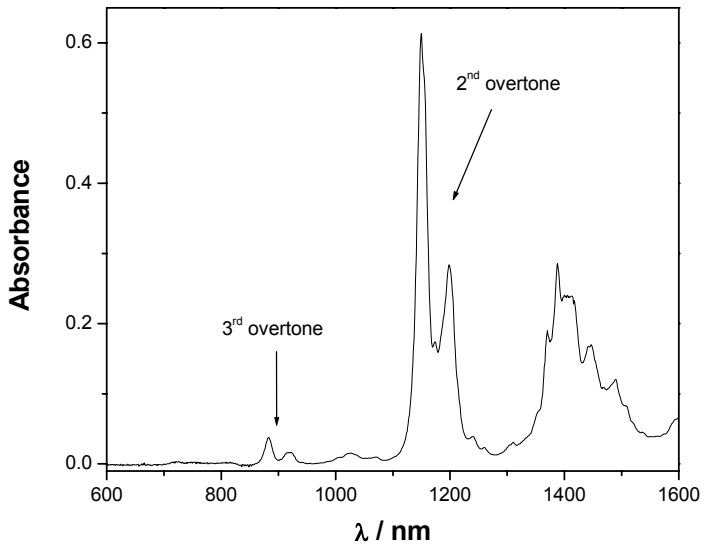

Fig. 5. Absorption spectrum of neat toluene over the spectral region pertinent to the present two-photon experiments. The 2nd and 3rd overtones of C-H stretching modes are marked. Data were recorded using a 1 cm path length cell.

C. **Resonance enhancement in two-photon transitions**. The observation that, in the Soret region, the porphycenes have a much larger two-photon absorption cross section than the corresponding porphyrin can be qualitatively explained using the concept of resonance enhancement. The latter has been invoked in discussing the nonlinear optical behaviour of other molecules [33,36,56,57] but, as outlined below, it is particularly relevant for porphyrins and related systems [20,21,58].

In describing the qualitative features of the two-photon transitions in the porphycenes as compared to that in the porphyrin TPP, we consider the condensed three-level scheme shown in Fig. 6 that shows the pertinent electronic eigenstates and transition frequencies (with no formal reference to state parity). Here 0 represents the ground state, and *S* and *Q* represent states in the Soret and Q regions, respectively. Simultaneous absorption of two photons is shown to occur via a virtual state.

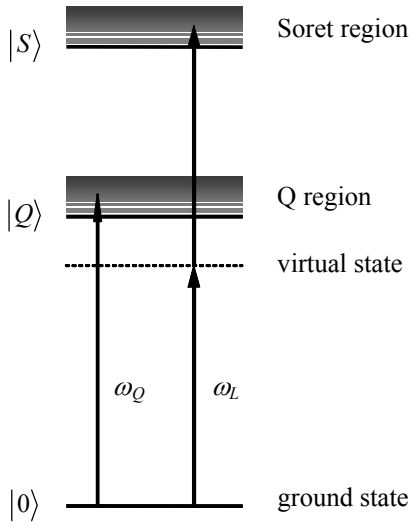

Fig. 6. Generalized three-level energy diagram describing resonance enhanced two-photon excitation in porphyrins and porphycenes. The laser frequency used in the two-photon experiment is ω_L and ω_Q is the frequency of an allowed one-photon transition in the Q region.

The salient features of this model are perhaps most easily understood in terms of the expression shown in Eq. (1) [58], where $\delta_{f\leftarrow 0}$ is the two-photon absorption cross section upon ground state excitation into a final state *f* :

$$\delta_{f\leftarrow o} \propto \sum_j \frac{\left|\mu_{oj}\right|^2 \left|\mu_{jf}\right|^2}{\left(\omega_j - \omega_L\right)^2 + \Gamma^2{}_{0j}} g_n(2\omega_L) \qquad (1)$$

Given that the virtual state is accurately described as a linear combination of all real eigenstates in the molecule, it is important to note that included in Eq. (1) are the transition dipole moments for the one-photon processes between the ground and j^{th}

state, $|\mu_{oj}|$, and between the j^{th} and final state, $|\mu_{jf}|$, summed over all real states *j*. Moreover, the denominator in Eq. (1) is dominated by the term ω_j - ω_L, whose magnitude depends on the difference between the excitation frequency of the j^{th} state and the frequency of the irradiating laser. Referring to Fig. 6 and Eq. (1), and recognizing that ω_Q denotes the frequency of an allowed one-photon transition to a state in the Q region, it is readily seen that a special case arises when the laser frequency ω_L approaches ω_Q. Under these conditions, the cross section for two-photon absorption into the Soret region will be dominated by terms in which the virtual state principally reflects states in the Q region. Although exact resonance is not achieved because $\omega_Q > \omega_L$, this condition of near resonance with an allowed one-photon transition can result in a significant enhancement of the two-photon transition in the Soret domain. A similar situation will not arise for two-photon absorption into the Q-region because there are no allowed one-photon transitions to a state *j* where $\omega_j \sim \omega_L$. Thus, on this basis one can generally rationalize why two-photon absorption cross sections in both porphyrins and porphycenes are greater in the Soret region than in the Q-region.

Application of these same arguments also explains why the Soret two-photon absorption cross sections for the porphycenes TPPo and PdTPPo are greater than that for TPP. In this case, the transition moments for one-photon absorption in the Q-region, $|\mu_{oj}|$, are far greater for the porphycenes than for TPP. This is clearly seen in the linear absorption spectra (Fig. 1). Moreover, for both TPPo and PdTPPo, the most intense Q-band is the 0-0 transition, thereby resulting in the greatest enhancement when the detuning term $\omega_Q - \omega_L$ is the smallest. In contrast, in TPP, the 0-0 transition in the Q domain is comparatively weak (Fig. 1).

D. **Experiments *vs* Calculations.** To go beyond the qualitative arguments presented above, and to address the relationship between molecular symmetry and the observed spectra, one- and two-photon quantum chemical calculations were performed on TPP and TPPo. As outlined in the section on computational details (*vide supra*), this was accomplished by Dr. Paterson from Heriot-Watt University (England) using density functional response theory.

> *Geometry Optimization.* Ground state geometries of both TPP and TPPo were optimized using density functional theory with the B3LYP functional and 6-31G* basis set, as implemented in the Gaussian program. Key parameters are collected in Table 2, while the structures are shown in Fig. 7 (for the complete coordinates: see Supporting Information of the original paper).

Table 2. Parameters for optimized conformers of ground state TPP and TPPo.

Molecule	Point Group	Dihedral Angles[a]				Energy (au)	ΔE (kJ/mol)[b]
		a	**b**	**c**	**d**		
TPP	D_{2h}	90°	90°	90°	90°	-1913.74947	4.20
	C_{2h}	69.1°	68.9°	110.9°	111.1°	-1913.75075	0.84
	D_2	71.2°	71.2°	71.2°	71.2°	-1913.75034	1.92
	C_2	66.1°	113.4°	66.1°	113.4°	-1913.75107	0
TPPo	C_{2h}	90°	90°	90°	90°	-1913.77265	30.56
	C_i	47.5°	134.2°	134.3°	44.0°	-1913.78411	0.47
	C_2	134.8°	134.6°	134.8°	134.6°	-1913.78429	0

a) Dihedral angle between the plane of the pyrrole ring and the adjacent phenyl substituent in TPPo and between the plane of the macrocycle and the phenyl ring in TPP, measured clockwise around the macrocycle such that **a**, **c** and **b**, **d** are on opposite sides (see Fig. 7). b) Energy difference, ΔE (kJ/mol), relative to the lowest energy conformer. Perpendicular geometries are 4^{th} order saddle points.

Through these calculations, three minima were found for TPP with geometries belonging to the point groups C_{2h}, D_2 and C_2, respectively. In all cases, the TPP macrocycle itself was planar, and the three geometries differ only in the dihedral angles between the plane of the macrocycle and the planes of the pendant phenyl rings. In general, these results are consistent with those of Kruk *et al.* [21], for example, who likewise find minima in which the pendant phenyl rings are twisted through a dihedral angle of about 60° with respect to the plane of the macrocycle. On the other hand, Kruk *et al.* identify two minimum energy conformers (*i.e.*, C_{2h} and C_2), whereas we have identified three.

The energy differences between these respective minima in TPP are small (<2 kJ/mol) and, as such, the actual geometry of the molecules studied will be a combination of all conformers (*i.e.*, our data would reflect a Boltzmann weighted average of these conformers). With this in mind, and with respect to our present study on two-photon transitions, it is important to recognize that, of the three TPP conformers shown, only one has a centre of inversion (C_{2h} point group); the others are non-centrosymmetric.

Likewise, two minima were found for TPPo with geometries that belong to the point groups C_i and C_2. In these cases, the TPPo macrocycle was slightly twisted out of planarity, but this twisting occurs such that the molecules still transform according to the point groups indicated. These geometries differ in the dihedral angles between the plane of a given pyrrole ring and the adjacent phenyl group. The energy difference between these conformers is likewise small (0.47 kJ/mol), and facile interconversion between the two will occur at room temperature. Moreover, the conclusion that the TPPo macrocycle is not planar is consistent with the photophysical behaviour ascribed to a macrocycle that is more flexible than that in TPP (*vide supra*). Finally, and again with respect to our present study on two-photon transitions, it is important to recognize that, of the TPPo conformers shown, only one has a centre of inversion; the other is non-centrosymmetric.

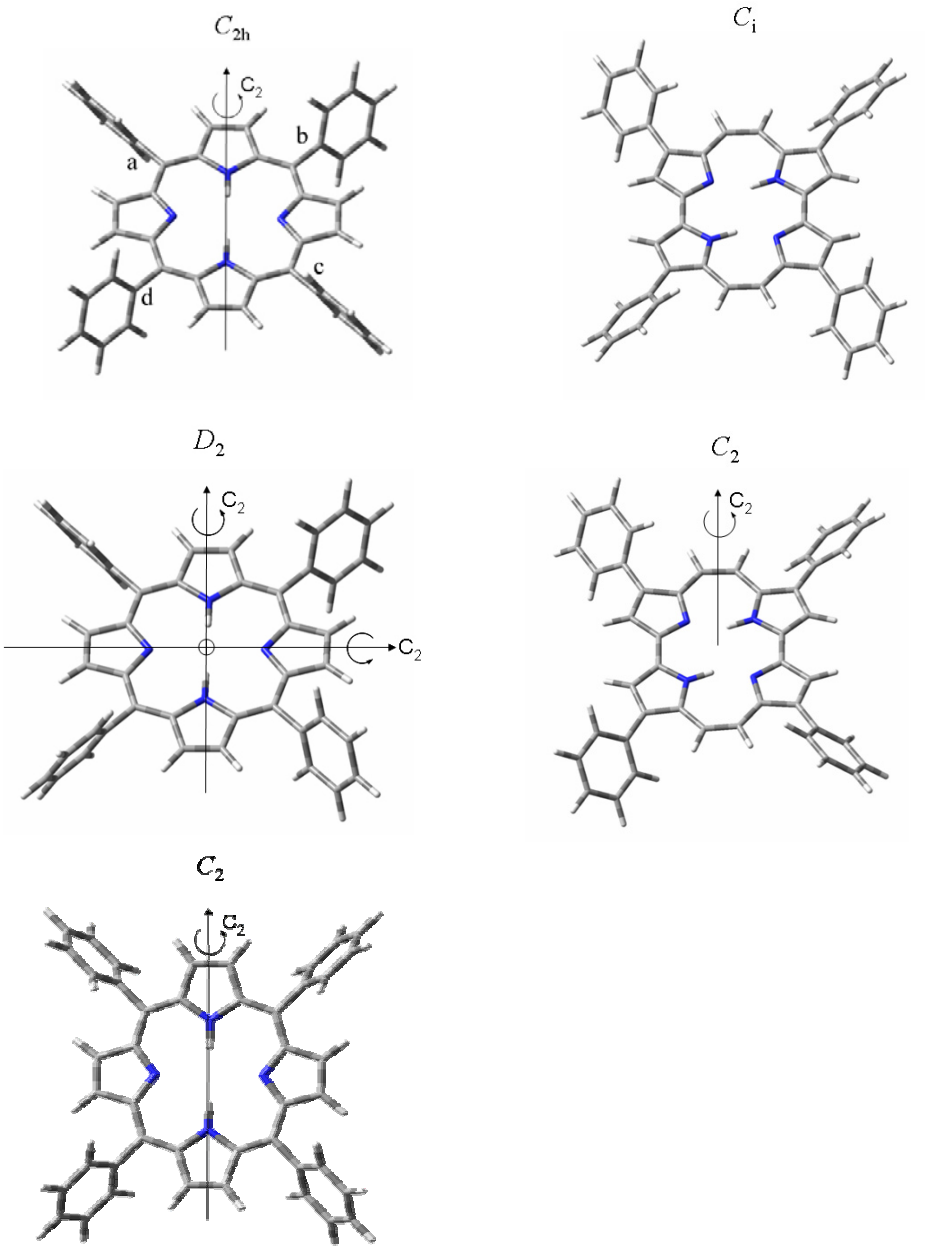

Fig. 7. Minimum energy conformers for TPP (left column) and TPPo (right column). The largest energy difference between the conformers for TPP, E(D_2) – E(C_2), is 1.92 kJ/mol, whereas for TPPo, E(C_i) – E(C_2), it is 0.47 kJ/mol. The letters shown on the upper left hand structure correspond to the columns shown in Table 2 in which dihedral angles are designated. This labeling holds for all of the structures.

In concluding this section, we reiterate the significant point that both TPP and TPPo are equally characterized by conformers that are centrosymmetric and conformers that are not. Thus, when interpreting the correspondence, or lack thereof, between one- and two-photon spectra such as those shown for TPP and TPPo in Fig. 3 and Fig. 4, one must exercise caution when invoking a qualitative discussion based on symmetry-derived parity selection rules. Rather, as outlined below, it is more prudent to carry out a more rigorous calculation.

One- and two- photon transitions. Fig. 8 shows the energies and probabilities for one- and two- photon transitions for each of the TPP and TPPo conformations. Importantly, for each molecule there is not a significant difference between the spectra calculated for the individual conformers (*i.e.*, the spectrum for C_{2h} TPP is almost identical with those for D_2 and C_2 TPP. Additional information can be found in the original paper). Thus, we can effectively compare a single TPP spectrum with a single TPPo spectrum, and this is done in Fig. 8 using conformers for which there is no inversion symmetry. Keeping in mind that the spectra calculated for TPP and TPPo correspond to rigid, non-vibrating gas-phase systems, these spectra agree quite well with the experimental data.

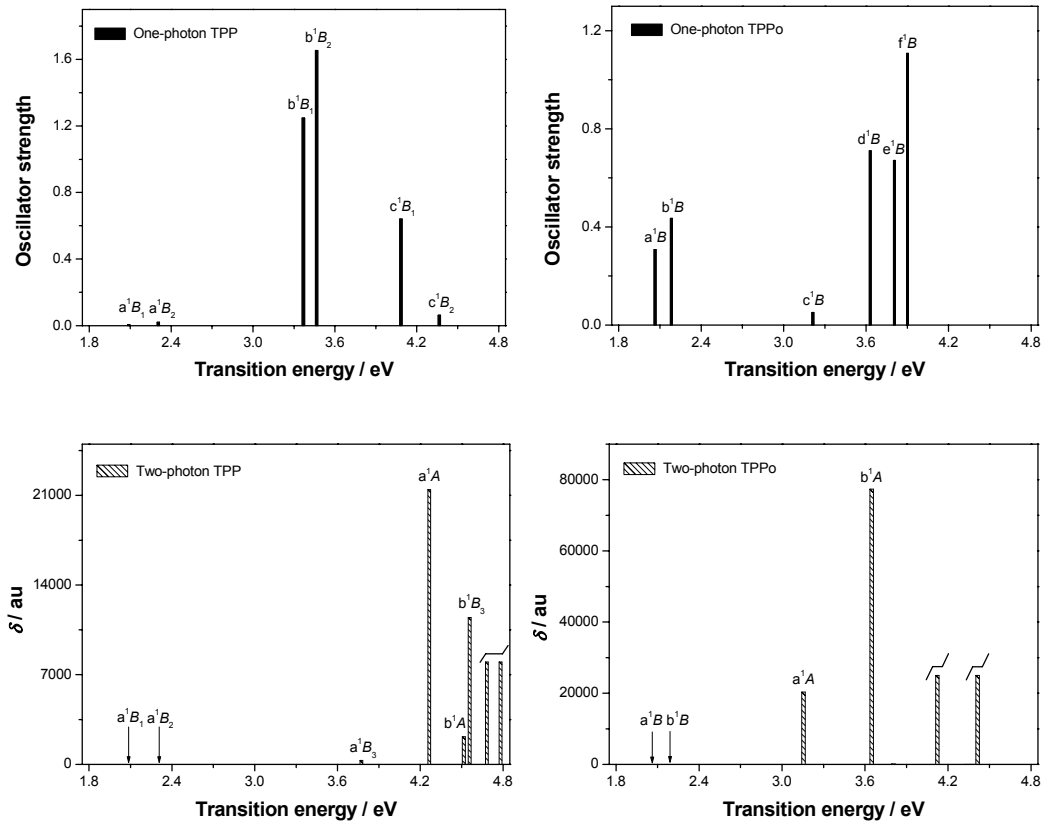

Fig. 8. Calculated one- and two-photon spectra for TPP (left) and TPPo (right). Transition probabilities are given in terms of oscillator strength for the one-photon spectra and rotationally-averaged δ values for the two-photon spectra (the latter are given in atomic units; see discussion in the text). The TPP spectrum shown is for the conformer that transforms according to the point group D_2, whereas the TPPo spectrum is for the conformer that transforms according to the C_2 point group. The irreducible representation to which a given transition transforms in the corresponding point group is shown. A complete list of the calculated transitions and transition probabilities is shown in tabular form in the Supporting Information.

We first focus on the one-photon transitions. The calculated spectrum of TPP readily reproduces the fact that the Q-bands in the spectral domain of 2.0-2.4 eV are much less intense than the Soret transitions in the spectral range of 3.3-3.5 eV. Likewise, the calculated spectrum of TPPo indicates that the Q-band transitions for this molecule are

more intense, not only relative to the TPPo Soret band but also relative to the Q band transitions in TPP. Finally, the transition energy of the TPPo Soret band is calculated to be slightly higher than that of TPP, and the intensity of the TPPo Soret transition to be less than that of TPP, as indeed observed experimentally.

The calculated two-photon spectra are equally as impressive. For TPP, the calculations indeed indicate that the principal two-photon absorption band will occur at a transition energy higher than that for the one-photon band. For TPPo, the calculations correctly indicate that, in the Soret region, the principal two-photon absorption band will be coincident with the one-photon band, just as we have observed experimentally (Fig. 3). The calculations also correctly reproduce a δ value for TPPo in the Soret domain that is significantly larger than the corresponding value for TPP. With respect to this latter point, however, it is important to note that the calculated ratio of TPPo/TPP δ values is not as large as the ratio of TPPo/TPP δ values experimentally obtained. In part, this discrepancy likely reflects the fact that, in the experimental spectrum of TPP, the band maximum of the two-photon absorption profile is not obtained at the shortest wavelength used (see Fig. 4).

There are several other more subtle points in the calculated spectra that deserve comment. First, for TPPo, the two-photon transitions shown at 4.12 and 4.35 eV are so close to being in resonance with the one-photon Q-band transitions at 2.07 and 2.18 eV, that reliable two-photon matrix elements can not be safely calculated for these specific transitions, but they are expected to be very large. Second, although the calculations yield two-photon TPPo Q-band transitions at 2.07 and 2.18 eV, respectively, they are not seen in the spectrum shown in Fig. 8 because, relative to the two-photon Soret transition, these calculated Q-band transitions are significantly less intense. Similarly, the calculated two-photon Q transitions for TPP at 2.09 and 2.31 eV are not seen in the spectrum because they, too, are small compared to the Soret transition (as with TPPo, there are also one photon transitions in TPP at these same energies). Nevertheless, despite the fact that these calculated two-photon Q transition probabilities are small relative to the Soret transitions, the TPPo Q-band transition probabilities are indeed calculated to be larger than those for TPP (see Supporting Information of the original manuscript).

The most important point that is realized through these calculations is that one must exercise caution when using qualitative molecular-symmetry-derived arguments to predict the expected relation between allowed one- and two-photon transitions. From a simplistic perspective, one might say that, because TPP appears to be centrosymmetric, it is expected that the first allowed two-photon transition will populate a state higher in energy than the state populated by a one-photon transition [59]. It is thus reassuring to observe that this expectation is indeed met in the experimental data (Fig. 4). By extension, because TPPo also appears to be centrosymmetric, one would

likewise expect the two-photon transition to populate a state higher in energy than that populated in a one-photon process. This latter expectation is not realized in the experimental data (Fig. 3). Rather, on the basis of the experimental data, one would infer that TPPo is, in fact, non-centrosymmetric. In reality, both TPP and TPPo are arguably best described in terms of a Boltzmann distribution of centrosymmetric and non-centrosymmetric conformers. Thus, attempts to predict the expected relation between allowed one- and two-photon transitions should ideally incorporate the results of reasonably rigorous computations; one can be misled by arguments based solely on apparent molecular symmetry. As illustrated in the case of TPPo, such computations can point to “accidental degeneracies” in which a state populated in a two-photon transition is energetically very close to a state populated in a one-photon transition (Fig. 8).

> *Cis porphycene tautomers.* Our presentation thus far has been based on the framework that TPPo exists as the *trans* tautomer, as shown in Chart 1 and Fig. 7. At this point, however, it is pertinent to note that, in our room temperature samples, the TPPo population could also contain some of the higher-energy *cis* tautomers that result as a consequence of changes in the position of the N-H bonds within the macrocycle [60]. Calculated minimum energy structures for these *cis* tautomers are indeed consistent with the notion that a room temperature population of TPPo will contain a mixture of *cis* and *trans* tautomers. On the other hand, corresponding calculations for TPP indicate, as expected [60], that the *cis* tautomer is significantly higher in energy than the *trans.* As such, it is only necessary for us to consider the *trans* tautomer of TPP, as shown in Chart 1 and Fig. 7.
>
> Of course, these *cis* tautomers of TPPo do not have inversion symmetry and, as such, the associated one- and two-photon spectra are expected to show similarities. Most importantly, if our ground state TPPo population is indeed accurately described as a weighted mixture of *cis* and *trans* tautomers, our central thesis developed in the previous sections is only further substantiated. Specifically, our spectroscopic data reflect a distribution of both centrosymmetric and non-centrosymmetric structures.

In conclusion, one must exercise caution when using qualitative molecular-symmetry-derived arguments to predict the expected spectral relationship between allowed one- and two-photon transitions. From a practical perspective, this study establishes that, in comparison to porphyrins and other tetrapyrrolic macrocyclic systems, porphycenes exhibit many desirable attributes for use as sensitizers in two-photon initiated photodynamic therapy.

6.4. CONCLUSIONS

Porphycenes are isomers of porphyrins and, as such, can be used to yield fundamental information about the relationship between structure and reactivity in tetrapyrrolic macrocycles found in a wide range of ubiquitous compounds. In their own right, porphycenes have unique properties that distinguish them from the commonly found porphyrins. In the present study, we have established that, in the spectral domain 750-850 nm (*i.e.*, the two-photon Soret region), the two-photon absorption cross sections for two porphycenes, TPPo and PdTPPo, are large compared to that from the porphyrin analogue, TPP. These observations are attributed to the fact that, for the porphycenes, the two-photon transition is nearly resonant with a comparatively intense one-photon Q-band transition. In this regard, these data corroborate a model based on resonance-enhancement that can be quite useful in qualitatively predicting the relative magnitudes of two-photon transitions in tetrapyrrolic systems. This work has also established, however, that qualitative symmetry-based arguments used to predict the spectral relationship between one- and two-photon transitions can be misleading, and that one should ideally rely on more rigorous quantum chemical calculations to predict nonlinear optical properties. To this end, it has been demonstrated that density functional response theory with appropriate functionals can provide useful results, even for these comparatively large porphycene and porphyrin systems. Furthermore, such calculations show that one can now apply fairly rigorous quantum mechanical methods to such nonlinear optical phenomena as two-photon absorption in large chemical systems without having to use arbitrary sum-over-states expressions.

In the Soret spectral region (~750-850 nm), the two-photon absorption cross sections obtained for these fundamental porphycenes are not only larger than that for TPP but they are also larger than those for other analogous tetrapyrrolic macrocyclic systems. For example, although tetraazaporphyrins (*i.e.*, porphyrazines) can have large two-photon absorption cross sections [24,61], the data reported herein indicate that the basic porphycene, TPPo, still has a larger two-photon transition probability in the Soret region.

Porphycenes sensitize the production of singlet molecular oxygen, $^1O_2$, upon two-photon irradiation and, with such large two-photon absorption cross sections in the spectral region around 800 nm, these molecules are good candidates for use in two-photon initiated photodynamic therapy. With this in mind, it is important to note that the efficiency of the two-photon absorption process in porphyrins can be enhanced by structural modifications [23], including the generation of porphyrin dimers [22,25].

Similar structural modification to the porphycene framework could likewise prove to be quite beneficial for use in PDT, particularly when combined with modifications that might enhance the selectivity with which these compounds either target a malignant cell or localize in a specific subcellular domain. To this end, a recently published diversity-oriented synthesis of porphycenes should facilitate such developments [62]. In any event, even in the absence of such modifications, the two-photon absorption cross sections reported herein for TPPo and PdTPPo, 2280 and 1750 GM, are significantly greater than the absorption cross sections for the porphyrin-based PDT drugs Photofrin® (δ < 10 GM over the spectral range 800-900 nm) [63] and protoporphyrin IX (δ < 3 GM over the spectral range 760-790 nm) [19].

At this juncture, it is pertinent to mention the ingenious approach of using a two-chromophore conjugate to increase the amount of $^1O_2$ produced upon two-photon excitation of a sensitizer [64,65]. In this approach, a chromophore that efficiently absorbs light in a two-photon process is covalently linked to a second chromophore designed principally to sensitize the production of $^1O_2$ in high yield. Upon nonlinear photoexcitation of the first chromophore, energy transfer to the second chromophore ensues with the resultant production of $^1O_2$. Although this approach is indeed clever, it has the potential limitation of a cumbersome synthetic procedure to make the rather sophisticated conjugate. On the other hand, working solely with the porphycene framework, one can combine a reasonably large two-photon absorption cross section, efficient $^1O_2$ production, and biocompatibility in a potentially simpler and more easily delivered molecular package.

The comparatively large two-photon absorption cross sections in the porphycenes can also be exploited for other nonlinear optical applications. One such application is as a sensitizer in the so-called two-photon $^1O_2$ microscope wherein a focused laser is used to create a discrete and localized population of $^1O_2$ in sub-cellular spatial domains [66,67]. General application of this tool is currently limited, in part, by the lack of biologically compatible $^1O_2$ sensitizers that have large two-photon absorption cross sections [66]. To this end, derivatives of the porphycenes described herein could prove to be beneficial in the use of this microscope to further elucidate spatially-resolved mechanisms of oxygen-dependent photoinduced cell death.

6.5. REFERENCES

[1] Vogel, E.; Kocher, M.; Schmickler, H.; Lex, J. Porphycene - A novel porphin isomer. *Angew. Chem. Int. Ed. Engl.* **25**:257-259; 1986.

[2] Nonell, S.; Bou, N.; Borrell, J. I.; Teixido, J.; Villanueva, A.; Juarranz, A.; Canete, M. Synthesis of 2,7,12,17-tetraphenylporphycene (TPPo) - First aryl-substituted porphycene for the photodynamic therapy of tumors. *Tetrahedron Lett.* **36**:3405-3408; 1995.

[3] Gavalda, A.; Borrell, J. I.; Teixido, J.; Nonell, S.; Arad, O.; Grau, R.; Canete, M. C.; Juarranz, A.; Villanueva, A.; Stockert, J. C. A non-tetradecarboxylative synthesis of 2,7,12,17-tetraphenylporphycene. *Journal of Porphyrins and Phthalocyanines* **5**:846-852; 2001.

[4] Cañete, M.; Ortiz, A.; Juarranz, A.; Villanueva, A.; Nonell, S.; Borrell, J. I.; Teixidó, J.; Stockert, J. C. Photosensitizing properties of palladium-tetraphenylporphycene on cultured tumour cells. *Anti-Cancer Drug Des.* **15**:143-150; 2000.

[5] Bonnett, R. *Chemical Aspects of Photodynamic Therapy*: Amsterdam: Gordon and Breach Science Publishers; 2000.

[6] MacDonald, I. J.; Dougherty, T. J. Basic Principles of photodynamic therapy. *J. Porphyrins Phthalocyanines* **5**:105-129; 2001.

[7] Sternberg, E. D.; Dolphin, D.; Brückner, C. Porphyrin-based photosensitisers for use in photodynamic therapy. *Tetrahedron* **54**:4151-4202; 1998.

[8] Nonell, S.; Aramendía, P. F.; Heihoff, K.; Martin-Negri, R.; Braslavsky, S. E. Laser-induced optoacoustics combined with near-infrared emission. An alternative approach for the determination of intersystem crossing quantum yields applied to porphycenes. *J. Phys. Chem.* **94**:5879-5883; 1990.

[9] Rubio, N.; Prat, F.; Bou, N.; Borrell, J. I.; Teixido, J.; Villanueva, A.; Juarranz, A.; Canete, M.; Stockert, J. C.; Nonell, S. A comparison between the photophysical and photosensitising properties of tetraphenyl porphycenes and porphyrins. *New J. Chem.* **29**:378-384; 2005.

[10] Weishaupt, K. R.; Gomer, C. J.; Dougherty, T. J. Identification of singlet oxygen as the cytotoxic agent in photo-inactivation of the murine tumor. *Cancer Res.* **36**:2326-2329; 1976.

[11] Villanueva, A.; Cañete, M.; Nonell, S.; Borrell, J. I.; Teixido, J.; Juarranz, A. Photodamaging effects of tetraphenylporphycene in a human carcinoma cell line. *Anti-Cancer Drug Des.* **11**:89-99; 1996.

[12] Cañete, M.; Lapena, M.; Juarranz, A.; Vendrell, V.; Borrell, J. I.; Teixido, J.; Nonell, S.; Villanueva, A. Uptake of tetraphenylporphycene and its photoeffects on actin and cytokeratin elements of HeLa cells. *Anti-Cancer Drug Des.* **12**:543-554; 1997.

[13] Cañete, M.; Ortega, C.; Gavalda, A.; Cristobal, J.; Juarranz, A.; Nonell, S.; Teixido, J.; Borrell, J. I.; Villanueva, A.; Rello, S.; Stockert, J. C. Necrotic cell death induced by photodynamic treatment of human lung adenocarcinoma A-549 cells with palladium(II)-tetraphenylporphycene. *Int. J. Oncol.* **24**:1221-1228; 2004.

[14] Kessel, D. Correlation between subcellular localization and photodynamic efficacy. *J. Porphyrins Phthalocyanines* **8**:1009-1014; 2004.

[15] Aramendia, P. F.; Redmond, R. W.; Nonell, S.; Schuster, W.; Braslavsky, S. E.; Schaffner, K.; Vogel, E. The photophysical properties of porphycenes - Potential photodynamic therapy agents. *Photochem. Photobiol.* **44**:555-559; 1986.

[16] Waluk, J.; Muller, M.; Swiderek, P.; Kocher, M.; Vogel, E.; Hohlneicher, G.; Michl, J. Electronic states of porphycenes. *J. Am. Chem. Soc.* **113**:5511-5527; 1991.

[17] Pifferi, A.; Swartling, J.; Chikoidze, E.; Torricelli, A.; Taroni, P.; Bassi, A.; ndersson-Engels, S.; Cubeddu, R. Spectroscopic time-resolved diffuse reflectance and transmittance measurements of the female breast at different interfiber distances. *J. Biomedical Optics* **9**:1143-1151; 2004.

[18] Masthay, M. B.; Findsen, L. A.; Pierce, B. M.; Bocian, D. F.; Lindsey, J. S.; Birge, R. R. A theoretical investigation of the one-photon and two-photon properties of porphyrins. *J. Chem. Phys.* **84**:3901-3915; 1986.

[19] Goyan, R. L.; Cramb, D. T. Near-infrared two-photon excitation of protoporphyrin IX: Photodynamics and photoproduct generation. *Photochem. Photobiol.* **72**:821-827; 2000.

[20] Drobizhev, M.; Karotki, A.; Kruk, M.; Rebane, A. Resonance enhancement of two-photon absorption in porphyrins. *Chem. Phys. Lett.* **355**:175-182; 2002.

[21] Kruk, M.; Karotki, A.; Drobizhev, M.; Kuzmitsky, V.; Gael, V.; Rebane, A. Two-photon absorption of tetraphenylporphin free base. *J. Lumin.* **105**:45-55; 2003.

[22] Drobizhev, M.; Stepanenko, Y.; Dzenis, Y.; Karotki, A.; Rebane, A.; Taylor, P. N.; Anderson, H. L. Extremely strong near-IR two-photon absorption in conjugated porphyrin dimers: Quantitative description with three-essential-states model. *J. Phys. Chem. B* **109**:7223-7236; 2005.

[23] Drobizhev, M.; Makarov, N. S.; Stepanenko, Y.; Rebane, A. Near-infrared two-photon absorption in phthalocyanines: Enhancement of lowest gerade-gerade transition by symmetrical electron-accepting substitution. *J. Chem. Phys.* **124**: 2006.

[24] Frederiksen, P. K.; McIlroy, S. P.; Nielsen, C. B.; Nikolajsen, L.; Skovsen, E.; Jorgensen, M.; Mikkelsen, K. V.; Ogilby, P. R. Two-photon photosensitized production of singlet oxygen in water . *J. Am. Chem. Soc.* **127**:255-269; 2005.

[25] Kim, D. Y.; Alm, T. K.; Kwon, J. H.; Kim, D.; Ikeue, T.; Aratani, N.; Osuka, A.; Shigeiwa, M.; Maeda, S. Large two-photon absorption (TPA) cross-section of directly linked fused diporphyrins. *J. Phys. Chem. A* **109**:2996-2999; 2005.

[26] Ogawa, K.; Ohashi, A.; Kobuke, Y.; Kamada, K.; Ohta, K. Strong two-photon absorption of self-assembled butadiyne-linked bisporphyrin. *J. Am. Chem. Soc.* **125**:13356-13357; 2003.

[27] Xu, C.; Webb, W. W. Nonlinear and two-photon-induced fluorescence. In: Lakowicz, J. R. eds. *Topics in fluorescence spectroscopy*. New York: Plenum Press; 1997:471-540.

[28] Sheik-Bahae, M.; Said, A. A.; Wei, T.-H.; Hagan, D. J.; Van Stryland, E. W. Sensitive measurement of optical nonlinearities using a single beam. *IEEE J. Quantum Electron.* **26**:760-769; 1990.

[29] Frederiksen, P. K.; Jorgensen, M.; Ogilby, P. R. Two-photon photosensitized production of singlet oxygen. *J. Am. Chem. Soc.* **123**:1215-1221; 2001.

[30] Arnbjerg, J.; Johnsen, M.; Frederiksen, P. K.; Braslavsky, S. E.; Ogilby, P. R. Two-photon photosensitized production of singlet oxygen: Optical and optoacoustic characterization of absolute two-photon absorption cross sections for standard sensitizers in different solvents. *J. Phys. Chem. A* **110**:7375-7385; 2006.

[31] Fisher, W. G.; Partridge, W. P.; Dees, C.; Wachter, E. A. Simultaneous two-photon activation of type-I photodynamic therapy agents. *Photochem. Photobiol.* **66**:141-155; 1997.

[32] King, B. A.; Oh, D. H. Spatial control of reactive oxygen species formation in fibroblasts using two-photon excitation. *Photochem. Photobiol.* **80**:1-6; 2004.

[33] Kogej, T.; Beljonne, D.; Meyers, F.; Perry, J. W.; Marder, S. R.; Bredas, J. L. Mechanisms for enhancement of two-photon absorption in donor-acceptor conjugated chromophores. *Chem. Phys. Lett.* **298**:1-6; 1998.

[34] Rubio-Pons, O.; Luo, Y.; Agren, H. Effects of conjugation length, electron donor and acceptor strengths on two-photon absorption cross sections of asymmetric zinc-porphyrin derivatives. *J. Chem. Phys.* **124**: 2006.

[35] Bhawalkar, J. D.; He, G. S.; Prasad, P. N. Nonlinear multiphoton processes in organic and polymeric materials. *Rep. Prog. Phys.* **59**:1041-1070; 1996.

[36] Poulsen, T. D.; Frederiksen, P. K.; Jorgensen, M.; Mikkelsen, K. V.; Ogilby, P. R. Two-photon singlet oxygen sensitizers: quantifying, modeling, and optimizing the two-photon absorption cross section. *J. Phys. Chem. A* **105**:11488-11495; 2001.

[37] Norman, P.; Luo, Y.; Agren, H. Large two-photon absorption cross sections in two-dimensional, charge-transfer, cumulene-containing aromatic molecules. *J. Chem. Phys.* **111**:7758-7765; 1999.

[38] Wang, C. K.; Macak, P.; Luo, Y.; Agren, H. Effects of pi centers and symmetry on two-photon absorption cross sections of organic chromophores. *J. Chem. Phys.* **114**:9813-9820; 2001.

[39] Olsen, J.; Jorgensen, P. Linear and nonlinear response functions for an exact state and for an MCSCF state. *J. Chem. Phys.* **82**:3235-3264; 1985.

[40] Jensen, F. *Introduction to computational chemistry*: Chichester: John Wiley and Sons; 1999.

[41] Paterson, M. J.; Christiansen, O.; Jensen, F.; Ogilby, P. R. Overview of theoretical and computational methods applied to the oxygen-organic molecule photosystem. *Photochem. Photobiol.* **82**:1136-1160; 2006.

[42] Dreuw, A.; Head-Gordon, M. Single-reference ab initio methods for the calculation of excited states of large molecules. *Chem. Rev.* **105**:4009-4037; 2005.

[43] Yanai, T.; Tew, D. P.; Handy, N. C. A new hybrid exchange-correlation functional using the Coulomb-attenuating method (CAM-B3LYP). *Chem. Phys. Lett.* **393**:51-57; 2004.

[44] Salek, P.; Vahtras, O.; Helgaker, T.; Agren, H. Density-functional theory of linear and nonlinear time-dependent molecular properties. *J. Chem. Phys.* **117**:9630-9645; 2002.

[45] Paterson, M. J.; Christiansen, O.; Pawlowski, F.; Jorgensen, P.; Hattig, C.; Helgaker, T.; Salek, P. Benchmarking two-photon absorption with CC3 quadratic response theory, and comparison with density-functional response theory. *J. Chem. Phys.* **124**: 2006.

[46] Wilkinson, F.; Helman, W. P.; Ross, A. B. Quantum yields for the photosensitized formation of the lowest electronically excited singlet state of molecular oxygen in solution. *J. Phys. Chem. Ref. Data* **22**:113-262; 1993.

[47] Wilkinson, F.; Helman, W. P.; Ross, A. B. Rate constants for the decay and reactions of the lowest electronically excited singlet state of molecular oxygen in solution. An expanded and revised compilation. *J. Phys. Chem. Ref. Data* **24**:663-1021; 1995.

[48] Ogilby, P. R.; Foote, C. S. Chemistry of Singlet Oxygen. 42. Effect of Solvent, Solvent Isotopic Substitution and Temperature on Lifetime of Singlet Molecular Oxygen ($^1\ddot{A}_g$). *J. Am. Chem. Soc.* **105**:3423-3430; 1983.

[49] Gorman, A. A.; Rodgers, M. A. J. The quenching of aromatic ketone triplets by oxygen: competing singlet oxygen and biradical formation ? *J. Am. Chem. Soc.* **108**:5074-5078; 1986.

[50] Kristiansen, M.; Scurlock, R. D.; Iu, K.; Ogilby, P. R. Charge-transfer state and singlet oxygen ($O_2(a^1\Delta_g)$) production in photoexcited organic molecule-molecular oxygen complexes. *J. Phys. Chem.* **95**:5190-5197; 1991.

[51] Flors, C.; Ogilby, P. R.; Luis, J. G.; Grillo, T. A.; Izquierdo, L. R.; Gentili, P. L.; Bussotti, L.; Nonell, S. Phototoxic phytoalexins. Processes that compete with the photosensitized production of singlet oxygen by 9-phenylphenalenones. *Photochem. Photobiol.* **82**:95-103; 2006.

[52] Rebane, A. and Drobizhev, M. Private Communication. 2007.

[53] Gouterman, M. *The porphyrins*: New York: Academic Press; 1978.

[54] Eisenberg, W. C.; Taylor, K.; Veltman, J.; Murray, R. W. Generation of $O_2(a^1\Delta_g)$ by direct absorption of radiation by ground-state oxygen. *J. Am. Chem. Soc.* **104**:1104-1105; 1982.

[55] Anastasakos, L.; Wildman, T. A. The effect of internal-rotation on the methyl CH-stretching overtone spectra of toluene and the xylenes. *J. Chem. Phys.* **99**:9453-9459; 1993.

[56] Birge, R. R.; Pierce, B. M. Theoretical-analysis of the two-photon properties of linear polyenes and the visual chromophores. *J. Chem. Phys.* **70**:165-178; 1979.

[57] Albert, I. D. L.; Marks, T. J.; Ratner, M. A. Large molecular hyperpolarizabilities. Quantitative analysis of aromaticity and auxiliary donor-acceptor effects. *J. Am. Chem. Soc.* **119**:6575-6582; 1997.

[58] Drobizhev, M.; Stepanenko, Y.; Dzenis, Y.; Karotki, A.; Rebane, A.; Taylor, P. N.; Anderson, H. L. Understanding strong two-photon absorption in pi-conjugated porphyrin dimers via double-resonance enhancement in a three-level model. *J. Am. Chem. Soc.* **126**:15352-15353; 2004.

[59] McClain, W. M. Two-photon molecular spectroscopy. *Acc. Chem. Res.* **7**:129-135; 1974.

[60] Waluk, J. Ground- and excited-state tautomerism in porphycenes. *Acc. Chem. Res.* **39**:945-952; 2006.

[61] Drobizhev, M.; Karotki, A.; Kruk, M.; Mamardashvili, N. Z.; Rebane, A. Drastic enhancement of two-photon absorption in porphyrins associated with symmetrical electron-accepting substitution. *Chem. Phys. Lett.* **361**:504-512; 2002.

[62] Arad, O.; Morros, J.; Batllori, X.; Teixido, J.; Nonell, S.; Borrell, J. I. Diethyl 2,7-dibromo-4*H*,5*H*-thieno[3,2-b4,5-b']dipyrrole-3,6-dicarboxylate: A key intermediate for a diversity oriented synthesis of 2,7,12,17-tetraarylporphycenes. *Org. Lett.* **8**:847-850; 2006.

[63] Karotki, A.; Khurana, M.; Lepock, J. R.; Wilson, B. C. Simultaneous two-photon excitation of photofrin in relation to photodynamic therapy. *Photochem. Photobiol.* **82**:443-452; 2006.

[64] Dichtel, W. R.; Serin, J. M.; Edder, C.; Frechet, J. M. J.; Matuszewski, M.; Tan, L. S.; Ohulchanskyy, T. Y.; Prasad, P. N. Singlet oxygen generation via two-photon excited FRET. *J. Am. Chem. Soc.* **126**:5380-5381; 2004.

[65] Oar, M. A.; Serin, J. A.; Dichtel, W. R.; Frechet, J. M. J. Photosensitization of singlet oxygen via two-photon-excited fluorescence resonance energy transfer in a water-soluble dendrimer. *Chem. Mater.* **17**:2267-2275; 2005.

[66] Skovsen, E.; Snyder, J. W.; Ogilby, P. R. Two-photon singlet oxygen microscopy: The challenges of working with single cells. *Photochem. Photobiol.* **82**:1187-1197; 2006.

[67] Snyder, J. W.; Skovsen, E.; Lambert, J. D. C.; Poulsen, L.; Ogilby, P. R. Optical detection of singlet oxygen from single cells. *Phys. Chem. Chem. Phys.* **8**:4280-4293; 2006.

Chapter 7

General Discussion

A general discussion of the whole work described in the previous chapters and their implications for photodynamic therapy, as well as some suggestions for future research in this field are given in this chapter.

7.1. GENERAL DISCUSSION

On the basis of the results presented along the previous chapters, it can be safely concluded that the novel photon-counting system developed for time-resolved singlet oxygen ($^1O_2$) phosphorescence detection is suitable for determination of the kinetics of this species in biological media. Studies in biological systems are more challenging than those in solution due to the plethora of interferences. However, the system described in chapter 2 has allowed the study of $^1O_2$ kinetics in cell suspensions and from intact proteins, mainly as the result of meaningful improvements in sensitivity, time resolution, and dynamic range over the conventional analog detection technique.

We have used this tool to examine the $^1O_2$ behaviour in human skin fibroblasts. Perhaps the most important result obtained in this regard is the determination of the $^1O_2$ lifetime in such eukaryotic cells and the implications that it has in relation to spatially-resolved mechanisms of oxygen-dependent photoinduced cell death. The experiments performed with two well-known porphyrins that show a preferential localisation in a single organelle, indicate that the $^1O_2$ lifetime is not only governed by solvent interactions but also by interactions with cellular constituents. The extent of $^1O_2$ quenching by cell constituents depends on the organelle where it has been photosensitised. The lifetime of $^1O_2$ is, however, in the microsecond range, which enlarge the diffusion-dependent sphere of $^1O_2$ activity up to ~1 μm in a D_2O-based environment [1]. These results are consistent with the recently proposed view of $^1O_2$ free to move along the cell [2-5], but also with several landmark studies that indicate a correlation between the subcellular localization of a photosensitiser and the outgoing photodynamic response [6,7]. It is generally accepted that those photosensitisers which show a preferential localisation for the lysosomes induce cell death by apoptosis [6] whereas nuclear photosensitisers produce mutagenic oxidations to DNA that lead to cell death by a different pathway [8].

In relation to $^1O_2$ photosensitised in the nucleus, the experiments with the protein bovine serum albumin (BSA) indicate that a fraction of the $^1O_2$ photosensitised in the nucleus is able to escape out the cell. The $^1O_2$ lifetime τ_Δ = 24 ± 2 μs measured in a D_2O cell suspension, is a scrambled number between the lifetimes within (τ_Δ~ 5 μs) and outside the cells (τ_Δ ~ 68 μs [9]). The resulting conclusion is that diffusional exchange of $^1O_2$ between the cell and the external aqueous phase is taking place.

The proposed mechanism is depicted in Fig. 1.

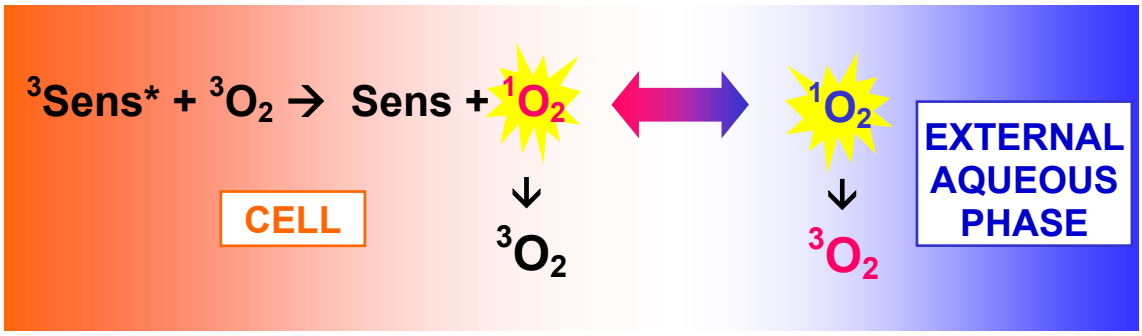

Figure 1. Proposed mechanism for the $^1O_2$ formation and decay in the cells.

The lifetime τ_Δ = 6 ± 2 μs measured in the presence of BSA represents thus the upper limit for the $^1O_2$ lifetime within the cells when photosensitised in the nucleus. This value indicates that even if all $^1O_2$ molecules were completely quenched by BSA, the measured lifetime would not go below ~6 μs. To verify this conclusion, it would be highly desirable to find another $^1O_2$ quencher that would scavenge even faster than BSA in the aqueous external phase. Ideally, this quencher should be stuck at the outer part of the cytoplasmic membrane in order to ensure the quenching of all $^1O_2$ molecules that were able to cross the membrane.

On the other hand, the lifetime of $^1O_2$ photosensitised in the lysosomes, τ_Δ ~13 μs, is unaffected by the presence of BSA. Then, $^1O_2$ generated in this organelle is not able to leave the cell before being quenched by its cellular constituents. The differences in $^1O_2$ kinetics as a function of its site of generation are consistent with the long-standing notion of highly localized damage induced by this species [1]. The importance of solvent deactivation pathways for H_2O-based cell suspensions indicates, however, that $^1O_2$ is more accurately described as a selective rather than a reactive species [5]. Thus, the results on human skin fibroblasts reconcile the two currently proposed versions for the $^1O_2$ kinetics in cells.

Thus far, we have photosensitised $^1O_2$ in the nucleus and the lysosomes of human skin fibroblasts. It is clearly desirable to expand our horizons and examine other kinds of cells, particularly tumour cells, and other subcellular localisations of the photosensitisers.

Selective and quantitative localisation of a photosensitiser is often difficult to achieve. The advances of molecular genetic techniques may shed light onto this issue. By means of these methods it is possible to codify the DNA to express selectively a photosensitising-protein in any single location of the cell. In fact, the development of the first fully genetically-encoded photosensitiser gave rise to several laboratories, including ours, to study the ability of green fluorescence protein (GFP) mutants to

photosensitise $^1O_2$. This family of compounds has a characteristic biosynthetic chromophore that is embedded in an 11-strand β-barrel. The protein scaffold not only plays a pivotal role in modulating the chromophore photophysical properties but has also a protective function from collisional quenching effects [10,11].

The β-can protective role from oxygen has been evidenced in our experiments by the long triplet state lifetimes measured for EGFP (τ_T ~25 μs, air-saturated solution), GFPmut2 (τ_T ~18 μs, oxygen-saturated solution) and GFPmut2-H148G (τ_T ~10 μs, oxygen-saturated solution) in comparison to the HBDI chromophore in solution (τ_T ~3 μs, air-saturated solution). Likewise, the $^1O_2$ lifetime measured for EGFP, GFPmut2-H148G and the HBDI chromophore is substantially shorter than that in solution. In addition to $^1O_2$ quenching by the chromophore itself, ~10% of the β-can aminoacids are potential $^1O_2$ quenchers. The presence of such number of $^1O_2$ quenchers in the chromophore surroundings is a negative factor for PDT purposes, as they reduce the $^1O_2$ lifetime and therefore, its maximum diffusion distance and action sphere. This factor should be taken into account for the future development of genetically-encoded photosensitisers.

In relation to this, the protein EGFP presents the best photosensitising properties of the GFP mutants studied, judging from its triplet state lifetime and k_q value. EGFP, GFPmut2 and GFPmut2-H148G are all class 2 mutants in which the phenolate form of the chromophore is stabilised by mutation of Ser 65, by Thr in EGFP, and by Ala in GFPmut2 and GFPmut2-H148G. From a chemical perspective, one would infer that, because the three proteins share the same form of the chromophore, the photosensitising properties must be almost the same for the three mutants. The experiments indicate, however, that the impact of the overall protein structure must be also taken into account. In this direction, experiments on GFPmut2 and GFPmut2-H148G have been very valuable since the only difference between them is the replacement of His 148 by Gly. This allows us to draw a conclusion about the role play by this aminoacid.

Removal of His148 destabilises the protein barrel, leading to more pronounced conformational fluctuations that result in higher solvent access to the chromophore [12,13]. This is shown in our experiments by a shorter triplet state lifetime in GFPmut2-H148G than in GFPmut2, due to more effective oxygen quenching. Then, suppression of His 148 is likely to be one the key mutations for improving the photosensitising properties of GFPs.

With the development of mutagenesis techniques, it is feasible to get a great variety of GFP-like proteins. On the basis on the direct detection of $^1O_2$ formation and decay, our results yield new information that will allow the rational re-engineering of GFPs with better photosensitising properties. Perhaps, they are only the first prototype of a collection of genetically-encoded, light-driven macromolecular reagents.

Genetically-encoded photosensitisers would open new perspectives for PDT as they provide a unique opportunity to spatially and temporally control cell killing. Alternatively, selective generation of $^1O_2$ in a well-defined subcellular spatial domain can be also achieved by two-photon excitation of the photosensitiser. This technique is free from ambiguities as to the primary site of $^1O_2$ photosensitisation but its main drawback relays on the lack of biologically compatible $^1O_2$ sensitisers with large two-photon absorption cross sections in the NIR region. This currently restricts its application for PDT purposes.

In this direction, tetraphenylporphycenes can play a key role as two-photon photosensitisers. Their maximum δ values, obtained upon two-photon excitation of the two compounds studied, fit into the so-called therapeutic window and result in the production of $^1O_2$ with efficiency ~100 times higher than with other photosensitisers used in PDT (Table 1). Also, *in vitro* studies have shown that tetraphenylporphycenes are biologically compatible and photoinactivate several cell lines, triggering the apoptotic pathway [14].

Table 1. Two-photon absorption cross sections of common one-photon photosensitisers, tetrapyrrolic frameworks and new two-photon photosensitisers[a].

	δ, GM	**Wavelength, nm**	
Photofrin®	7.4	850	Common one-photon photosensitisers
HPD	15	750	
Photosens	5	1064	
Protoporphyrin IX	2	790	
Photolon	60	800	
Visudyne® [b]	51	930	
TPP	59	760	Basic tetrapyrrolic frameworks
TBP	20	780	
Bu_4TAP	70	783	
Pc	250	830	
TPPo	**1750**	770	
Porphyrin dimers	3100-10100	825-875	Two-photon photosensitisers

[a] adapted from Karotki *et al*. [15]. [b] from Khurana *et al*. [16]. HPD: hematoporphyrin derivative; TBP: tetrabenzoporhyrin; TAP: tetraazaporphyrin or porphyrazin; Pc: phthalocyanine or tetrabenzoazaporphyrin.

The porphycenes' two-photon properties can be further improved by adequate synthetic modifications. A number of factors influence the TPA magnitudes, in particular, π-electronic delocalisation and charge separation efficiency. Molecular designs involving donor/acceptor sets inserted with a π-conjugation system in a symmetrical (D-π-D or A-π-A) or asymmetrical (D-π-A) arrangement have been proposed to enhance the TPA cross section values [17]. Larger enhancements and/or properties' final tuning can be achieved by the additional introduction of electron-accepting or electron-donating substituents in the end groups [18-22]. The approach of extending the π-electron delocalization throughout porphyrin dimers has produced, however, the largest enhancements measured in any organic molecule (~10^3 times) [23,24,24].

In this regard, tetraphenylporphycenes are very attractive for a number of reasons. First, the special reactivity of the 9 position [25] makes feasible to synthesise porphycene dimers linked by this point. Second, the new diversity-oriented methodology developed for their synthesis allows to introduce a variety of aromatic substituents in the 2,7,12,17 positions [26]. These two structural modifications make us confident that the future development of new tetraphenylporphycenes with improved two-photon properties is now feasible.

Altogether, the results presented herein open new possibilities for $^1O_2$-mediated cell death studies, the design of new photosensitising GFP-like proteins, as well as for the emerging two-photon initiated PDT.

7.2 REFERENCES

[1] Moan, J. On the diffusion length of singlet oxygen in cells and tissues. *J. Photochem. Photobiol. B:Biol.* **6**:343-347; 1990.

[2] Snyder, J. W.; Skovsen, E.; Lambert, J. D. C.; Ogilby, P. R. Subcellular, time-resolved studies of singlet oxygen in single cells. *J. Am. Chem. Soc.* **127**:14558-14559; 2005.

[3] Skovsen, E.; Snyder, J. W.; Lambert, J. D. C.; Ogilby, P. R. Lifetime and diffusion of singlet oxygen in a cell. *J. Phys. Chem. B* **109**:8570-8573; 2005.

[4] Snyder, J. W.; Skovsen, E.; Lambert, J. D. C.; Poulsen, L.; Ogilby, P. R. Optical detection of singlet oxygen from single cells. *Phys. Chem. Chem. Phys.* **8**:4280-4293; 2006.

[5] Hatz, S.; Lambert, J. D. C.; Ogilby, P. R. Measuring the lifetime of singlet oxygen in a single cell: addressin the issue of cell viability. *Photochem. Photobiol. Sci.* **6**:1106-1116; 2007.

[6] Kessel, D. Correlation between subcellular localization and photodynamic efficacy. *J. Porphyrins Phthalocyanines* **8**:1009-1014; 2004.

[7] Peng, Q.; Moan, J.; Nesland, J. M. Correlation of subcellular and intratumoral photosensitizer localization with ultrastructural features after photodynamic therapy. *Ultrastruct. Pathol.* **20**:109-129; 1996.

[8] Ravanat, J. L.; Di Mascio, P.; Martinez, G. R.; Medeiros, M. H. G.; Cadet, J. Singlet oxygen induces oxidation of cellular DNA. *J. Biol. Chem.* **275**:40601-40604; 2000.

[9] Wilkinson, F.; Helman, W. P.; Ross, A. B. Rate constants for the decay and reactions of the lowest electronically excited singlet state of molecular oxygen in solution. An expanded and revised compilation. *J. Phys. Chem. Ref. Data* **24**:663-1021; 1995.

[10] Tsien, R. Y. The Green Fluorescent Protein. *Annu. Rev. Biochem.* **67**:509-544; 1998.

[11] Swaminathan, R.; Hoang, C. P.; Verkman, A. S. Photobleaching recovery and anisotropy decay of green fluorescent protein GFP-S65T in solution and cells: Cytoplasmic viscosity probed by green fluorescent protein translational and rotational diffusion. *Biophys. J.* **72**:1900-1907; 1997.

[12] Abbruzzetti, S.; Grandi, E.; Viappiani, C.; Bologna, S.; Campanini, B.; Raboni, S.; Bettati, S.; Mozzarelli, A. Kinetics of acid-induced spectral changes in the GFPmut2 chromophore. *J. Am. Chem. Soc.* **127**:626-635; 2005.

[13] Wachter, R. M.; Elsliger, M. A.; Kallio, K.; Hanson, G. T.; Remington, S. J. Structural basis of spectral shifts in the yellow-emission variants of green fluorescent protein. *Structure* **6**:1267-1277; 1998.

[14] Stockert, J. C.; Cañete, M.; Juarranz, A.; Villanueva, A.; Horobin, R. W.; Borrell, J.; Teixido, J.; Nonell, S. Porphycenes: Facts and prospects in photodynamic therapy of cancer. *Curr. Med. Chem.* **14**:997-1026; 2007.

[15] Karotki, A.; Khurana, M.; Lepock, J. R.; Wilson, B. C. Simultaneous two-photon excitation of photofrin in relation to photodynamic therapy. *Photochem. Photobiol.* **82**:443-452; 2006.

[16] Khurana, M.; Collins.H.A.; Karotki, A.; Anderson, H. L.; Cramb, D. T.; Wilson, B. C. Quantitative *in vitro* demostration of two-photon photodynamic therapy using Photofrin and Visudyne. *Photochem. Photobiol.* **83**:1-8; 2007.

[17] Albota, M.; Beljonne, D.; Bredas, J. L.; Ehrlich, J. E.; Fu, J. Y.; Heikal, A. A.; Hess, S. E.; Kogej, T.; Levin, M. D.; Marder, S. R.; Cord-Maughon, D.; Perry, J. W.; Rockel, H.; Rumi, M.; Subramaniam, C.; Webb, W. W.; Wu, X. L.; Xu, C. Design of organic molecules with large two-photon absorption cross sections. *Science* **281**:1653-1656; 1998.

[18] Karotki, A.; Kruk, M.; Drobizhev, M.; Rebane, A.; Nickel, E.; Spangler, C. W. Efficient singlet oxygen generation upon two-photon excitation of new porphyrin with enhanced nonlinear absorption. *IEEE J. Select. Top. Quant. Electron.* **7**:971-975; 2001.

[19] Morone, M.; Beverina, L.; Abbotto, A.; Silvestri, F.; Collini, E.; Ferrante, C.; Bozio, R.; Pagani, G. A. Enhancement of two-photon absorption cross-section and singlet-oxygen generation in porphyrins upon beta-functionalization with donor-acceptor substituents. *Org. Lett.* **8**:2719-2722; 2006.

[20] Drobizhev, M.; Karotki, A.; Kruk, M.; Mamardashvili, N. Z.; Rebane, A. Drastic enhancement of two-photon absorption in porphyrins associated with symmetrical electron-accepting substitution. *Chem. Phys. Lett.* **361**:504-512; 2002.

[21] Karotki, A.; Drobizhev, M.; Kruk, M.; Spangler, C.; Nickel, E.; Mamardashvili, N.; Rebane, A. Enhancement of two-photon absorption in tetrapyrrolic compounds. *J. Opt. Soc. Am. B: Optical Phys.***20**:321-332; 2003.

[22] Drobizhev, M.; Makarov, N. S.; Stepanenko, Y.; Rebane, A. Near-infrared two-photon absorption in phthalocyanines: Enhancement of lowest gerade-gerade transition by symmetrical electron-accepting substitution. *J. Chem. Phys.* **124**: 2006.

[23] Kim, D. Y.; Alm, T. K.; Kwon, J. H.; Kim, D.; Ikeue, T.; Aratani, N.; Osuka, A.; Shigeiwa, M.; Maeda, S. Large two-photon absorption (TPA) cross-section of directly linked fused diporphyrins. *J. Phys. Chem. A* **109**:2996-2999; 2005.

[24] Drobizhev, M.; Stepanenko, Y.; Dzenis, Y.; Karotki, A.; Rebane, A.; Taylor, P. N.; Anderson, H. L. Understanding strong two-photon absorption in pi-conjugated porphyrin dimers via double-resonance enhancement in a three-level model. *J. Am. Chem. Soc.* **126**:15352-15353; 2004.

[25] Vogel, E.; Köcher, M.; Lex, J.; Ermer, O. Steric Modulation of the Porphycene System by alkyl substituents: 9,10,19,20-Tetraalkylporphycenes. *Israel J. Chem.* **29**:257-266; 1989.

[26] Arad, O.; Morros, J.; Batllori, X.; Teixido, J.; Nonell, S.; Borrell, J. I. Diethyl 2,7-dibromo-4H,5H-thieno[3,2-b : 4,5-b ']dipyrrole-3,6-dicarboxylate: A key intermediate for a diversity oriented synthesis of 2,7,12,17-tetraarylporphycenes. *Org. Lett.***8**:847-850; 2006.

Chapter 8

Conclusions

1. An ultrasensitive spectrometer capable to detect the phosphorescence of singlet oxygen with nanosecond time resolution has been built and compared to previous systems based on analog detectors.
2. The kinetics of singlet oxygen production and decay in human skin fibroblasts depend on the organelle when it has been generated, but both processes being slower in the lysosomes than in the nucleus.
3. Singlet oxygen photosensitised in the cell nucleus of D_2O-based suspensions is in a fast equilibrium with that in the external aqueous phase, whereas singlet oxygen photosensitised in the lysosomes is not able to cross the cell membrane.
4. The triplet state of the green fluorescent protein mutant GFPmut2 is effectively shielded from oxygen by the β-can. The additional mutation H148G increases the protein's permeability to oxygen. Access of oxygen to the protein's chromophore is highest in the mutant EGFP.
5. Production of singlet oxygen by green fluorescent mutants follows the same trend as above. Neither KillerRed nor its photobleached form produces singlet oxygen to any measurable extent.
6. 2,7,12,17-Tetraphenylporphycene and its palladium (II) complex are efficient singlet oxygen two-photon photosensitisers for the 700-800 nm therapeutic window. The maximum values of the two-photon absorption cross sections are 2280 and 1750 GM for the 2,7,12,17- tetraphenylporphycene and its palladium (II) complex, respectively. These values are ~100 times larger than those for commonly used photosensitisers due to resonance enhancement in the Soret region.